Thomas Traub

A Kinetic Transport Model for the Coupled Dynamics of Electrons and Phonons in One-dimensional Systems and its Application to Metallic Carbon Nanotubes

DIPLOMARBEIT

Zur Erlangung des akademischen Grades
Diplom-Ingenieur

Diplomstudium Technische Physik

Graz University of Technology

Technische Universität Graz

betreut von
Ao. Univ.-Prof. Dr. Ferdinand Schürrer
Institute of Theoretical and Computational Physics
Graz, Oktober 2010

Ein kinetisches Transportmodell für die gekoppelte Dynamik von Elektronen und Phononen in eindimensionalen Systemen und dessen Anwendung auf metallische Kohlenstoffnanoröhrchen

Ziel dieser Arbeit ist die Entwicklung eines kinetischen Transportmodells für die gekoppelte Dynamik von Elektronen und Phonon in eindimensionalen Systemen, wobei keine Information über die Bandstruktur des Elektronen und Phononen Sytems vorausgesetzt wird. Um die Transportgleichungen zu lösen, wird ein numerisches Modell entwickelt, für welches die Teilchenzahlerhaltung der Elektronen sowie die Energie- und Impulserhaltung gezeigt wird. Zur Überwindung der numerische Problem bei der Berechnung der Stoßintegrale wird eine spezielle Abtastmethode entwicket, welche ebenfalls die Erhaltungssätze erfüllt. Die Diskretisierung der Verteilungsfunktionen erfolgt über den k-Raum, entgegen der üblichen Energiedisketisierung, sodass auch flache Elektronenbänder behandelt werden können. Für das numerische Modell ist nur die Kentniss der Dispersionsrelation an den Gitterpunkten notwendig, weshalb auch mit Bandstrukturen geabeitet werden kann, die nicht in analytischer Form gegeben sind. Abschließend wird das Modell an metallischen Kohlenstoffnanoröhrchen erprobt.

A kinetic transport model for the coupled dynamics of electrons and phonons in one-dimensional systems and its application to metallic carbon nanotubes

The aim of this work is the development of a kinetic transport model for the coupled dynamics of electrons and phonons in one-dimensional systems without using prior information on the band structure of the electron and phonon system. A numerical model is developed to solve the transport equations for which the conservation of electron number, energy and momentum is proved. To overcome numerical sampling problems, when calculating the collision integrals, a supersampling method that fulfills the conservation laws, is introduced. To be able to deal with flat electron bands, all distribution functions are discretized in k-space as opposed to the common energy discretization. The numerical model is designed to work with dispersion relations only known at the discretization grid points, therefore, no analytical expression for the band structure is explicitly needed. Finally, the model is tested for metallic carbon nanotubes.

Contents

1 Introduction

Carbon nanotubes have been extensively studied since their discovery [1]. They represent a very interasting functional material due to their unique electrical, thermal and mechanical properties. For a detailed description of carbon nanotube properties we refer to the review articles of M.S. Dresselhaus et al. [2], E. Thune et. al. [3], J.-C. Charlier et. al. [4] and the book of S. Reich et al.[5]. Carbon nanotubes can exhibit either a metallic or semiconducting behavior, depending on their atomic structure. Metallic nanotubes can be seen as one-dimensional conductors. Their ability to carry very high current densities and ballistic transport properties in the low bias regime [6] makes them attractive candidates for interconnections in future electronic devices. Consequently, they have been investigated thoroughly both experimentally [6, 7] and theoretically [8, 9, 10, 11, 12]. Semiconducting nanotubes, on the other hand, can be used in field-effect transistors (FETs) [13, 14]. New developments show that they can be also utilized as sense-FETs [15] for instance by immobilizing functional groups along the nanotube [16] and, thus, changing the band structure [17]. To effectivley describe such a system one needs to develop a kinetic transtport model that does not depend on the specific form of the band structure. Furthermore, as opposed to the common energy discretization of the electron bands, one needs to employ a k-space discetization in order to be able to work with very flat bands. The focus of this thesis is to develop such a model to describe the coupled dynamics of electrons and phonons in one-dimensional systems.

Chapter 2 presents an analytical description of the carrier transport in one-dimensional systems that does not rely on any specific band structure. This idea is further pursued in the development of the numerical model, in Chapter 3. Conservation of electron number, energy and momentum is proved for arbitrary band structures, where the dispersion relation only needs to be known at the grid points. Therefore, even band structures obtained by DFT calculations can be used. To overcome sampling problems, when calculating the collision integrals, a supersampling method is presented in Section 3.7 which retains the conservational properties of the original method. In Chapter 4 the properties of metallic carbon nanotubes are discussed and used to test the transport model. The results are presented in Chapter 5.

2 The kinetic transport model

In this chapter we develop the kinetic transport model that describes the flow of electrons and phonons throughout the device. Since the main focus of this thesis aims at one-dimensional systems, we will start with the one-dimensional semi-classical Boltzmann equation for electrons. Subsequently, we need to formulate the collision operator. Thereafter, the same steps are repeated for phonons. Finally, we will check if the corresponding conservation laws are still fulfilled within the framework of the obtained equations. These steps are crucial to develop a fully discretized model.

2.1 Moments of the distribution function

The semi-classical Boltzmann equation is an evolution equation for distribution functions. In our case we will calculate the time evolution of the electron and phonon distributions. Evaluated distribution functions, however, are difficult to verify experimentally. Moments of the distribution function, like the electron, current or the energy densities are macroscopic quantities and can be measured easily. Hence, these quantities need to be defined before we start with the development of our model.

In order to calculate local densities, a summation over all electron states needs to be performed. Since we are using the classical limit, this summation will be replaced by an integral over the first Brillouin zone. In the d-dimensional case by assuming an equal extension L of the crystal in all directions this transformation is of the form

$$\sum_{\mathbf{k}} \to \left(\frac{L}{2\pi}\right)^d \int_{\mathcal{BZ}} d\mathbf{k} \tag{2.1}$$

according to [18], where $\mathbf{k}$ denotes the wave vector also called quasi momentum. The constant $\left(\frac{L}{2\pi}\right)^d$ accounts for the density of states in k-space.

Consequently, we can define the electron density for a band α in a one-dimensional system following [19] as

$$\mathcal{N}_\alpha(x,t) = \frac{1}{L}\sum_k f_\alpha(x,k,t) = \frac{1}{2\pi}\int_{\mathcal{BZ}} f_\alpha(x,k,t)dk \qquad \text{with } x,k \in \mathbb{R}, \quad t \in \mathbb{R}^+, \tag{2.2}$$

where $f_\alpha(x,k,t)$ denotes the electron distribution function of band α.

The distribution function $f_\alpha(x,k,t)$ is the probability density of finding a carrier at position x with quasi momentum k at time t. The number of carriers at this point in the infinitesimal phase space volume $dxdk$ is therefore $(L/2\pi)f_\alpha(x,k,t)dxdk$ [18].

The total carrier density is then given by the sum over all electron bands:

$$\mathcal{N}(x,t) = \sum_\alpha \mathcal{N}_\alpha(x,t). \tag{2.3}$$

Similarly, the current density reads

$$\mathcal{J}_\alpha(x,t) = -\frac{e_0}{L}\sum_k v_\alpha(k) f_\alpha(x,k,t) = -\frac{e_0}{2\pi}\int_{\mathcal{BZ}} v_\alpha(k) f_\alpha(x,k,t)dk, \tag{2.4}$$

with the elementary charge e_0 and the group velocity $v_\alpha(k)$. Finally, the energy density is defined as

$$\mathcal{E}_\alpha(x,t) = \frac{1}{L}\sum_k E_\alpha(k) f_\alpha(x,k,t) = \frac{1}{2\pi}\int_{\mathcal{BZ}} E_\alpha(k) f_\alpha(x,k,t)dk, \tag{2.5}$$

where $E(k)$ denotes the dispersion relation. The total current and energy densities are then again given by a sum over all relevant bands:

$$\mathcal{J}_(x,t) = \sum_\alpha \mathcal{J}_\alpha(x,t), \tag{2.6}$$

$$\mathcal{E}_(x,t) = \sum_\alpha \mathcal{E}_\alpha(x,t) + \sum_\eta \mathcal{E}^\eta(x,t). \tag{2.7}$$

While $\mathcal{J}$ comprises the sum over all electron bands, the total energy density consists of the energy stored in the electron as well as in the phonon system. Therefore, the second sum represents the phonon energy density of band η defined likewise as

$$\mathcal{E}^\eta(x,t) = \frac{1}{2\pi}\int_{\mathcal{BZ}} W^\eta(q) N^\eta(x,q,t)dq. \tag{2.8}$$

Here, $W_\eta(q)$ stands for the phonon dispersion relation, $N^\eta(x,q,t)$ is the phonon distribution function and q the phonon quasi momentum. The total momentum density, consequently, reads

$$\mathcal{K}(x,t) = \sum_\alpha \mathcal{K}_\alpha(x,t) + \sum_\eta \mathcal{Q}^\eta(x,t), \tag{2.9}$$

with

$$\mathcal{K}_\alpha(x,t) = \frac{1}{2\pi}\int_{\mathcal{BZ}} k f_\alpha(x,k,t)dk \qquad \text{and} \tag{2.10}$$

$$\mathcal{Q}^\eta(x,t) = \frac{1}{2\pi}\int_{\mathcal{BZ}} q N^\eta(x,q,t)dq. \tag{2.11}$$

Adhering to this pattern generalized moments $\mathcal{M}$ of the electron and phonon distribution functions can be defined as

$$\mathcal{M}_\alpha(x,t) = \frac{1}{2\pi}\int_{\mathcal{BZ}} \Psi_\alpha(k) f_\alpha(x,k,t)dk \qquad \text{and} \tag{2.12}$$

$$\mathcal{M}^\eta(x,t) = \frac{1}{2\pi}\int_{\mathcal{BZ}} \Psi^\eta(q) N^\eta(x,q,t)dq. \tag{2.13}$$

with arbitrary functions Ψ of the quasi momenta k and q, respectively. Therefore, the total generalized moment reads

$$\mathcal{M}_(x,t) = \sum_\alpha \mathcal{M}_\alpha(x,t) + \sum_\eta \mathcal{M}^\eta(x,t). \tag{2.14}$$

2.2 Electron collision operator

The one-dimensional semi-classical Boltzmann equation is given by [18]

$$\frac{\partial f_\alpha(x,k,t)}{\partial t} + v_\alpha(k)\frac{\partial f_\alpha(x,k,t)}{\partial x} + \frac{eE}{\hbar}\frac{\partial f_\alpha(x,k,t)}{\partial k} = \left.\frac{\partial f_\alpha(x,k,t)}{\partial t}\right|_{Coll} \tag{2.15}$$

where $f_\alpha(x,k,t)$ denotes the distribution function of the electrons for the band α, $v_\alpha(k) = \partial_k E_\alpha(k)/\hbar$ the group velocity, E the electric field strength and e the electric charge ($e = -e_0$ for electrons, where e_0 denotes the elementary charge). We can express the rate of change of the distribution function due to collisions, in summing over all relevant collision operators $C^\eta_{\alpha\beta}(k)$. Each one takes into account interactions of electrons in the bands α,β with phonons of the branch η:

$$\left.\frac{\partial f_\alpha(k)}{\partial t}\right|_{Coll} = C_\alpha(k) = \sum_\eta \sum_\beta C^\eta_{\alpha\beta}(k), \qquad \alpha,\beta \in I_{el}, \quad \eta \in I_{ph}. \tag{2.16}$$

Here, I_{el} and I_{ph} stands for the set of electron and phonon band indices. Since scattering events are local and instantaneous, the time and position dependency is omitted for the sake of a compact notation $f_\alpha(k) = f_\alpha(x,k,t)$. Note that only electron-phonon scattering is accounted for. No electron-electron or impurity scattering is included, since

phonon scattering events plays the dominant role in limiting the conductivity in our systems under investigation. This is especially true for phonon distributions far from equilibrium, which we will see later. Following [20] the collision operator for electrons can now be expressed as

$$C^{\eta}_{\alpha\beta}(k) = \sum_{k'} \left\{ W^{\eta}_{\beta\alpha}(k',k) f_{\beta}(k') \left[1 - f_{\alpha}(k)\right] - W^{\eta}_{\alpha\beta}(k,k') f_{\alpha}(k) \left[1 - f_{\beta}(k')\right] \right\}, \quad (2.17)$$

where k' runs over the whole Brillouin zone and $W^{\eta}_{\beta\alpha}(k',k)$ is the probability for processes that transfer electrons from state k' to k and from band β to α due to a scattering event. It, therefore, contributes to the gain term of the collision operator, whereas $W^{\eta}_{\alpha\beta}(k,k')$ is part of the loss term and describes the inverse processes. The total scattering rate is proportional to the probability of the occurrence of the scattering process, the occupation probability of the initial states f' and the Pauli-blocking factor $(1-f)$, which denotes the probability that the final state is free. The scattering probability $W^{\eta}_{\alpha\beta}(k_1,k_2)$ can be expressed as

$$W^{\eta}_{\alpha\beta}(k_1,k_2) = W^{EM}_{\alpha\beta\,\eta}(k_1,k_2) + W^{ABS}_{\alpha\beta\,\eta}(k_1,k_2) \quad (2.18)$$

with W^{EM} and W^{ABS} being the probabilities for emission and absorption of phonons. These quantities can be calculated by time-dependent, first-order perturbation theory, which leads to

$$W^{EM}_{\alpha\beta\,\eta}(k_1,k_2) = \sum_{q} s^{\eta}_{\alpha\beta}(k_1,k_2) \left[N^{\eta}(q)+1\right] \delta(E_{\alpha}(k_1) - E_{\beta}(k_2) - W^{\eta}(q)) \delta_{q,k_1-k_2}, \quad (2.19)$$

$$W^{ABS}_{\alpha\beta\,\eta}(k_1,k_2) = \sum_{q} s^{\eta}_{\alpha\beta}(k_1,k_2) N^{\eta}(q) \delta(E_{\beta}(k_2) - E_{\alpha}(k_1) - W^{\eta}(q)) \delta_{q,k_2-k_1}, \quad (2.20)$$

where $s^{\eta}_{\alpha\beta}(k_1,k_2)$ denotes the matrix element of the scattering potential [18], $N^{\eta}(q)$ the phonon distribution function, $E_{\alpha}(k_1)$ and $E_{\beta}(k_2)$ the electron and $W^{\eta}(q)$ the phonon dispersion relation. The delta function stems from Fermi's golden rule and ensures energy conservation. The Kronecker delta ensures conservation of quasi momentum.

It should be noted that this formulation is not completely general. In principle, we also need to account for the reciprocity of the Brillouin zone which would modify the conservation condition of quasi momentum to

$$k_1 - k_2 \pm q = G \quad (2.21)$$

with G being the reciprocal lattice constant. Since we do not deal with Umklapp pro-

cesses, or rather circumvent this problem by choosing a convenient collision geometry the more simple condition

$$k_1 - k_2 \pm q = 0 \tag{2.22}$$

suffices. Note that this simplification does not affect the generality of the later proofs of conservation laws.

The matrix element $s^{\eta}_{\alpha\beta}(k_1, k_2)$ still needs to be evaluated. It depends on the phonon type η (acoustical or optical) involved and is symmetric with respect to the exchange of electron bands α and β and the exchange of quasi momenta k_1 and k_2.

Inserting everything back into (2.17) yields

$$\begin{aligned} C^{\eta}_{\alpha\beta}(k) = \sum_{k'}\sum_{q} \big\{ & s^{\eta}_{\alpha\beta}(k,k')\left[N^{\eta}(q)+1\right]\delta(E_\beta(k') - E_\alpha(k) - W^{\eta}(q))\delta_{q,k'-k} f_\beta(k')\left[1-f_\alpha(k)\right] \\ & + s^{\eta}_{\alpha\beta}(k,k') N^{\eta}(q)\delta(E_\alpha(k) - E_\beta(k') - W^{\eta}(q))\delta_{q,k-k'} f_\beta(k')\left[1-f_\alpha(k)\right] \\ & - s^{\eta}_{\alpha\beta}(k,k')\left[N^{\eta}(q)+1\right]\delta(E_\alpha(k) - E_\beta(k') - W^{\eta}(q))\delta_{q,k-k'} f_\alpha(k)\left[1-f_\beta(k')\right] \\ & - s^{\eta}_{\alpha\beta}(k,k') N^{\eta}(q)\delta(E_\beta(k') - E_\alpha(k) - W^{\eta}(q))\delta_{q,k'-k} f_\alpha(k)\left[1-f_\beta(k')\right] \big\}. \end{aligned} \tag{2.23}$$

Examining (2.23), we can identify gain (G) and loss (L) terms via emission (EM) and absorption (ABS)(see Figure 2.1):

$$\begin{aligned} G^{EM}_{\beta\alpha\,\eta}(k',k) &= \delta(E_\beta(k') - E_\alpha(k) - W^{\eta}(k'-k)) \\ &\quad \times s^{\eta}_{\alpha\beta}(k,k')[N^{\eta}(k'-k)+1] f_\beta(k')[1-f_\alpha(k)], && (2.24) \\ L^{ABS}_{\beta\alpha\,\eta}(k',k) &= \delta(E_\beta(k') - E_\alpha(k) - W^{\eta}(k'-k)) \\ &\quad \times s^{\eta}_{\alpha\beta}(k,k') N^{\eta}(k'-k) f_\alpha(k)[1-f_\beta(k')], && (2.25) \\ G^{ABS}_{\beta\alpha\,\eta}(k',k) &= \delta(E_\alpha(k) - E_\beta(k') - W^{\eta}(k-k')) \\ &\quad \times s^{\eta}_{\alpha\beta}(k,k') N^{\eta}(k-k') f_\beta(k')[1-f_\alpha(k)], && (2.26) \\ L^{EM}_{\beta\alpha\,\eta}(k',k) &= \delta(E_\alpha(k) - E_\beta(k') - W^{\eta}(k-k')) \\ &\quad \times s^{\eta}_{\alpha\beta}(k,k')[N^{\eta}(k-k')+1] f_\alpha(k)[1-f_\beta(k')]. && (2.27) \end{aligned}$$

Consequently, we can express the collision operator by these four elementary processes

$$C^{\eta}_{\alpha\beta}(k) = \sum_{k'} \left\{ G^{EM}_{\beta\alpha\,\eta}(k',k) - L^{ABS}_{\beta\alpha\,\eta}(k',k) + G^{ABS}_{\beta\alpha\,\eta}(k',k) - L^{EM}_{\beta\alpha\,\eta}(k',k) \right\}. \tag{2.28}$$

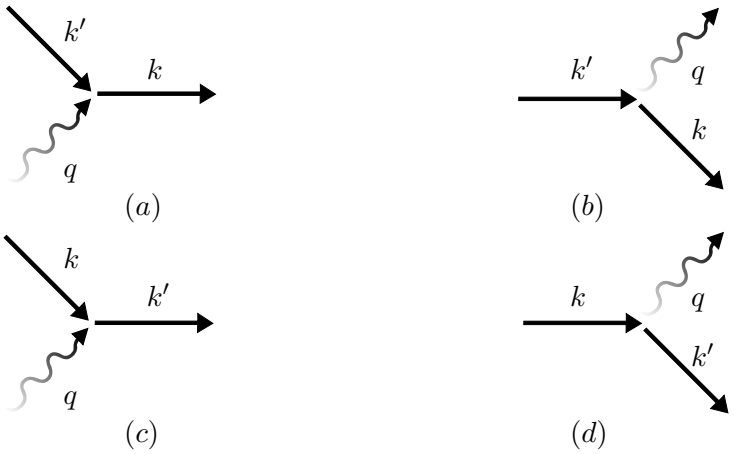

Figure 2.1: Illustration of gain and loss terms by absorption and emission of a phonon: gain by absorption (a), or emission (b) and loss by absorption (c), or emission (d)

This form is not suitable for our further investigations, but gives a good overview of the physical processes involved. If we, however, rearrange (2.23),

$$\begin{aligned} C^{\eta}_{\alpha\beta}(k) = \sum_{k'}\sum_{q} \big\{ & \delta(E_\beta(k') - E_\alpha(k) - W^\eta(q))\delta_{q,k'-k} \\ & \times s^{\eta}_{\alpha\beta}(k,k')\{[N^\eta(q)+1]\, f_\beta(k')\,[1-f_\alpha(k)] - N^\eta(q) f_\alpha(k)\left[1-f_\beta(k')\right]\} \\ & + \delta(E_\alpha(k) - E_\beta(k') - W^\eta(q))\delta_{q,k-k'} \\ & \times s^{\eta}_{\alpha\beta}(k,k')\{N^\eta(q) f_\beta(k')\,[1-f_\alpha(k)] - [N^\eta(q)+1]\, f_\alpha(k)\left[1-f_\beta(k')\right]\}\big\} \end{aligned} \tag{2.29}$$

and then sum over the phonon wave number q by evaluating the Kronecker delta, we

get:

$$C^{\eta}_{\alpha\beta}(k) = \sum_{k'} \big\{ \delta(E_\beta(k') - E_\alpha(k) - W^\eta(k'-k)) s^\eta_{\alpha\beta}(k',k) \\ \times \{[N^\eta(k'-k)+1] f_\beta(k')[1-f_\alpha(k)] - N^\eta(k'-k) f_\alpha(k)[1-f_\beta(k')]\} \\ + \delta(E_\alpha(k) - E_\beta(k') - W^\eta(k-k')) s^\eta_{\alpha\beta}(k,k') \\ \times \{N^\eta(k-k') f_\beta(k')[1-f_\alpha(k)] - [N^\eta(k-k')+1] f_\alpha(k)[1-f_\beta(k')]\}\big\}. \tag{2.30}$$

The first term in the sum represents scattering events that involve interactions with higher energies than the current state k under consideration, which is represented by $E_\beta(k') - E_\alpha(k) - W^\eta(k'-k)$. The second term accounts for scattering processes that involve lower energies $E_\alpha(k) - E_\beta(k') - W^\eta(k-k')$. Therefore, we can define symbols leading to a compact notation of the collision operator. The symbol "+" denotes higher and "−" lower energies than the current state k. For this purpose we define

$$q^{\pm}(k',k) = \pm(k'-k) \tag{2.31}$$

and the following statistic terms:

$$g^{+\,\eta}_{\beta\alpha}(k',k) = \left\{ \left[N^\eta(q^+)+1\right] f_\beta(k') \left[1-f_\alpha(k)\right] - N^\eta(q^+) f_\alpha(k) \left[1-f_\beta(k')\right] \right\}, \tag{2.32}$$

$$g^{-\,\eta}_{\beta\alpha}(k',k) = \left\{ N^\eta(q^-) f_\beta(k') \left[1-f_\alpha(k)\right] - \left[N^\eta(q^-)+1\right] f_\alpha(k) \left[1-f_\beta(k')\right] \right\}. \tag{2.33}$$

Furthermore, we introduce

$$H^{+\,\eta}_{\beta\alpha}(k',k) = E_\beta(k') - E_\alpha(k) - W^\eta(q^+), \tag{2.34}$$

$$H^{-\,\eta}_{\beta\alpha}(k',k) = E_\alpha(k) - E_\beta(k') - W^\eta(q^-) \tag{2.35}$$

expressing the energy dependences. By means of this abbreviations, the collision operator can be written as

$$C^{\eta}_{\alpha\beta}(k) = \sum_{k'} \left[\delta(H^{+\,\eta}_{\beta\alpha}(k',k)) s^\eta_{\alpha\beta}(k,k') g^{+\,\eta}_{\beta\alpha}(k',k) + \delta(H^{-\,\eta}_{\beta\alpha}(k',k)) s^\eta_{\alpha\beta}(k,k') g^{-\,\eta}_{\beta\alpha}(k',k) \right]. \tag{2.36}$$

We are dealing with a macroscopic system. Therefore, the k-states are very dense,

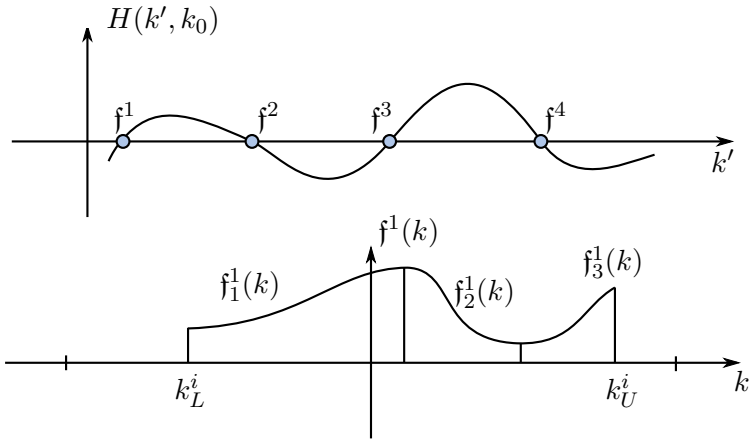

Figure 2.2: Illustration of finding the roots $k' = \mathfrak{f}^i(k)$ of $H(k', k)$ with respect to k' and the construction of bijective functions and the corresponding partition into subintervals.

which justifies our semi-classical approach of describing the charge carrier transport. Consequently, the sum over all k-states can be expressed as an integral over the first Brillouin zone:

$$\sum_k \to \frac{L}{2\pi} \int_{\mathcal{BZ}} dk, \tag{2.37}$$

where L denotes the spatial extension of our one-dimensional system. Using this transformation yields

$$C_{\alpha\beta}^{\eta}(k) = \frac{L}{2\pi} \int dk' \left[\delta(H_{\beta\alpha}^{+\,\eta}(k', k)) s_{\alpha\beta}^{\eta}(k, k') g_{\beta\alpha}^{+\,\eta}(k', k) + \delta(H_{\beta\alpha}^{-\,\eta}(k', k)) s_{\alpha\beta}^{\eta}(k, k') g_{\beta\alpha}^{-\,\eta}(k', k) \right]. \tag{2.38}$$

The integral in (2.38) over the Brillouin zone now needs to be evaluated. To that end, we need the relation

$$\int \delta\left(f(x)\right) g(x) dx = \sum_{x_0} \left. \frac{1}{|f'(x)|} \right|_{x=x_0} g(x_0) \tag{2.39}$$

with x_0 being the roots of the function $f(x)$. Furthermore, we start by considering the elementary expression

$$C(k) = \int \delta\left(H(k', k)\right) F(k', k) dk' \tag{2.40}$$

to understand the implications of the evaluating (2.38).

At a given $k = k_0$ we are searching for the roots of $H(k', k_0)$ with respect to k'. The

result is a set of $\mathfrak{f}^i$ roots, with $i \in \{1, \ldots, N\}$ as depicted in Figure 2.2. Remembering that k is not a fixed parameter, we see that each root defines implicitly the function $k' = \mathfrak{f}^i(k)$ within a certain interval $k \in (k^i_L, k^i_U)$. This function, as illustrated in Figure 2.2, is not necessarily bijective and we, therefore, partition it into N^i smaller subintervals and label the function within this interval by $k' = \mathfrak{f}^i_j(k) = \mathfrak{f}^i(k)$ for $k \in (k^i_{j\,L}, k^i_{j\,U})$.

During our previous calculations we have eliminated the phonon quasi momentum q by using (2.31). For the sake of argument, let us now consider $\mathfrak{g}^i_j(k) = \mathfrak{f}^i_j(k) + k$, corresponding to $q^+(k', k)$ in the first term of (2.38). Since for each subinterval this is still not necessarily a bijective function, we further split the N^i-th interval into N^i_j subintervals and use the notation $\mathfrak{f}^{i\,l}_j(k) = \mathfrak{f}^i_j(k)$ and $\mathfrak{g}^{i\,l}_j(k) = \mathfrak{f}^{i\,l}_j(k) - k$ for $k \in (k^{i\,l}_{j\,L}, k^{i\,l}_{j\,U})$.

Let us elaborate on this interim result. We have found a partition for $k \in (k^{i\,l}_{j\,L}, k^{i\,l}_{j\,U})$ and corresponding partitions for $k' \in (k'^{i\,l}_{j\,L}, k'^{i\,l}_{j\,U})$ and $q \in (q^{i\,l}_{j\,L}, q^{i\,l}_{j\,U})$. These partitions for k, k' and q as well as the corresponding bijective functions are not unique. They can, however, always be constructed for the given set of equations $H(k', k) = 0$ and $q = k' - k$, by using the rules outlined above, resulting in a total number of $\sum_{i=1}^{N} \sum_{j=1}^{N^i} N^i_j$ intervals and functions. Furthermore, we can define the function $k' = \mathfrak{h}^{i\,l}_j(q)$ as the function composition $\mathfrak{h}^{i\,l}_j = \mathfrak{f}^{i\,l}_j \mathfrak{g}^{-1\,i\,l}_j$.

Finally, we need to define a set of functions in order to extend $\mathfrak{f}^i(k)$, $\mathfrak{f}^i_j(k)$ and $\mathfrak{f}^{i\,l}_j(k)$ over the whole domain:

$$\chi^i(k) = \begin{cases} 1 & \forall k \in (k^i_L, k^i_U) \\ 0 & \text{otherwise} \end{cases}, \qquad \chi^i_j(k) = \begin{cases} 1 & \forall k \in (k^i_{j\,L}, k^i_{j\,U}) \\ 0 & \text{otherwise} \end{cases}, \tag{2.41}$$

$$\chi^{i\,l}_j(k) = \begin{cases} 1 & \forall k \in (k^{i\,l}_{j\,L}, k^{i\,l}_{j\,U}) \\ 0 & \text{otherwise} \end{cases}. \tag{2.42}$$

Consequently, we can write

$$C(k) = \sum_{i=1}^{N} \left(\sum_{j=1}^{N^i} \left(\sum_{l=1}^{N^i_j} \left(\frac{1}{|\partial_{k'} H(k', k)|} F(k', k) \right)_{k' = \mathfrak{f}^{i\,l}_j(k)} \chi^{i\,l}_j(k) \right) \chi^i_j(k) \right) \chi^i(k) \tag{2.43}$$

and since $\chi^{i\,l}_j(k) \chi^i_j(k) \chi^i(k) = \chi^{i\,l}_j(k)$ this turns into:

$$= \sum_{i=1}^{N} \sum_{j=1}^{N^i} \sum_{l=1}^{N^i_j} \left(\frac{1}{|\partial_{k'} H(k', k)|} F(k', k) \chi^{i\,l}_j(k) \right)_{k' = \mathfrak{f}^{i\,l}_j(k)}. \tag{2.44}$$

Now, we collect all bijective partitions into one sum by defining the sets

$$\mathfrak{f}^p(k) \in \{\mathfrak{f}_j^{i\,l}(k) | i \in \{1,\dots,N\} \wedge j \in \{1,\dots,N^i\} \wedge l \in \{1,\dots,N_j^i\}\}, \tag{2.45}$$

$$\mathfrak{g}^p(k) \in \{\mathfrak{g}_j^{i\,l}(k) | i \in \{1,\dots,N\} \wedge j \in \{1,\dots,N^i\} \wedge l \in \{1,\dots,N_j^i\}\}, \tag{2.46}$$

$$\mathfrak{h}^p(k) \in \{\mathfrak{h}_j^{i\,l}(k) | i \in \{1,\dots,N\} \wedge j \in \{1,\dots,N^i\} \wedge l \in \{1,\dots,N_j^i\}\}, \tag{2.47}$$

$$\chi^p \in \{\chi_j^{i\,l}(k) | i \in \{1,\dots,N\} \wedge j \in \{1,\dots,N^i\} \wedge l \in \{1,\dots,N_j^i\}\} \tag{2.48}$$

and the index set

$$I_p = \{1,\dots,N_{\text{total}}\} \qquad \text{with} \quad N_{\text{total}} = \sum_{i=1}^{N}\sum_{j=1}^{N^i} N_j^i. \tag{2.49}$$

Replacing the indices i, j and l with a single index $p \in I_p$ leads to

$$C(k) = \sum_{p=1}^{N_{\text{total}}} \left(\frac{1}{|\partial_{k'} H(k',k)|} F(k',k)\chi^p(k) \right)_{k'=\mathfrak{f}^p(k)}. \tag{2.50}$$

Consequently, we can apply the same analysis to evaluate (2.38). Doing so, leaves us with $N_{\beta\alpha}^{+\,\eta}$ bijective functions and corresponding intervals for k, k' and q:

$$H_{\beta\alpha}^{+\,\eta}\left(k' = \mathfrak{f}_{\beta\alpha\,p}^{+\,\eta}(k), k\right) = 0\,, \quad \mathfrak{g}_{\beta\alpha\,p}^{+\,\eta}(k) = q^+\left(\mathfrak{f}_{\beta\alpha\,p}^{+\,\eta}(k), k\right)\,, \quad \mathfrak{h}_{\beta\alpha\,p}^{+\,\eta} = \mathfrak{f}_{\beta\alpha\,p}^{+\,\eta}\mathfrak{g}_{\beta\alpha\,p}^{-1\,+\,\eta} \tag{2.51}$$

$$\Rightarrow \quad \left\{\mathfrak{f}_{\beta\alpha\,p}^{+\,\eta}(k)\right\}\,, \quad \left\{\mathfrak{g}_{\beta\alpha\,p}^{+\,\eta}(k)\right\}\,, \quad \left\{\mathfrak{h}_{\beta\alpha\,p}^{+\,\eta}(q)\right\} \text{ with } p = 1,\dots,N_{\beta\alpha}^{+\,\eta}, \tag{2.52}$$

where

$$\mathfrak{f}_{\beta\alpha\,p}^{+\,\eta}(k) : k \to k' \text{ with} \quad k \in (k_{\beta\alpha\,p\,L}^{+\,\eta}, k_{\beta\alpha\,p\,U}^{+\,\eta}), \tag{2.53}$$

$$\mathfrak{g}_{\beta\alpha\,p}^{+\,\eta}(k) : k \to q \text{ with} \quad k \in (k_{\beta\alpha\,p\,L}^{+\,\eta}, k_{\beta\alpha\,p\,U}^{+\,\eta}), \tag{2.54}$$

$$\mathfrak{h}_{\beta\alpha\,p}^{+\,\eta}(q) : q \to k' \text{ with} \quad q \in (q_{\beta\alpha\,p\,L}^{+\,\eta}, q_{\beta\alpha\,p\,U}^{+\,\eta}), \tag{2.55}$$

and

$$k' \in (k_{\beta\alpha\,p\,L}^{\prime\,+\,\eta} = \mathfrak{f}_{\beta\alpha\,p}^{+\,\eta}(k_{\beta\alpha\,p\,L}^{+\,\eta}), k_{\beta\alpha\,p\,U}^{\prime\,+\,\eta} = \mathfrak{f}_{\beta\alpha\,p}^{+\,\eta}(k_{\beta\alpha\,p\,U}^{+\,\eta})), \tag{2.56}$$

$$q \in (q_{\beta\alpha\,p\,L}^{+\,\eta} = \mathfrak{g}_{\beta\alpha\,p}^{+\,\eta}(k_{\beta\alpha\,p\,L}^{+\,\eta}), q_{\beta\alpha\,p\,U}^{+\,\eta} = \mathfrak{g}_{\beta\alpha\,p}^{+\,\eta}(k_{\beta\alpha\,p\,U}^{+\,\eta})). \tag{2.57}$$

Repeating this procedure for $H^{-\,\eta}_{\beta\alpha}(k',k)$ leads to

$$H^{-\,\eta}_{\beta\alpha}\left(\mathfrak{f}^{-\,\eta}_{\beta\alpha\,p}(k),k\right)=0 \quad \Rightarrow \quad \left\{\mathfrak{f}^{-\,\eta}_{\beta\alpha\,p}(k)\right\} \text{ with } p=1,\ldots,N^{-\,\eta}_{\beta\alpha}, \tag{2.58}$$

where

$$\mathfrak{f}^{-\,\eta}_{\beta\alpha\,p}(k): k\to k' \text{ with } \quad k\in(k^{-\,\eta}_{\beta\alpha\,p\,L},k^{-\,\eta}_{\beta\alpha\,p\,U}) \tag{2.59}$$

and

$$k'\in(k'^{-\,\eta}_{\beta\alpha\,p\,L}=\mathfrak{f}^{-\,\eta}_{\beta\alpha\,p}(k^{-\,\eta}_{\beta\alpha\,p\,L}),k'^{-\,\eta}_{\beta\alpha\,p\,U}=\mathfrak{f}^{-\,\eta}_{\beta\alpha\,p}(k^{-\,\eta}_{\beta\alpha\,p\,U})). \tag{2.60}$$

Furthermore, we introduce the functions $\chi^{+\,\eta}_{\beta\alpha\,p}$, $\chi^{-\,\eta}_{\beta\alpha\,p}$, $\chi'^{+\,\eta}_{\beta\alpha\,p}$, $\chi'^{-\,\eta}_{\beta\alpha\,p}$ and $\phi^{+\,\eta}_{\beta\alpha\,p}$ defined by

$$\chi^{+\,\eta}_{\beta\alpha\,p}(k)=\begin{cases}1 & \forall k\in(k^{+\,\eta}_{\beta\alpha\,p\,L},k^{+\,\eta}_{\beta\alpha\,p\,U})\\ 0 & \text{otherwise}\end{cases}, \qquad \chi^{-\,\eta}_{\beta\alpha\,p}(k)=\begin{cases}1 & \forall k\in(k^{-\,\eta}_{\beta\alpha\,p\,L},k^{-\,\eta}_{\beta\alpha\,p\,U})\\ 0 & \text{otherwise}\end{cases}, \tag{2.61}$$

$$\chi'^{+\,\eta}_{\beta\alpha\,p}(k')=\begin{cases}1 & \forall k'\in(k'^{+\,\eta}_{\beta\alpha\,p\,L},k'^{+\,\eta}_{\beta\alpha\,p\,U})\\ 0 & \text{otherwise}\end{cases}, \qquad \chi'^{-\,\eta}_{\beta\alpha\,p}(k')=\begin{cases}1 & \forall k'\in(k'^{-\,\eta}_{\beta\alpha\,p\,L},k'^{-\,\eta}_{\beta\alpha\,p\,U})\\ 0 & \text{otherwise}\end{cases}, \tag{2.62}$$

$$\phi^{+\,\eta}_{\beta\alpha\,p}(q)=\begin{cases}1 & \forall q\in(q^{+\,\eta}_{\beta\alpha\,p\,L},q^{+\,\eta}_{\beta\alpha\,p\,U}).\\ 0 & \text{otherwise}\end{cases}. \tag{2.63}$$

It is usually sufficient to determine the distribution functions within a small region of the Brillouin zone. Therefore, we need to limit the collision operator in a way, so that electrons are not scattered out of the physical domain of interest. This can be done by choosing the intervals $(k^{+\,\eta}_{\beta\alpha\,p\,L},k^{+\,\eta}_{\beta\alpha\,p\,U})$ and $(k^{-\,\eta}_{\beta\alpha\,p\,L},k^{-\,\eta}_{\beta\alpha\,p\,U})$ accordingly. Of course, this implies that outside these interval scattering rates need to be sufficiently small as to be neglected. Otherwise this would yield unphysical solutions.

Consequently, we can define $C^{+\,\eta}_{\alpha\beta}(k)$ as a sum of collision operators each representing

one bijective partition p. The final general representation reads

$$C_{\alpha\beta}^{+\,\eta\,p}(k) = \frac{L}{2\pi}\left(\left|\frac{\partial H_{\beta\alpha}^{+\,\eta}(k',k)}{\partial k'}\right|^{-1} \chi_{\beta\alpha\,p}^{+\,\eta}(k) s_{\alpha\beta}^{\eta}(k,k') g_{\beta\alpha}^{+\,\eta}(k',k)\right)_{k'=\mathfrak{f}_{\beta\alpha\,p}^{+\,\eta}(k),\,k=k}, \quad (2.64)$$

$$C_{\alpha\beta}^{-\,\eta\,p}(k) = \frac{L}{2\pi}\left(\left|\frac{\partial H_{\beta\alpha}^{-\,\eta}(k',k)}{\partial k'}\right|^{-1} \chi_{\beta\alpha\,p}^{-\,\eta}(k) s_{\alpha\beta}^{\eta}(k,k') g_{\beta\alpha}^{-\,\eta}(k',k)\right)_{k'=\mathfrak{f}_{\beta\alpha\,p}^{-\,\eta}(k),\,k=k}, \quad (2.65)$$

$$C_{\alpha\beta}^{+\,\eta}(k) = \sum_{p=1}^{N_{\beta\alpha}^{+\,\eta}} C_{\alpha\beta}^{+\,\eta\,p}(k), \quad (2.66)$$

$$C_{\alpha\beta}^{-\,\eta}(k) = \sum_{p=1}^{N_{\beta\alpha}^{-\,\eta}} C_{\alpha\beta}^{-\,\eta\,p}(k), \quad (2.67)$$

$$C_{\alpha\beta}^{\eta}(k) = \left[C_{\alpha\beta}^{+\,\eta}(k) + C_{\alpha\beta}^{-\,\eta}(k)\right], \quad (2.68)$$

where $q^{\pm} = q^{\pm}(k',k) = \pm(k'-k)$ denotes the phonon quasi momentum. Inserting our result back into (2.16), the total collision operator now reads:

$$\left.\frac{\partial f_\alpha(k)}{\partial t}\right|_{Coll} = C_\alpha(k) = \sum_\eta \sum_\beta \left[C_{\alpha\beta}^{+\,\eta}(k) + C_{\alpha\beta}^{-\,\eta}(k)\right]. \quad (2.69)$$

2.3 Phonon Collision Operator

The time evolution of the phonon distribution function is given by

$$\frac{\partial N^\eta(x,q,t)}{\partial t} + v_\eta(q)\frac{\partial N^\eta(x,q,t)}{\partial x} = \left.\frac{\partial N^\eta(x,q,t)}{\partial t}\right|_{Coll} \quad (2.70)$$

where N^η is the distribution function of the phonons of band η and q denotes the quasi momentum of the phonons. The group velocity of the phonons is determined by $v_\eta(q) = \partial_q W_\eta(q)/\hbar$, where $W_\eta(q)$ stands for the dispersion relation of band η. There is no force acting on the phonons, as they are uncharged particles, and, therefore, move freely through the device. The collision term can be written as

$$\left.\frac{\partial N^\eta(x,q,t)}{\partial t}\right|_{Coll} = C_{e,ph}(x,q,t) + C_{ph,ph}(x,q,t), \quad (2.71)$$

where $C_{e,ph}$ describes the interaction of phonons with electrons and $C_{ph,ph}$ represents the phonon-phonon interaction, which can be expressed by the relaxation time approxi-

mation [18]

$$C_{ph,ph}(x,q,t) = -\frac{1}{\tau_{rel}^{\eta}}\left[N^{\eta}(x,q,t) - \tilde{N}^{\eta}(q)\right] \tag{2.72}$$

with τ_{rel}^{η} being the relaxation time and $\tilde{N}^{\eta}(q)$ the equilibrium distribution function of the phonon system η at system temperature T. The electron-phonon collision operator is the sum of all interactions $C_{\eta}^{\alpha\beta}$, each involving two electron bands(α,β) and one phonon band(η):

$$C_{e,ph}(q) = \sum_{\alpha}\sum_{\beta} C_{\eta}^{\alpha\beta}(q). \tag{2.73}$$

The position and time variables are again dropped due to the local and instantaneous nature of scattering events. Following [19], a general form of the electron-phonon collision operator reads

$$C_{\eta}^{\alpha\beta}(q) = \left\{W_{\eta\,\beta\alpha}^{EM}(q)\left[1 + N^{\eta}(q)\right] - W_{\eta\,\alpha\beta}^{ABS}(q)N^{\eta}(q)\right\} \tag{2.74}$$

with $W_{\eta\,\beta\alpha}^{EM}$ being the emission probability which is also the gain term and $W_{\eta\,\alpha\beta}^{ABS}$ the absorption probability or loss term. Both can be further expressed as

$$W_{\eta\,\beta\alpha}^{EM}(q) = \sum_{k_1}\sum_{k_2} s_{\alpha\beta}^{\eta}(k_1,k_2) f_{\beta}(k_2)\left[1 - f_{\alpha}(k_1)\right]\delta(E_{\beta}(k_2) - E_{\alpha}(k_1) - W^{\eta}(q))\delta_{k_1+q,k_2}, \tag{2.75}$$

$$W_{\eta\,\alpha\beta}^{ABS}(q) = \sum_{k_1}\sum_{k_2} s_{\alpha\beta}^{\eta}(k_1,k_2) f_{\alpha}(k_1)\left[1 - f_{\beta}(k_2)\right]\delta(E_{\beta}(k_2) - E_{\alpha}(k_1) - W^{\eta}(q))\delta_{k_1+q,k_2}. \tag{2.76}$$

Comparing (2.75) and (2.76) to (2.19) and (2.20) reveals that

$$\sum_{q} W_{\eta\,\beta\alpha}^{EM}(q)\left[N^{\eta}(q) + 1\right] = \sum_{k_1}\sum_{k_2} W_{\beta\alpha\,\eta}^{EM}(k_2,k_1) f_{\beta}(k_2)\left[1 - f_{\alpha}(k_1)\right], \tag{2.77}$$

$$\sum_{q} W_{\eta\,\alpha\beta}^{ABS}(q)N^{\eta}(q) = \sum_{k_1}\sum_{k_2} W_{\alpha\beta\,\eta}^{ABS}(k_1,k_2) f_{\alpha}(k_1)\left[1 - f_{\beta}(k_2)\right]. \tag{2.78}$$

By using our previously introduced notation we obtain

$$C_\eta^{\alpha\beta}(q) = \sum_k \sum_{k'} \delta(E_\beta(k') - E_\alpha(k) - W^\eta(q))\delta_{k',k+q} \times s_{\alpha\beta}^\eta(k,k')\{[N^\eta(q)+1]f_\beta(k')[1-f_\alpha(k)] - N^\eta(q)f_\alpha(k)[1-f_\beta(k')]\} \tag{2.79}$$

$$= \sum_k \sum_{k'} \delta(H_{\beta\alpha}^{+\,\eta}(k',k))\ \delta_{k',k+q} s_{\alpha\beta}^\eta(k,k') g_{\beta\alpha}^{+\,\eta}(k',k). \tag{2.80}$$

We can now further analyze this result, starting by evaluating the sum over k:

$$C_\eta^{\alpha\beta}(q) = \sum_{k'} \left(\delta(H_{\beta\alpha}^{+\,\eta}(k',k)) s_{\alpha\beta}^\eta(k,k') g_{\beta\alpha}^{+\,\eta}(k',k)\right)_{k=k'-q}. \tag{2.81}$$

Again using (2.1), we turn the sum into an integral resulting in

$$C_\eta^{\alpha\beta}(q) = \frac{L}{2\pi} \int_{\mathcal{BZ}} \left(\delta(H_{\beta\alpha}^{+\,\eta}(k',k)) s_{\alpha\beta}^\eta(k,k') g_{\beta\alpha}^{+\,\eta}(k',k)\right)_{k=k'-q} dk' \tag{2.82}$$

Finally, we integrate using (2.51) (2.52) (2.54) (2.55) and (2.63), leading us to the final representation

$$C_\eta^{\alpha\beta}(q) = \sum_{p=1}^{N_{\beta\alpha}^{+\,\eta}} C_\eta^{\alpha\beta\,p}(q), \tag{2.83}$$

with

$$C_\eta^{\alpha\beta\,p}(q) = \frac{L}{2\pi} \left(\left| \frac{\partial H_{\beta\alpha}^{+\,\eta}(k',k'-q)}{\partial k'} \right|^{-1} \phi_{\beta\alpha\,p}^{+\,\eta}(q) s_{\alpha\beta}^\eta(k,k') g_{\beta\alpha}^{+\,\eta}\left(k',k\right) \right)_{k'=\mathfrak{h}_{\beta\alpha\,p}^{+\,\eta}(q),\, k=\mathfrak{g}_{\beta\alpha\,p}^{-1\,+\,\eta}(q)}. \tag{2.84}$$

2.4 Collision operator in thermal equilibrium

In thermal equilibrium the collision operators $C_{\alpha\beta}^\eta(k)$ vanish for all k, due to the structure of the statistic terms $g_{\beta\alpha}^{+\,\eta}(k',k)$ and $g_{\beta\alpha}^{-\,\eta}(k',k)$ and the equilibrium distribution functions. For phonons (N^η) and electrons (f_α and f_β) they are given by the Bose-Einstein (phonons) and Fermi-Dirac (electrons) distribution, respectively. The Fermi-Dirac dis-

tribution function is defined as

$$\tilde{f}(k) = \frac{1}{\exp(\frac{E(k)-\mu}{k_B T}) + 1}, \tag{2.85}$$

where $E(k)$ is the electron dispersion relation, μ is the chemical potential, k_B the Boltzmann constant and T the temperature of the system under investigation. The Bose-Einstein distribution function is given by

$$\tilde{N}(q) = \frac{1}{\exp(\frac{W(q)}{k_B T}) - 1} \tag{2.86}$$

with $W(q)$ being the phonon dispersion relation.

We will now proof that $C^{+\,\eta}_{\beta\alpha}(k)$ vanishes for an arbitrary partition p, $k' = \mathfrak{f}^{+\,\eta}_{\beta\alpha\,i}(k)$ of $H^{+\,\eta}_{\beta\alpha}(k', k)$:

$$E_\beta(\mathfrak{f}^{+\,\eta}_{\beta\alpha\,p}(k)) - E_\alpha(k) - W^\eta(\mathfrak{f}^{+\,\eta}_{\beta\alpha\,p}(k) - k) = 0. \tag{2.87}$$

We will continue to use the symbol k' instead of $\mathfrak{f}^{+\,\eta}_{\beta\alpha\,p}(k)$ for the sake of a compact notation, bearing in mind that k' is now an dependent variable of k. Rewriting consequently yields:

$$E_\beta(k') = W^\eta(k' - k) + E_\alpha(k). \tag{2.88}$$

As stated before the statistics term, which is given by (2.32), must vanish:

$$[N^\eta(k' - k) + 1] f_\beta(k')[1 - f_\alpha(k)] - N^\eta(k' - k) f_\alpha(k)[1 - f_\beta(k')] \stackrel{!}{=} 0 \tag{2.89}$$

One can now search for distribution functions f and N satisfying this condition which would lead to the already mentioned equilibrium functions. For our purpose it suffices to show that the collision operator vanishes in thermal equilibrium. Therefore, we rearrange (2.89)

$$[N^\eta(k' - k) + 1] f_\beta(k')[1 - f_\alpha(k)] = N^\eta(k' - k) f_\alpha(k)[1 - f_\beta(k')] \tag{2.90}$$

and then insert the equilibrium electron and phonon distribution functions:

$$\frac{f_\alpha(k)}{1 - f_\alpha(k)} = \frac{N^\eta(k' - k) + 1}{N^\eta(k' - k)} \frac{f_\beta(k')}{1 - f_\beta(k')}. \tag{2.91}$$

First, we evaluate the left hand side of this equation:

$$\begin{aligned}\frac{f_\alpha(k)}{1-f_\alpha(k)} &= \left(\frac{1}{\exp\left(\frac{E_\alpha(k)-\mu}{k_BT}\right)+1}\right)\left(1-\frac{1}{\exp\left(\frac{E_\alpha(k)-\mu}{k_BT}\right)+1}\right)^{-1}, \\ &= \frac{1}{\exp\left(\frac{E_\alpha(k)-\mu}{k_BT}\right)}. \end{aligned} \tag{2.92}$$

Similar considerations by taking into account (2.88) lead to

$$\begin{aligned}\frac{f_\beta(k')}{1-f_\beta(k')} &= \frac{1}{\exp\left(\frac{E_\beta(k')-\mu}{k_BT}\right)}, \\ &= \frac{1}{\exp\left(\frac{E_\alpha(k)+W^\eta(k'-k)-\mu}{k_BT}\right)}, \end{aligned} \tag{2.93}$$

Subsequently, we evaluate the expression dependent on the phonon distribution:

$$\begin{aligned}\frac{N^\eta(k'-k)+1}{N^\eta(k'-k)} &= \left(\frac{1}{\exp\left(\frac{W^\eta(k'-k)}{k_BT}\right)-1}+1\right)\left(\frac{1}{\exp\left(\frac{W^\eta(k'-k)}{k_BT}\right)-1}\right)^{-1}, \\ &= \exp\left(\frac{W^\eta(k'-k)}{k_BT}\right). \end{aligned} \tag{2.94}$$

Finally, we insert (2.92) (2.93) and (2.94) into (2.91)

$$\frac{1}{\exp\left(\frac{E_\alpha(k)-\mu}{k_BT}\right)} = \frac{\exp\left(\frac{W^\eta(k'-k)}{k_BT}\right)}{1}\frac{1}{\exp(\frac{E_\alpha(k)+W^\eta(k'-k)-\mu}{k_BT})} \tag{2.95}$$

and after canceling we obtain

$$\frac{1}{\exp\left(\frac{E_\alpha(k)-\mu}{k_BT}\right)} = \frac{1}{\exp\left(\frac{E_\alpha(k)-\mu}{k_BT}\right)}. \tag{2.96}$$

which proves that the collision operator vanishes.

2.5 Conservation laws

Since our transport model is now complete, we need to check if all conservation laws still hold. First, we will concentrate on the conservation of the electron number and

thereafter verify that energy and quasi momentum conservation are still valid within our system of equations.

2.5.1 Conservation of electron number

A very important property of electron-phonon scattering events is the conservation of the electron number, since no electron is created or destroyed. Note, however, that this is not true for phonons , since a phonon is absorbed or emitted in this process. After formulating the main transport equations, we need to check if the property of electron conservation holds. The total electron density is given by (2.2) and (2.3):

$$\mathcal{N}(x,t) = \frac{1}{2\pi}\sum_{\alpha}\int_{\mathcal{BZ}} f_\alpha(x,k,t)dk.$$

The quantity $\mathcal{N}(x,t)$ must be constant under collisions, which means that the time derivative needs to vanish:

$$\left.\frac{\partial \mathcal{N}}{\partial t}\right|_{Coll} = \frac{1}{2\pi}\sum_{\alpha}\frac{\partial}{\partial t}\int_{\mathcal{BZ}} f_\alpha(x,k,t)dk = \frac{1}{2\pi}\sum_{\alpha}\int_{\mathcal{BZ}}\left.\frac{\partial f_\alpha(x,k,t)}{\partial t}\right|_{Coll} dk = 0. \quad (2.97)$$

Since collisions are local and instantaneous events, we can neglect the x and t dependence, because the condition needs to be satisfied independently of x for all times t. In the second step, we exchanged the differential and the integral operation. Now, we insert the collision operator, (2.69), into (2.97) and get

$$\begin{aligned}
\left.\frac{\partial \mathcal{N}}{\partial t}\right|_{Coll} &= \frac{1}{2\pi}\sum_{\alpha}\sum_{\beta}\sum_{\eta}\int_{\mathcal{BZ}}\left[C^{+\,\eta}_{\alpha\beta}(k) + C^{-\,\eta}_{\alpha\beta}(k)\right]dk, && (2.98)\\
&= \frac{1}{2\pi}\sum_{\eta}\sum_{\alpha}\sum_{\beta}\int_{\mathcal{BZ}} C^{+\,\eta}_{\alpha\beta}(k)dk + \frac{1}{2\pi}\sum_{\eta}\sum_{\beta}\sum_{\alpha}\int_{\mathcal{BZ}} C^{-\,\eta}_{\beta\alpha}(k)dk, && (2.99)\\
&= \frac{1}{2\pi}\sum_{\eta}\sum_{\alpha}\sum_{\beta}\int_{\mathcal{BZ}} C^{+\,\eta}_{\alpha\beta}(k)dk + \frac{1}{2\pi}\sum_{\eta}\sum_{\alpha}\sum_{\beta}\int_{\mathcal{BZ}} C^{-\,\eta}_{\alpha\beta}(k)dk, && (2.100)\\
&= \frac{1}{2\pi}\sum_{\alpha}\sum_{\beta}\sum_{\eta}\int_{\mathcal{BZ}}\left[C^{+\,\eta}_{\alpha\beta}(k) + C^{-\,\eta}_{\beta\alpha}(k)\right]dk = 0. && (2.101)
\end{aligned}$$

We will now show that each term in (2.101) vanishes independently. To that end, we split the integral and rename the integration variable k for the second term:

$$\int_{\mathcal{BZ}} \left[C^{+\,\eta}_{\alpha\beta}(k) + C^{-\,\eta}_{\beta\alpha}(k) \right] dk = 0 \tag{2.102}$$

$$\int_{\mathcal{BZ}} C^{+\,\eta}_{\alpha\beta}(k) dk + \int_{\mathcal{BZ}} C^{-\,\eta}_{\beta\alpha}(k') dk' = 0 \tag{2.103}$$

Equation (2.34) transforms into (2.35) if we swap α for β and k for k':

$$H^{+\,\eta}_{\beta\alpha}(k', k) = H^{-\,\eta}_{\alpha\beta}(k, k') = E_\beta(k') - E_\alpha(k) - W^\eta(k' - k) = 0. \tag{2.104}$$

This is also true for the quasi momenta (2.31):

$$q^+(k', k) = q^-(k, k') = k' - k. \tag{2.105}$$

Therefore, we use (2.34), (2.35), (2.51), (2.52), (2.58) and by choosing the a certain partition into subintervals for (2.53) and a corresponding one for (2.59) to construct bijective functions we see:

$$H^{+\,\eta}_{\beta\alpha}(k' = \mathfrak{f}^{+\,\eta}_{\beta\alpha\,p}(k), k) = E_\beta(\mathfrak{f}^{+\,\eta}_{\beta\alpha\,p}(k)) - E_\alpha(k) - W^\eta(\mathfrak{f}^{+\,\eta}_{\beta\alpha\,p}(k) - k), \tag{2.106}$$

$$H^{-\,\eta}_{\alpha\beta}(k, k' = \mathfrak{f}^{-1\,-\,\eta}_{\alpha\beta\,p}(k)) = E_\beta(\mathfrak{f}^{-1\,-\,\eta}_{\alpha\beta\,p}(k)) - E_\alpha(k) - W^\eta(\mathfrak{f}^{-1\,-\,\eta}_{\alpha\beta\,p}(k) - k) \tag{2.107}$$

By comparing (2.106) to (2.107) we conclude that

$$k' = \mathfrak{f}^{+\,\eta}_{\beta\alpha\,p}(k) = \mathfrak{f}^{-1\,-\,\eta}_{\alpha\beta\,p}(k), \tag{2.108}$$

and also

$$k = \mathfrak{f}^{-\,\eta}_{\alpha\beta\,p}(k') = \mathfrak{f}^{-1\,+\,\eta}_{\beta\alpha\,p}(k'). \tag{2.109}$$

We use corresponding intervals for $\mathfrak{f}^{+\,\eta}_{\beta\alpha\,p}(k)$ and $\mathfrak{f}^{-\,\eta}_{\alpha\beta\,p}(k')$ and, therefore,

$$N^{-\,\eta}_{\alpha\beta} = N^{+\,\eta}_{\beta\alpha}. \tag{2.110}$$

Furthermore, the limits of the intervals need to coincide:

$$k^{+\,\eta}_{\beta\alpha\,p\,L} = k^{-\,\eta}_{\alpha\beta\,p\,L}, \qquad k^{+\,\eta}_{\beta\alpha\,p\,U} = k^{-\,\eta}_{\alpha\beta\,p\,U}, \tag{2.111}$$

$$k'^{+\,\eta}_{\beta\alpha\,p\,L} = k'^{-\,\eta}_{\alpha\beta\,p\,L}, \qquad k'^{+\,\eta}_{\beta\alpha\,p\,U} = k'^{-\,\eta}_{\alpha\beta\,p\,U}, \tag{2.112}$$

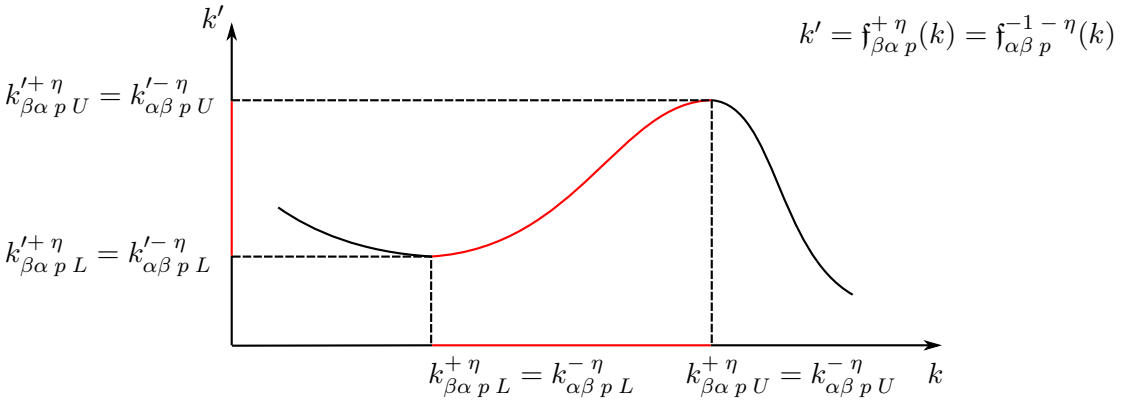

Figure 2.3: Illustration of one interval and its limits for which $\mathfrak{f}^{+\,\eta}_{\beta\alpha\,p}(k) = \mathfrak{f}^{-1\,-\,\eta}_{\alpha\beta\,p}(k)$

which is illustrated in Figure 2.3.

Since $H^{+\,\eta}_{\beta\alpha}(k', k)$ and $H^{-\,\eta}_{\alpha\beta}(k, k')$, are equal we conclude that

$$\frac{\partial H^{-\,\eta}_{\alpha\beta}(k, k')}{\partial k} = \frac{\partial H^{+\,\eta}_{\beta\alpha}(k', k)}{\partial k}. \tag{2.113}$$

If we then compare (2.32) to (2.33), we notice that the relation

$$g^{+\,\eta}_{\beta\alpha}(k', k) = -g^{-\,\eta}_{\alpha\beta}(k, k') \tag{2.114}$$

holds. We can now evaluate the second integral by using (2.65), (2.67) (2.104), (2.105),

(2.110),(2.109), (2.113), (2.114) and the symmetry of the matrix element $s^{\eta}_{\alpha\beta}$

$$\int_{\mathcal{BZ}} C^{-\,\eta}_{\beta\alpha}(k')dk' = \sum_{p=1}^{N^{-\,\eta}_{\alpha\beta}} \int_{\mathcal{BZ}} C^{-\,\eta\,p}_{\beta\alpha}(k')dk' \tag{2.115}$$

$$= \sum_{p=1}^{N^{-\,\eta}_{\alpha\beta}} \int_{\mathcal{BZ}} \frac{L}{2\pi} \left(\frac{1}{\left| \frac{\partial H^{-\,\eta}_{\alpha\beta}(k,k')}{\partial k} \right|} \chi'^{-\,\eta}_{\alpha\beta\,p}(k') s^{\eta}_{\alpha\beta}(k,k') g^{-\,\eta}_{\alpha\beta}(k,k') \right) dk', \quad k=\mathfrak{f}^{-\,\eta}_{\alpha\beta\,p}(k'),\, k'=k' \tag{2.116}$$

$$= \frac{L}{2\pi} \sum_{p=1}^{N^{-\,\eta}_{\alpha\beta}} \int_{k^{\prime-\,\eta}_{\alpha\beta\,p\,L}}^{k^{\prime-\,\eta}_{\alpha\beta\,p\,U}} \left(\frac{1}{\left| \frac{\partial H^{-\,\eta}_{\alpha\beta}(k,k')}{\partial k} \right|} s^{\eta}_{\alpha\beta}(k,k') g^{-\,\eta}_{\alpha\beta}(k,k') \right) dk', \quad k=\mathfrak{f}^{-1\,+\,\eta}_{\beta\alpha\,p}(k'),\, k'=k' \tag{2.117}$$

$$= -\frac{L}{2\pi} \sum_{p=1}^{N^{+\,\eta}_{\beta\alpha}} \int_{k^{\prime+\,\eta}_{\beta\alpha\,p\,L}}^{k^{\prime+\,\eta}_{\beta\alpha\,p\,U}} \left(\frac{1}{\left| \frac{\partial H^{+\,\eta}_{\beta\alpha}(k',k)}{\partial k} \right|} s^{\eta}_{\alpha\beta}(k,k') g^{+\,\eta}_{\beta\alpha}(k',k) \right) dk'. \quad k'=k',\, k=\mathfrak{f}^{-1\,+\,\eta}_{\beta\alpha\,p}(k') \tag{2.118}$$

For every p-th interval of $k \in (k^{+\,\eta}_{\beta\alpha\,p\,L}, k^{+\,\eta}_{\beta\alpha\,p\,U})$ and $k' \in (k^{\prime+\,\eta}_{\beta\alpha\,p\,L}, k^{\prime+\,\eta}_{\beta\alpha\,p\,U})$ we know that (2.34)

$$H^{+\,\eta}_{\beta\alpha}(k',k) = E_{\beta}(k') - E_{\alpha}(k) - W^{\eta}(k'-k) = 0 \tag{2.119}$$

is an implicit definition of $k' = \mathfrak{f}^{+\,\eta}_{\beta\alpha\,p}(k)$ or $k = \mathfrak{f}^{-1+\,\eta}_{\beta\alpha\,p}(k')$. Applying the rules for differentiation of implicit functions we get

$$\frac{\partial H^{+\,\eta}_{\beta\alpha}(k',k)}{\partial k'} \frac{dk'}{dk} + \frac{\partial H^{+\,\eta}_{\beta\alpha}(k',k)}{\partial k} = 0, \tag{2.120}$$

which we can transform into

$$\frac{dk'}{dk} = -\left(\frac{\frac{\partial H^{+\,\eta}_{\beta\alpha}(k',k)}{\partial k}}{\frac{\partial H^{+\,\eta}_{\beta\alpha}(k',k)}{\partial k'}} \right)_{k'=\mathfrak{f}^{+\,\eta}_{\beta\alpha\,p}(k)}. \tag{2.121}$$

Consequently, we can express the total derivative dk' as

$$dk' = \left| \frac{dk'}{dk} \right| dk \tag{2.122}$$

with dk'/dk in (2.121) being the Jacobian of the coordinate transformation.

Finally, we perform a variable transformation $k' \to k$ by using (2.121) and (2.122)

$$\int_{\mathcal{BZ}} C^{-\,\eta}_{\beta\alpha}(k')dk' =$$

$$= -\frac{L}{2\pi}\sum_{p=1}^{N^{+\,\eta}_{\beta\alpha}} \int_{\mathfrak{f}^{-1\,+\,\eta}_{\beta\alpha\;p}(k'^{+\,\eta}_{\beta\alpha\;p\;L})}^{\mathfrak{f}^{-1\,+\,\eta}_{\beta\alpha\;p}(k'^{+\,\eta}_{\beta\alpha\;p\;U})} \left(\left(\frac{1}{\left|\frac{\partial H^{+\,\eta}_{\beta\alpha}(k',k)}{\partial k}\right|} s^{\eta}_{\alpha\beta}(k,k') g^{+\,\eta}_{\beta\alpha}(k',k) \right)_{k'=k',\, k=\mathfrak{f}^{-1\,+\,\eta}_{\beta\alpha\;p}(k')} \right) \left|\frac{dk'}{dk}\right| dk \Bigg|_{k'=\mathfrak{f}^{+\,\eta}_{\beta\alpha\;p}(k)} \tag{2.123}$$

$$= -\frac{L}{2\pi}\sum_{p=1}^{N^{+\,\eta}_{\beta\alpha}} \int_{k^{+\,\eta}_{\beta\alpha\;p\;L}}^{k^{+\,\eta}_{\beta\alpha\;p\;U}} \left(\frac{1}{\left|\frac{\partial H^{+\,\eta}_{\beta\alpha}(k',k)}{\partial k}\right|} s^{\eta}_{\alpha\beta}(k,k') g^{+\,\eta}_{\beta\alpha}(k',k) \right) \left|\frac{dk'}{dk}\right| dk \Bigg|_{k'=\mathfrak{f}^{+\,\eta}_{\beta\alpha\;p}(k),\, k=\mathfrak{f}^{-1\,+\,\eta}_{\beta\alpha\;p}(\mathfrak{f}^{+\,\eta}_{\beta\alpha\;p}(k))} \tag{2.124}$$

$$= -\frac{L}{2\pi}\sum_{p=1}^{N^{+\,\eta}_{\beta\alpha}} \int_{\mathcal{BZ}} \left(\frac{1}{\left|\frac{\partial H^{+\,\eta}_{\beta\alpha}(k',k)}{\partial k}\right|} \chi^{+\,\eta}_{\beta\alpha\;p}(k) s^{\eta}_{\alpha\beta}(k,k') g^{+\,\eta}_{\beta\alpha}(k',k) \right)_{k'=\mathfrak{f}^{+\,\eta}_{\beta\alpha\;p}(k),\, k=k}$$

$$\times \left(\frac{\left|\frac{\partial H^{+\,\eta}_{\beta\alpha}(k',k)}{\partial k}\right|}{\left|\frac{\partial H^{+\,\eta}_{\beta\alpha}(k',k)}{\partial k'}\right|} \right)_{k'=\mathfrak{f}^{+\,\eta}_{\beta\alpha\;p}(k),\, k=k} dk, \tag{2.125}$$

$$= -\sum_{p=1}^{N^{+\,\eta}_{\beta\alpha}} \int_{\mathcal{BZ}} \frac{L}{2\pi} \left(\frac{1}{\left|\frac{\partial H^{+\,\eta}_{\beta\alpha}(k',k)}{\partial k'}\right|} \chi^{+\,\eta}_{\beta\alpha\;p}(k) s^{\eta}_{\alpha\beta}(k,k') g^{+\,\eta}_{\beta\alpha}(k',k) \right)_{k'=\mathfrak{f}^{+\,\eta}_{\beta\alpha\;p}(k),\, k=k} dk, \tag{2.126}$$

$$= -\sum_{p=1}^{N^{+\,\eta}_{\beta\alpha}} \int_{\mathcal{BZ}} C^{+\,\eta\;p}_{\alpha\beta}(k)dk, \tag{2.127}$$

where we have taken into account (2.64). By comparing (2.115) to (2.127) and remembering (2.110) we see that

$$\int_{\mathcal{BZ}} C^{+\,\eta\;p}_{\alpha\beta}(k)dk = -\int_{\mathcal{BZ}} C^{-\,\eta\;p}_{\beta\alpha}(k')dk'. \tag{2.128}$$

Inserting (2.66) and (2.115) into (2.103) yields

$$\sum_{p=1}^{N_{\beta\alpha}^{+\,\eta}} \int_{\mathcal{BZ}} C_{\alpha\beta}^{+\,\eta\,p}(k)dk + \sum_{p=1}^{N_{\alpha\beta}^{-\,\eta}} \int_{\mathcal{BZ}} C_{\beta\alpha}^{-\,\eta\,p}(k')dk' = 0. \tag{2.129}$$

We use (2.110) and interchange sum and integral to obtain

$$\sum_{p=1}^{N_{\beta\alpha}^{+\,\eta}} \left(\int_{\mathcal{BZ}} C_{\alpha\beta}^{+\,\eta\,p}(k)dk + \int_{\mathcal{BZ}} C_{\beta\alpha}^{-\,\eta\,p}(k')dk' \right) = 0. \tag{2.130}$$

This equation is fulfilled due to (2.128), which implies that the electron number is indeed conserved. This is a very important result for two reasons: First of all, it is a good indicator that our equations are correct. Second, we see that the collision integrals for each bijective partition cancel independently. Furthermore, we have shown that $\int_{\mathcal{BZ}} C_{\alpha\beta}^{+\,\eta\,p}(k)dk$ can be transformed into $-\int_{\mathcal{BZ}} C_{\beta\alpha}^{-\,\eta\,p}(k')dk'$ by the variable transformation $k \to k'$.

2.5.2 Conservation of energy and momentum

Now we will show that our model also conserves energy and momentum. Thus we will consider a generalized moment $\mathcal{M}$ defined in (2.14) by using the definitions (2.12) and (2.13):

$$\begin{aligned} \mathcal{M} &= \sum_{\alpha} \mathcal{M}_\alpha + \sum_{\eta} \mathcal{M}_\eta \\ &= \frac{1}{2\pi} \sum_{\alpha} \int_{\mathcal{BZ}} \Psi_\alpha(k) f_\alpha(k,t)dk + \frac{1}{2\pi} \sum_{\eta} \int_{\mathcal{BZ}} \Psi^\eta(q) N^\eta(q,t)dq. \end{aligned} \tag{2.131}$$

The sum is taken over all electron and phonon bands to get the total momentum. The moment $\mathcal{M}$ is a conserved quantity under collisions if its time derivative vanishes:

$$\left.\frac{\partial \mathcal{M}}{\partial t}\right|_{Coll} = 0. \tag{2.132}$$

If we insert (2.131) into (2.132) and interchange differentiation and integration we get

$$\frac{1}{2\pi} \sum_{\alpha} \int_{\mathcal{BZ}} \Psi_\alpha(k) \left.\frac{\partial f_\alpha}{\partial t}\right|_{Coll} dk + \frac{1}{2\pi} \sum_{\eta} \int_{\mathcal{BZ}} \Psi^\eta(q) \left.\frac{\partial N^\eta}{\partial t}\right|_{Coll} dq = 0. \tag{2.133}$$

The arbitrary function Ψ is assumed to have no time dependence. Consequently we can now insert the definitions of the collision operators (2.16), (2.68) and (2.71), (2.73) which leads to

$$\sum_{\alpha\beta\eta}\int_{\mathcal{BZ}}\Psi_\alpha(k)\left[C^{+\,\eta}_{\alpha\beta}(k)+C^{-\,\eta}_{\alpha\beta}(k)\right]dk+\sum_{\alpha\beta\eta}\int_{\mathcal{BZ}}\Psi^\eta(q)C^{\alpha\beta}_\eta(q)dq=0. \tag{2.134}$$

The phonon-phonon interaction $C_{ph,ph}(x,q,t)$ in (2.71) needs to be neglected in this case, since it violates the energy and momentum conservation. We then split up the first term, exchange α and β and rename the integration variable, as we did before in Section 2.5.1:

$$\sum_{\alpha\beta\eta}\int_{\mathcal{BZ}}\Psi_\alpha(k)C^{+\,\eta}_{\alpha\beta}(k)dk+\sum_{\alpha\beta\eta}\int_{\mathcal{BZ}}\Psi_\beta(k')C^{-\,\eta}_{\beta\alpha}(k')dk'+\sum_{\alpha\beta\eta}\int_{\mathcal{BZ}}\Psi^\eta(q)C^{\alpha\beta}_\eta(q)dq=0. \tag{2.135}$$

Again combining the three sums yields

$$\sum_{\alpha\beta\eta}\Bigg[\underbrace{\int_{\mathcal{BZ}}\Psi_\alpha(k)C^{+\,\eta}_{\alpha\beta}(k)dk}_{I}+\underbrace{\int_{\mathcal{BZ}}\Psi_\beta(k')C^{-\,\eta}_{\beta\alpha}(k')dk'}_{II}+\underbrace{\int_{\mathcal{BZ}}\Psi^\eta(q)C^{\alpha\beta}_\eta(q)dq}_{III}\Bigg]=0. \tag{2.136}$$

Now, we evaluate each integral separately. From (2.66) and (2.127) we obtain

$$I:\quad\sum_{i=1}^{N^{+\,\eta}_{\beta\alpha}}\int_{\mathcal{BZ}}\Psi_\alpha(k)C^{+\,\eta\,p}_{\alpha\beta}(k)dk, \tag{2.137}$$

$$II:\quad-\sum_{i=1}^{N^{+\,\eta}_{\beta\alpha}}\int_{\mathcal{BZ}}\Psi_\beta(\mathfrak{f}^{+\,\eta}_{\beta\alpha\,p}(k))C^{+\,\eta\,p}_{\alpha\beta}(k)dk, \tag{2.138}$$

where $C^{+\,\eta\,p}_{\alpha\beta}(k)$ is given by (2.64). Term III still needs some further investigation. Inserting the definition of the phonon collision operator (2.80) yields

$$\int_{\mathcal{BZ}}\Psi^\eta(q)C^{\alpha\beta}_\eta(q)dq=\int_{\mathcal{BZ}}\sum_k\sum_{k'}\Psi^\eta(q)\delta(H^{+\,\eta}_{\beta\alpha}(k',k))\delta_{k',k+q}s^\eta_{\alpha\beta}(k,k')g^{+\,\eta}_{\beta\alpha}(k',k)dq. \tag{2.139}$$

The sum over k' is calculated by evaluating the Kronecker delta resulting in

$$k' = k + q, \tag{2.140}$$

which is now a dependent variable of k and q:

$$\int_{\mathcal{BZ}} \Psi^\eta(q) C_\eta^{\alpha\beta}(q) dq = \int_{\mathcal{BZ}} \sum_k \Psi^\eta(q) \delta(H_{\beta\alpha}^{+\,\eta}(k',k)) s_{\alpha\beta}^\eta(k,k') g_{\beta\alpha}^{+\,\eta}(k',k) dq. \tag{2.141}$$

In the next step we transform the sum over k into an integral by using (2.1)

$$\int_{\mathcal{BZ}} \Psi^\eta(q) C_\eta^{\alpha\beta}(q) dq = \frac{L}{2\pi} \iint_{\mathcal{BZ}} \Psi^\eta(q) \delta(H_{\beta\alpha}^{+\,\eta}(k',k)) s_{\alpha\beta}^\eta(k,k') g_{\beta\alpha}^{+\,\eta}(k',k) dk dq. \tag{2.142}$$

It is now useful to perform a variable transformation from q again to k' using (2.140):

$$\int_{\mathcal{BZ}} \Psi^\eta(q) C_\eta^{\alpha\beta}(q) dq = \frac{L}{2\pi} \iint_{\mathcal{BZ}} \Psi^\eta(q^+) \delta(H_{\beta\alpha}^{+\,\eta}(k',k)) s_{\alpha\beta}^\eta(k,k') g_{\beta\alpha}^{+\,\eta}(k',k) dk dk'. \tag{2.143}$$

Finally, we integrate over k' as we have done in (2.38) by using (2.51), (2.52), (2.53), (2.64) resulting in

$$\int_{\mathcal{BZ}} \Psi^\eta(q) C_\eta^{\alpha\beta}(q) dq = \sum_{p=1}^{N_{\beta\alpha}^{+\,\eta}} \int_{\mathcal{BZ}} \Psi^\eta(\mathfrak{g}_{\beta\alpha\,p}^{+\,\eta}(k)) C_{\alpha\beta}^{+\,\eta\,p}(k) dk. \tag{2.144}$$

By comparing (2.144) for $\Psi^\eta = const$ to (2.83) and (2.128), we get the important relation that

$$\int_{\mathcal{BZ}} C_\eta^{\alpha\beta\,p}(q) dq = \int_{\mathcal{BZ}} C_{\alpha\beta}^{+\,\eta\,p}(k) dk = -\int_{\mathcal{BZ}} C_{\beta\alpha}^{-\,\eta\,p}(k') dk'. \tag{2.145}$$

Again we see that each collision integral can be transformed into the other by performing a variable transformation.

Inserting (2.137), (2.138) and (2.144) back into (2.136) yields

$$\sum_{p=1}^{N_{\beta\alpha}^{+\,\eta}} \int_{\mathcal{BZ}} (\Psi_\alpha(k) - \Psi_\beta(\mathfrak{f}_{\beta\alpha\,p}^{+\,\eta}(k)) + \Psi^\eta(\mathfrak{g}_{\beta\alpha\,p}^{+\,\eta}(k))) C_{\alpha\beta}^{+\,\eta\,p}(k) \stackrel{!}{=} 0. \tag{2.146}$$

This is the final result. The conservation of the total generalized moment $\mathcal{M}$ depends only on Ψ and must be fulfilled by each addend independently. We will now search for

functions fulfilling this relation. If we choose Ψ to be the dispersion relation of the given bands, with $\Psi_\alpha(k) = E_\alpha(k)$, $\Psi_\beta(k) = E_\beta(k)$ and $\Psi^\eta(q) = W^\eta(q)$ we get

$$\int_{\mathcal{BZ}} (E_\alpha(k) - E_\beta(\mathfrak{f}^{+\,\eta}_{\beta\alpha\,p}(k)) + W^\eta(\mathfrak{g}^{+\,\eta}_{\beta\alpha\,p}(k)))C^{+\,\eta\,p}_{\alpha\beta}(k)dk \stackrel{!}{=} 0. \tag{2.147}$$

This is valid according to (2.34) and (2.51), which represents the energy conservation in each collision:

$$E_\alpha(k) - E_\beta(\mathfrak{f}^{+\,\eta}_{\beta\alpha\,p}(k)) + W^\eta(\mathfrak{g}^{+\,\eta}_{\beta\alpha\,p}(k)) = 0. \tag{2.148}$$

We can also choose Ψ to be equal to the quasi momentum, with $\Psi_\alpha(k) = k$, $\Psi_\beta(k) = k$ and $\Psi^\eta(q) = q$ resulting in

$$\int_{\mathcal{BZ}} (k - \mathfrak{f}^{+\,\eta}_{\beta\alpha\,p}(k) + \mathfrak{g}^{+\,\eta}_{\beta\alpha\,p}(k))C^{+\,\eta\,p}_{\alpha\beta}(k)dk \stackrel{!}{=} 0. \tag{2.149}$$

Again wee see that this is valid because of (2.31), (2.51) which represents the conservation of quasi momentum in each collision:

$$\mathfrak{g}^{+\,\eta}_{\beta\alpha\,p}(k) = \mathfrak{f}^{+\,\eta}_{\beta\alpha\,p}(k) - k. \tag{2.150}$$

3 Numerical treatment

In the previous chapter we have defined all necessary equations representing the transport model. Since it is not possible to find analytical solutions to this system, one needs to turn to numerical simulations. Hence we need to develop a fully discretized model.

3.1 Conservation laws and finite volume methods

A special class of homogeneous hyperbolic partial differential equations (PDEs) are called conservation laws. Conservation laws usually arise from physical principles expressed in their integral form and represent physical properties like conservation of mass, energy and momentum.

A general form of conservation laws for a one-dimnsional system reads

$$\frac{\partial u(x,t)}{\partial t} + \frac{\partial h(u(x,t))}{\partial x} = 0, \tag{3.1}$$

where $h(u(x,t))$ is the so called flux function. If we use a linear flux function

$$h(u(x,t)) = au(x,t) \qquad \text{with} \quad a \in \mathbb{R}, \tag{3.2}$$

and insert (3.2) back into (3.1) we get the so called advection equation:

$$\frac{\partial u(x,t)}{\partial t} + a\frac{\partial u(x,t)}{\partial x} = 0 \tag{3.3}$$

The Boltzmann-equation for electrons (2.15) is obviously of that type although mult-dimensional. It is therefore possible to apply an approach called dimensional splitting or fractional step [21] based on one-dimensional advection equations for x- and k-directions. Hence we will concentrate on solving the one-dimensional hyperbolic PDEs.

As mentioned before conservation laws lead to conserved quantities, therefore, we need to employ numerical schemes which are designed to preserve these physical quantities as well. To this end, finite volume methods have been developed which are closely related to finite difference schemes but based on the integral form of the PDE. The basic idea is

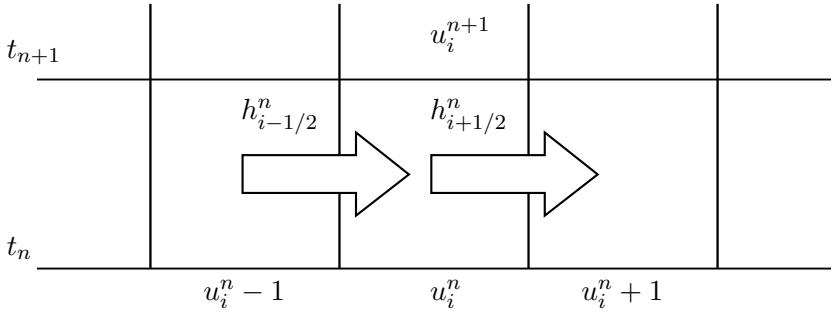

Figure 3.1: Illustration of finite volume methods update process. The cell average u_i^{n+1} is determined by the value of u_i^n and the numerical fluxes $h_{i+1/2}^n$, $h_{i-1/2}^n$ at the cell boundaries.

to divide the physical domain into grid cells $\mathcal{C}_i$ and approximate the unknown function at time t_n via its cell average:

$$u_i^n \approx \frac{1}{\Delta_x} \int_{\mathcal{C}_i} u(x, t_n) dx. \tag{3.4}$$

The derivative of the flux function can be expressed as numerical fluxes at the cell boundaries:

$$\left.\frac{\partial h(u, x, t)}{\partial x}\right|_{x=x_i} = \frac{h_{i+1/2} - h_{i-1/2}}{\Delta_x}. \tag{3.5}$$

Consequently, the cell averages are then updated by these fluxes:

$$u_i^{n+1} = u_i^n - \frac{\Delta_t}{\Delta_x}(h_{i+1/2}^n - h_{i-1/2}^n). \tag{3.6}$$

The challenge is to find a good approximation for these numerical fluxes. Figure 3.1 illustrates the basic idea behind this method. Please note that in (3.6) a simple forward Euler time stepping method is used.

For the simple advection equation with the constant coefficient $a \in \mathbb{R}^+$, a first order approximation of the numerical fluxes read

$$h_{i-1/2}^n = a u_{i-1}^n. \tag{3.7}$$

Inserting (3.7) back into (3.6) yields:

$$u_i^{n+1} = u_i^n - \frac{a\Delta_t}{\Delta_x}\left[u_i^n - u_{i-1}^n\right] = 0. \tag{3.8}$$

This is called the upwind scheme. If we choose the time and position discretization in a way that $a = \Delta_x/\Delta_t$ the result of the numerical scheme will be equal to the analytical solution. This is due to the fact that information in the advection equation travels at the speed of a. Lets consider an infinitely long system $-\infty < x < \infty$. The solution is the uniquely defined by the initial condition $u_o(x)$ at time $t = 0$. Using the method of characteristics, we can find characteristic curves on which the solution is constant and find the solution to be

$$u(x,t) = u_o(x - at) \qquad \text{for} \quad t > 0. \tag{3.9}$$

Because we have chosen our grid and step size exactly to coincide with the characteristic of the equation all the information contained in one cell can travel to the next within one time step. If the information moves faster than one cell per time step i.e. $\Delta_x/\Delta_t < a$ this method becomes unstable. This is expressed by CFL condition

$$\nu = \left| \frac{a\Delta_t}{\Delta_x} \right| \leq 1, \tag{3.10}$$

named after Courant, Friedrichs, and Lewy, which is an necessary condition for convergence. The symbol ν is also referred to as the Courant number. This obviously limits the maximal time step width that can be achieved, given a certain x discretization and advection constant a. For a system of equations the time step size is limited by:

$$\max(\nu_i) \leq 1 \qquad \text{or} \qquad \Delta_t \leq \min(a_i \Delta_{x\,i}). \tag{3.11}$$

The symbols ν_i, a_i and $\Delta_{x\,i}$ denote the Courant number, the advection constant and the position discretization size of the i^{th} equation, respectively.

If ν is smaller than one, the numerical solution differs from the analytical one due to numerical diffusion. Figure 3.2 shows the numerical diffusion caused by the upwind scheme. This effect is especially pronounced if $u(x,t)$ varies rapidly in the presence of shock waves. We will therefore turn to higher order schemes to be able to handle smooth regions as well as capture shock waves properly. Although we face strong numerical diffusion, upwind is still useful for the mere fact that it is, being a first order accurate scheme, the fastest one available. It is also non oscillatory, which is a very desired property, since distribution functions with values larger than one, or smaller than zero are unphysical.

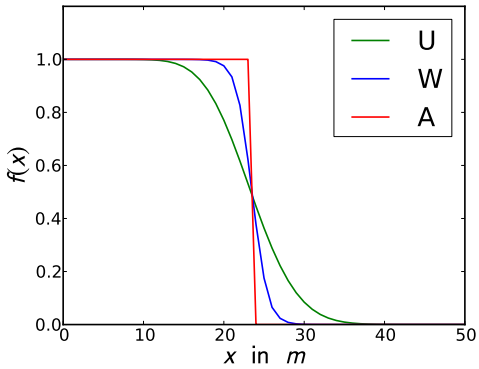

Figure 3.2: Comparison of the numerical diffusion caused by upwind and WENO scheme: analytical solution (A), upwind (U) and WENO method (W). Simulation parameters: $\Delta_x = 1\,\mathrm{m}$, $\Delta_t = 0.1\,\mathrm{s}$, advection constant $a = 1\,\mathrm{m/s}$, left boundary condition $f_L = 1$ and simulation time $t_{\mathrm{end}} = 25\,\mathrm{s}$

3.1.1 The WENO reconstruction

Having discussed the upwind method, let us turn to a far more advanced numerical scheme. As mentioned before, to capture shocks we need a numerical method that can calculate the numerical fluxes accurately to a higher order than one. Some higher order schemes, however, create oscillations at strong discontinuities and therefore tend to over- and under-shoot. This is due the fact that higher-order polynomials are used for function interpolation, which is oscillatory near discontinuities, a behavior called Gibbs phenomena. This is especially unfavorable concerning the calculation of the statistic terms of the collision operator, as they are designed to operate with electron distribution functions within the limits $[0, 1]$, which can lead to divergence of the system.

In order to prevent unwanted oscillations and still be able to use a higher order scheme, weighted essentially non oscillatory schemes or short WENO schemes have been developed. They were first introduced by Liu, Osher and Chan [22] and are an extension of the very successful ENO schemes developed by Harten et al. [23, 24]. We will use a fifth order accurate WENO scheme presented in [25, 26]. The basic idea behind ENO and WENO is to choose an appropriate stencil, instead of a fixed one, based on a smoothness indicator. ENO just uses the best indicated stencil. WENO on the other hand uses the results of all stencils and combines them via a convex sum, which leads to a higher accuracy, while still maintaining the desired non oscillatory behavior.

Let us turn to the actual scheme and see how the numerical flux is calculated, a

process, which is called reconstruction within this terminology. To calculate the flux at point $x_{i+1/2}$ one might consider to use the stencil $S^{(1)} = \{i-2, i-1, i\}$, which leads to

$$h^{(1)}_{i+1/2} = \frac{1}{3}h_{i-2} - \frac{7}{6}h_{i-1} + \frac{11}{6}h_i, \tag{3.12}$$

which is a third-order accurate approximation. We could, however, use $S^{(2)} = \{i-1, i, i+1\}$ and $S^{(3)} = \{i, i+1, i+2\}$ as well. This leads to

$$h^{(2)}_{i+1/2} = -\frac{1}{6}h_{i-1} + \frac{5}{6}h_i + \frac{1}{3}h_{i+1} \tag{3.13}$$

and

$$h^{(2)}_{i+1/2} = \frac{1}{3}h_i + \frac{5}{6}h_{i+1} - \frac{1}{6}h_{i+2}, \tag{3.14}$$

again both are third-order accurate approximations. For the choice of stencils we assumed $a > 0$. To obtain a polynomial of fourth degree one could use the union of these three stencils $S = \{i-2, i-1, i, i+1, i+2\}$. The formula for the flux now reads:

$$h_{i+1/2} = \frac{1}{30}h_{i-2} - \frac{13}{60}h_{i-1} + \frac{47}{60}h_i + +\frac{9}{20}h_{i+1} - \frac{1}{20}h_{i+2}. \tag{3.15}$$

This flux can also be constructed by linear combination, using the smaller stencils $S^{(1)}$,$S^{(2)}$ and $S^{(3)}$

$$h_{i+1/2} = \gamma_1 h^{(1)}_{i+1/2} + \gamma_2 h^{(2)}_{i+1/2} + \gamma_3 h^{(3)}_{i+1/2}, \tag{3.16}$$

with the linear weights:

$$\gamma_1 = \frac{1}{10}, \qquad \gamma_2 = \frac{3}{5}, \qquad \gamma_2 = \frac{3}{10}. \tag{3.17}$$

Figure (3.3) illustrates this concept.

The idea behind WENO now is to modify these weights according to the smoothness of the function. To this end, we introduce a new set of linear weights ω_1, ω_2 and ω_3:

$$h_{i+1/2} = \omega_1 h^{(1)}_{i+1/2} + \omega_2 h^{(2)}_{i+1/2} + \omega_3 h^{(3)}_{i+1/2}, \tag{3.18}$$

with normalized

$$\omega_n = \frac{\tilde{\omega}_n}{\sum_{l=1}^{3} \tilde{\omega}_l}. \tag{3.19}$$

This ensures that the weights yield a convex combination of fluxes. The weights $\tilde{\omega}_n$ in

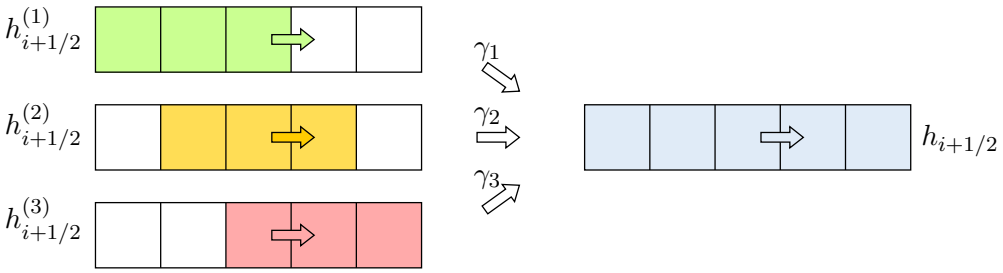

Figure 3.3: Illustration of stencils and linear weights used to construct the numerical fluxes.

turn are calculated by using the original weights γ_n:

$$\tilde{\omega}_n = \frac{\gamma_n}{(\beta_n + \delta)^2}, \tag{3.20}$$

where β_n is called the smoothness indicator and δ is a small constant preventing division by zero. For each stencil the indicators read

$$\beta_1 = \frac{13}{12}\left(h_{i-2} - 2h_{i-1} + h_i\right)^2 + \frac{1}{4}\left(h_{i-2} - 4h_{i-1} + 3h_i\right)^2, \tag{3.21}$$

$$\beta_2 = \frac{13}{12}\left(h_{i-1} - 2h_i + h_{i+1}\right)^2 + \frac{1}{4}\left(h_{i-1} - h_i\right)^2, \tag{3.22}$$

$$\beta_2 = \frac{13}{12}\left(h_i - 2h_{i+1} + h_{i+2}\right)^2 + \frac{1}{4}\left(3h_i - 4h_{i+1} + h_{i+2}\right)^2. \tag{3.23}$$

3.1.2 The dimensional splitting method and time interagtion

To solve the Boltzmann equation using the previously discussed upwind and WENO methods for one-dimensional system we need to employ a so called splitting or fractional step method. For a detailed description of splitting schemes please referre to the book of E. Toro [21]. This enables us to use the high order WENO scheme as well as to incorporate the source term. The idea is to split, for a time Δ_t, the problem into the advection and the source part. We further solve the advection problem for each direction seperately. Let us considern an initilal-value problem (IVP) of the form

$$\left.\begin{aligned} &\text{PDE:} && \partial_t u + a_x \partial_x u + a_k \partial_k u = C(u), \\ &\text{IC:} && u(x,k,t^n) = u_0(x,k) \equiv u^n. \end{aligned}\right\} \tag{3.24}$$

where a_x and a_k denote the advection constants for the x- and k-direction and $C(u)$ denotes the source term. The initial condition (IC) at time t_n is u^n. This partial differential equation (PDE) is is of the same form as (2.15). To apply the splitting method we start by solving

$$\left.\begin{array}{ll} \text{PDE:} & \partial_t u + a_x \partial_x u = 0 \\ \text{IC:} & u^n \end{array}\right\} \overset{\Delta_t}{\Longrightarrow} u^{n+\frac{1}{3}}, \tag{3.25}$$

where we use the initial condition (IC) of the original IPV u^n. The solution after time Δ_t is called $u^{n+\frac{1}{3}}$ Susquently, we use this as IC for the k-direction IPV

$$\left.\begin{array}{ll} \text{PDE:} & \partial_t u + a_k \partial_k u = 0 \\ \text{IC:} & u^{n+\frac{1}{3}} \end{array}\right\} \overset{\Delta_t}{\Longrightarrow} u^{n+\frac{2}{3}}, \tag{3.26}$$

where $u^{n+\frac{2}{3}}$ denotes the solution after time Δ_t. Finally, $u^{n+\frac{2}{3}}$ is used as the IC for the ordinary differential equation (ODE):

$$\left.\begin{array}{ll} \text{ODE:} & \frac{d}{dt} u = C(u) \\ \text{IC:} & u^{n+\frac{2}{3}} \end{array}\right\} \overset{\Delta_t}{\Longrightarrow} u^{n+1}. \tag{3.27}$$

The solution u^{n+1} is regarded as the solution to the full problem (3.24) after time Δ_t. To solve the IVP of (3.27) we use the Euler Method. For a first-order ODE

$$\frac{d}{dt} u(t) = C(t, u(t)) \tag{3.28}$$

and an IC u^n, the Euler method reads

$$u^{n+1} = u^n + \Delta_t C(t^n, u^n) \tag{3.29}$$

where Δ_t again denotes the time step. We also use the forward euler as the time inetragtion scheme to solve (3.25) and (3.26) as discussed in (3.6).

3.2 The simulation grid and discrete moments of the distribution function

The starting point of our numerical model is the discretization of distribution functions for phonons and electrons. For this purpose we need to introduce a two-dimensional

grid on which the functions will be defined. The physical domain we are interested in is the whole length (L) of the device $\mathbb{I}_x = [0, L]$ in the x-direction and the first Brillouin zone $\mathbb{I}_k = [-\pi/a, \pi/a]$ in the k-direction, where a denotes the lattice constant of the one-dimensional system.

A uniform grid is used, with grid points centered at each cell. Hence, we introduce the set $\mathcal{I}_x = \{x_n | n = 0, \ldots, N_x - 1\}$ for the interval $\mathbb{I}_x$ with

$$x_n = (n + \frac{1}{2})\Delta_x \qquad \text{for} \quad n \in I_x = \{0, \ldots, N_x - 1\} \tag{3.30}$$

that will spread grid points equally over the whole length of the device. The cell size can be calculated from $\Delta_x = L/N_x$ where N_x is a simulation parameter.

Similar, we introduce the set $\mathcal{I}_k = \{k_n | n = 0, \ldots, 2N_k - 1\}$

$$k_n = (n - N_k)\Delta_k \qquad \text{for} \quad n \in I_k = \{0, \cdots, 2N_k - 1\}\,, \tag{3.31}$$

which will cover the whole Brillouin zone uniformly. This time the discretization size Δ_k is the simulation parameter. One can, therefore, calculate the number of grid points needed

$$N_k = \left\lfloor \frac{\pi}{a} \frac{1}{\Delta_k} \right\rfloor . \tag{3.32}$$

Although each band extends over the whole k-space it is usually sufficient, to consider a smaller section that covers all important physical processes. This saves computation time and memory and allows us to use a finer discretization of k. Hence, we introduce the subsets $\mathcal{I}_k^\alpha = \{k_n | k_n \in \mathbb{I}_k^\alpha \wedge n \in I_k\}$ and $I_k^\alpha = \{n | n \in I_k \wedge k_n \in \mathbb{I}_k^\alpha\}$ for each electron band $\alpha \in I_{\text{el}}$ and interval $\mathbb{I}_k^\alpha = [k_{\min}^\alpha, k_{\max}^\alpha]$. Since we are using the same grid to discretize the electron and phonon distribution function, we can use the large sets $\mathbb{I}_k$, $\mathcal{I}_k$ and I_k again to define subsets for the phonon bands $\eta \in I_{\text{ph}}$: $I_q^\eta = [-q_{\max}^\eta, q_{\max}^\eta]$, $\mathcal{I}_q^\eta = \{q_n | q_n \in \mathbb{I}_q^\eta \wedge n \in I_k\}$, $I_q^\eta = \{n | n \in I_k \wedge q_n \in \mathbb{I}_q^\eta\}$. It is important to mention that one needs to choose $q_{\max}$ as large as not to limit possible scattering events.

We can now define the simulation grids with grid points centered at each cell. For an electron band α this reads $\mathcal{I}_x \times \mathcal{I}_k^\alpha$ and for phonon band η, $\mathcal{I}_x \times \mathcal{I}_k^\eta$.

Finally, we need to define the distribution functions on that grid. Although we are using finite volume methods to calculate numerical fluxes we can assume the values at the cell midpoints to be a good approximation for the cell averages [27]. We therefore set

$$f_{\alpha\, ij} := f_\alpha(x_i, k_j) \tag{3.33}$$

for the electron distribution function of band α and

$$N_{ij}^{\eta} := N^{\eta}(x_i, q_j) \tag{3.34}$$

for the phonon distribution of branch η.

Consequently, we are now able to define the discretized moments of the distribution function. The electron density of band α reads

$$\mathcal{N}_{\alpha\, i} = \frac{\Delta_k}{2\pi} \sum_{j \in I_k^{\alpha}} f_{\alpha\, ij} \tag{3.35}$$

and the total carrier density is defined as:

$$\mathcal{N}_i = \sum_{\alpha} \mathcal{N}_{\alpha\, i}. \tag{3.36}$$

Similarly, the current density of band α and the total current density read

$$\mathcal{J}_{\alpha\, i} = -\frac{e_0 \Delta_k}{2\pi} \sum_{j \in I_k^{\alpha}} v_{\alpha\, j} f_{\alpha\, ij}, \tag{3.37}$$

$$\mathcal{J}_i = \sum_{\alpha} \mathcal{J}_{\alpha\, i}, \tag{3.38}$$

where $v_{\alpha\, j} = v_{\alpha}(k_j)$ denotes the discretized group velocity of the electrons in band α. We can also use the numerical fluxes in x-direction, $h^x_{\alpha\, i\pm\frac{1}{2}j}$, to calculate the current density, resulting in

$$\mathcal{J}_{\alpha\, i\pm\frac{1}{2}} = -\frac{e_0 \Delta_k}{2\pi} \sum_{j \in I_k^{\alpha}} h^x_{\alpha\, i\pm\frac{1}{2}j}. \tag{3.39}$$

Furthermore, the discrete energy densities of the electrons in band α and the phonons in branch η can be written as

$$\mathcal{E}_{\alpha\, i} = \frac{\Delta_k}{2\pi} \sum_{j \in I_k^{\alpha}} E_{\alpha\, j} f_{\alpha\, ij}, \tag{3.40}$$

$$\mathcal{W}_i^{\eta} = \frac{\Delta_k}{2\pi} \sum_{j \in I_q^{\eta}} W_j^{\eta} N_{ij}^{\eta}, \tag{3.41}$$

with $E_{\alpha\, j} = E_{\alpha}(k_j)$ and $W_j^{\eta} = W^{\eta}(q_j)$ being the discrete electron and phonon dispersion

relations. Consequently, the total energy density is given by

$$\mathcal{E}_i = \sum_\alpha \mathcal{E}_{\alpha\, i} + \sum_\eta \mathcal{W}_{\eta\, i}, \tag{3.42}$$

Similarly, the momentum densities of electrons in band α and phonons in branch η and the total momentum density read

$$\mathcal{K}_{\alpha\, i} = \frac{\Delta_k}{2\pi} \sum_{j \in I_k^\alpha} k_j f_{\alpha\, ij}, \tag{3.43}$$

$$\mathcal{Q}_i^\eta = \frac{\Delta_k}{2\pi} \sum_{j \in I_q^\eta} q_j N_{ij}^\eta, \tag{3.44}$$

$$\mathcal{K}_i = \sum_\alpha \mathcal{K}_{\alpha\, i} + \sum_\eta \mathcal{Q}_i^\eta. \tag{3.45}$$

Finally, we can define a general moment of the electron and phonon distribution function, as we have done it in the analytical case, that consequently read

$$\mathcal{M}_{\alpha\, i} = \frac{\Delta_k}{2\pi} \sum_{j \in I_k^\alpha} \Psi_{\alpha\, j} f_{\alpha\, ij}, \tag{3.46}$$

$$\mathcal{M}_i^\eta = \frac{\Delta_k}{2\pi} \sum_{j \in I_q^\eta} \Psi_j^\eta N_{ij}^\eta. \tag{3.47}$$

The total momentum is therefore given by:

$$\mathcal{M}_i = \sum_\alpha \mathcal{M}_{\alpha\, i} + \sum_\eta \mathcal{M}_i^\eta. \tag{3.48}$$

3.3 Partial derivatives and boundary conditions

Having discretized the distribution functions we turn to the Boltzmann transport equation. For electrons it can be written as

$$\partial_t(f_{\alpha,ij}) + \partial_x(h^x_{\alpha,ij}) + \partial_k(h^k_{\alpha,ij}) = C_{\alpha,ij}, \tag{3.49}$$

with $h^x_{\alpha,ij} = v_{\alpha,j} f_{\alpha,ij}$ and $h^k_{\alpha,ij} = \frac{-e_0 E}{\hbar} f_{\alpha,ij}$ being the discretized flux functions at the grid points in x- and k-direction, respectively. The symbol $C_{\alpha,ij}$ denotes the discrete electron collision operator, which we will further discuss in Section (3.4). In the context of finite volume methods we can approximate the partial derivative of the flux functions

via the numerical fluxes at the cell boundaries, which leads to

$$\partial_t(f_{\alpha,ij}) + \frac{h^x_{\alpha,i+\frac{1}{2}j} - h^x_{\alpha,i-\frac{1}{2}j}}{\Delta_x} + \frac{h^k_{\alpha,ij+\frac{1}{2}} - h^k_{\alpha,;ij-\frac{1}{2}}}{\Delta_x} = C_{\alpha,ij}, \tag{3.50}$$

where $h^x_{\alpha,i+\frac{1}{2}j}$ and $h^k_{\alpha,ij+\frac{1}{2}}$ denote the numerical fluxes in x- and k-direction, respectively. These numerical fluxes can be calculated using either the upwind or WENO method.

Subsequently, we need to specify the boundary conditions for the system. To that end, we need to define so-called ghost cells extending the simulation grid used to calculate the numerical fluxes at the grid boundaries. The number of ghost points needed depends on the numerical scheme used to calculate the fluxes. For the upwind scheme only one ghost cell is needed, whereas for the WENO scheme, described before, we need to provide three ghost cells.

Let us start, by treating the boundary condition in x-direction. Requiring the contacts to be in thermal equilibrium, the Fermi-Dirac distribution function (2.85) can be used to calculate the cell values. This leads to

$$f_{\alpha\, ij} = \begin{cases} \tilde{f}_\alpha(x = 0, k_j) & \text{for} \quad i = \{-3, -2, -1\} \\ \tilde{f}_\alpha(x = L, k_j) & \text{for} \quad i = \{N_x, N_x + 1, N_x + 2\} \end{cases} \tag{3.51}$$

extending the grid for $i \notin \mathcal{I}_x = \{x_n|0, \ldots, N_x - 1\}$. These boundary conditions represent perfect contacts, since they provide a constant flow of electrons and absorb all outgoing electrons [19].

To model more realistic contacts one can additionally modify the flux of electrons, so that a certain percentage of electrons is reflected at the junction using a transmission coefficient t^2 [9]. These reflected electrons stay within their band but flip their quasi momentum from k to $-k$. For the left boundary condition at $x = 0$ this can be expressed as

$$h_{\alpha,-\frac{1}{2}j} = t^2 h_{\alpha,-\frac{1}{2}j} + (1 - t^2) h_{\alpha,-\frac{1}{2}l}, \quad \text{with} \quad l : k_l = -k_j. \tag{3.52}$$

Now, we will turn to the boundary conditions in k-direction. Due to the periodicity of the Brillouin zone, one would be inclined to impose periodic boundary conditions along the k-axis. This is, however, only valid if the simulation grid covers the whole k-space. As mentioned before we will focus only on small sections of the Brillouin zone. Therefore, we will use the same approach as for the x-direction and will set the ghost

cell values to corresponding Fermi-Dirac distribution function. This now reads

$$f_{\alpha\, ij} = \begin{cases} \tilde{f}_\alpha(x_i, k = k_{min}) & \text{for} \quad j = \{j_{min} - 3, j_{min} - 2, j_{min} - 1\} \\ \tilde{f}_\alpha(x_i, k = k_{max}) & \text{for} \quad j = \{j_{max} + 1, j_{max} + 2, j_{max} + 3\} \end{cases} \tag{3.53}$$

where j_{min} denotes the lower and j_{max} the upper bound for the index j within the set $I_k^\alpha = \{j | j \in I_k \wedge k_n \in \mathbb{I}_k^\alpha\}$. It should be noted that this definition is only valid far away from the Fermi-surface. Therefore, we need to define the upper and lower limit of each section with extreme caution, since the Fermi-surface will be shifted and deformed along the device due to the applied electric field and scattering events. If we choose our section to be too narrow, electrons will be lost along the boundaries, which leads to a wrong current. A possibility to circumvent this problem is to set the outgoing electron flow at the k-boundries to zero.

We will now perform the same analysis for the phonon transport equation (2.70) and corresponding boundary conditions. As before, we approximate the partial derivative in x-direction with numerical fluxes, $h^{\eta\, x}_{i+\frac{1}{2}j}$ and $h^{\eta\, x}_{i-\frac{1}{2}j}$, over the cell boundaries resulting in

$$\partial_t(N_{ij}^\eta) + \frac{h^{\eta\, x}_{i+\frac{1}{2}j} - h^{\eta\, x}_{i-\frac{1}{2}j}}{\Delta_x} = C_{e,ph\, ij} + C_{ph,ph\, ij}. \tag{3.54}$$

We will assume perfect contacts for phonons and, therefore, use the same boundary condition as before in x-direction. In this case we use the Bose-Einstein distribution (2.86) as equilibrium distribution function, which leads to

$$N_{ij}^\eta = \begin{cases} \tilde{N}^\eta(x = 0, q_j) & \text{for} \quad i = \{-3, -2, -1\} \\ \tilde{N}^\eta(x = L, q_j) & \text{for} \quad i = \{N_x, N_x + 1, N_x + 2\} \end{cases} \tag{3.55}$$

As before the boundary condition for phonons in k-direction reads

$$N_{ij}^\eta = \begin{cases} \tilde{N}^\eta(x_i, q = q_{min}) & \text{for} \quad j = \{j_{min} - 3, j_{min} - 2, j_{min} - 1\} \\ \tilde{N}^\eta(x_i, q = q_{max}) & \text{for} \quad j = \{j_{max} + 1, j_{max} + 2, j_{max} + 3\} \end{cases} \tag{3.56}$$

with j_{min} and j_{max} again beeing the lower and upper bound for the index j.

3.4 Electron collision operator

We will now discuss the electron collision operator and its discretization. At the grid points k_i (2.64) reads

$$C_{\alpha\beta}^{+\,\eta\,p}(k_i) = \frac{L}{2\pi}\left(\left|\frac{\partial H_{\beta\alpha}^{+\,\eta}(k',k)}{\partial k'}\right|^{-1} \chi_{\beta\alpha}^{+\,\eta\,p}(k) s_{\alpha\beta}^{\eta}(k,k') g_{\beta\alpha}^{+\,\eta}(k',k)\right)_{k'=\mathfrak{f}_{\beta\alpha\,p}^{+\,\eta}(k_i),k=k_i}, \tag{3.57}$$

We are searching for an approximation: $C_{\alpha\beta,i}^{+\,\eta} \approx C_{\alpha\beta}^{+\,\eta}(k_i)$. The function $\mathfrak{f}_{\beta\alpha\,p}^{+\,\eta}(k_i)$ obeys the equation

$$H_{\beta\alpha}^{+\,\eta}(k' = \mathfrak{f}_{\beta\alpha\,p}^{+\,\eta}(k_i), k_i) = 0. \tag{3.58}$$

A direct discretization of (2.34), $H_{\beta\alpha,ij}^{+\,\eta} = H_{\beta\alpha}^{+\,\eta}(k'_j, k_i)$, at the grid points reads

$$H_{\beta\alpha,ij}^{+\,\eta} = E_\beta(k'_j) - E_\alpha(k_i) - W^\eta(k'_j - k_i) = 0. \tag{3.59}$$

The solution $k' = \mathfrak{f}_{\beta\alpha\,p}^{+\,\eta}(k_i)$ does not necessarily fall on a grid point and is, therefore, not part of the set $\mathcal{I}_k^\beta$. We can, however, find two indices $(u^i, u^i + 1)$ with

$$k'_{u^i} < \mathfrak{f}_{\beta\alpha\,p}^{+\,\eta}(k_i) < k'_{u^i+1}. \tag{3.60}$$

In order to safe CPU time, we approximate $\mathfrak{f}_{\beta\alpha\,p}^{+\,\eta}(k_i)$ and define

$$k'_{u^i+x} \approx \mathfrak{f}_{\beta\alpha\,p}^{+\,\eta}(k_i), \tag{3.61}$$

with $x \in [0,1]$. We can describe k'_{u^i+x} to be the convex sum of the linear weights (r_0^i, r_1^i)

$$k'_{u^i+x} = r_0^i k'_{u^i} + r_1^i k'_{u^i+1}, \tag{3.62}$$

where r_0^i and r_1^i need to satisfy:

$$r_1^i = 1 - r_0^i. \tag{3.63}$$

The goal is to find these weights, which can be done by a linear interpolation of $H_{\beta\alpha,ij}^{+\,\eta}$ within the interval (k'_{u^i}, k'_{u^i+1}). This process is illustrated in Figure (3.4). We can find

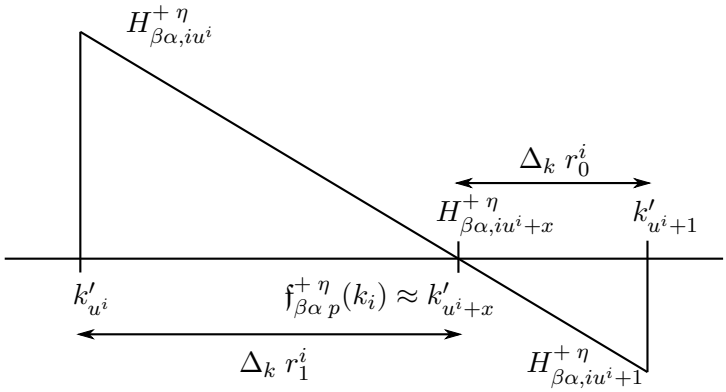

Figure 3.4: Illustration of root-finding using linear interpolation of energy.

the root by setting up a linear equation over the normalized interval that reads

$$f(0) = H^{+\,\eta}_{\beta\alpha,iu^i}, \qquad f(1) = H^{+\,\eta}_{\beta\alpha,iu^i+1}, \tag{3.64}$$

$$f(x) = \left(H^{+\,\eta}_{\beta\alpha,iu^i+1} - H^{+\,\eta}_{\beta\alpha,iu^i}\right) x + H^{+\,\eta}_{\beta\alpha,iu^i} = 0. \tag{3.65}$$

The root is given by

$$x = -\frac{H^{+\,\eta}_{\beta\alpha,iu^i}}{H^{+\,\eta}_{\beta\alpha,iu^i+1} - H^{+\,\eta}_{\beta\alpha,iu^i}}, \tag{3.66}$$

and with

$$r^i_0 = 1 - x, \qquad r^i_1 = x, \tag{3.67}$$

the linear weights finally read

$$r^i_0 = \frac{H^{+\,\eta}_{\beta\alpha,iu^i+1}}{H^{+\,\eta}_{\beta\alpha,iu^i+1} - H^{+\,\eta}_{\beta\alpha,iu^i}}, \qquad r^i_1 = -\frac{H^{+\,\eta}_{\beta\alpha,iu^i}}{H^{+\,\eta}_{\beta\alpha,iu^i+1} - H^{+\,\eta}_{\beta\alpha,iu^i}}. \tag{3.68}$$

These weights can now be used to interpolate the electron and the phonon quasi momentum $k'_{u^i+x} \approx \mathfrak{f}^{+\,\eta}_{\beta\alpha\,p}(k_i)$, $q^+_{v^i+x} \approx \mathfrak{g}^{+\,\eta}_{\beta\alpha\,p}(k_i)$

$$q^+_{v^i+x} = k'_{u^i+x} - k_i \tag{3.69}$$

and their distribution functions $f_{\beta,u^i+x} \approx f_\beta(k'_{u^i+x})$ and $N^\eta_{v^i+x} \approx N^\eta(q^+_{v^i+x})$, respec-

tively. The statistics term $g^{+\,\eta}_{\beta\alpha}(k'_{u^i+x}, k_i)$ can thus be approximated by

$$g^{+\,\eta}_{\beta\alpha\, iu^i+x} = \left(N^{\eta}_{v^i+x}+1\right) f_{\beta,u^i+x}\left(1-f_{\alpha,i}\right) - N^{\eta}_{v^i+x} f_{\alpha,i}\left(1-f_{\beta,u^i+x}\right) \tag{3.70}$$

Where f_{β,u^i+x} and $N^{\eta}_{v^i+x}$ still need to be determined, see Section 3.5.

Furthermore, $\frac{\partial H^{+\,\eta}_{\beta\alpha}(k',k)}{\partial k}$ needs to be approximated. We start from (2.34):

$$\left|\frac{\partial H^{+\,\eta}_{\beta\alpha}(k',k)}{\partial k'}\right|^{-1}_{k'=f^{+\,\eta}_{\beta\alpha\, p}(k_i),\, k=k_i} = \left|\frac{1}{\partial_{k'}E_\beta(k') - \partial_{k'}W^{\eta}(k'-k)}\right|^{-1}_{k'=f^{+\,\eta}_{\beta\alpha\, p}(k_i),\, k=k_i} \tag{3.71}$$

an by using (2.31)

$$\frac{\partial W^{\eta}(k'-k)}{\partial k'} = \frac{\partial W^{\eta}(q^+)}{\partial q^+}\frac{dq^+}{dk'} = \frac{\partial W^{\eta}(q^+)}{\partial q^+} \tag{3.72}$$

we obtain

$$\left|\frac{\partial H^{+\,\eta}_{\beta\alpha}(k',k)}{\partial k'}\right|^{-1}_{k'=f^{+\,\eta}_{\beta\alpha\, p}(k_i),\, k=k_i} \approx \left|\frac{1}{\left(r^i_0 E'_{\beta,u^i} + r^i_1 E'_{\beta,u^i+1} - r^i_0 W'^{\eta}_{v^i} - r^i_1 W'^{\eta}_{v^i+1}\right)}\right|^{-1} \tag{3.73}$$

where E'_{β,u^i} and $W'^{\eta}_{v^i}$ denote the derivatives of the electron and phonon dispersion relation with respect to k' and q^+, respectively, at the grid points. By defining $s^{\eta}_{\alpha\beta,iu^i} := s^{\eta}_{\alpha\beta}(k_i, k'_{u^i})$ we can approximate $s^{\eta}_{\alpha\beta}(k_i, k'_{u^i+x})$ by:

$$s^{\eta}_{\alpha\beta,iu^i+x} = r_0 s^{\eta}_{\alpha\beta,iu^i} + r_1 s^{\eta}_{\alpha\beta,iu^i+1} \tag{3.74}$$

We further define $\chi^{+\,\eta\, p}_{\beta\alpha,i} := \chi^{+\,\eta}_{\beta\alpha\, p}(k_i)$. Consequently, the final approximation $C^{+\,\eta\, p}_{\alpha\beta,i}$ at a grid point k_i reads:

$$C^{+\,\eta\, p}_{\alpha\beta,i} = \frac{L}{2\pi}\left|\frac{1}{\left(r^i_0 E'_{\beta,u^i} + r^i_1 E'_{\beta,u^i+1} - r^i_0 W'^{\eta}_{v^i} - r^i_1 W'^{\eta}_{v^i+1}\right)}\right|^{-1} \tag{3.75}$$

$$\times\, \chi^{+\,\eta\, p}_{\beta\alpha,i} s^{\eta}_{\alpha\beta,iu^i+x} g^{+\,\eta}_{\beta\alpha,iu^i+x}. \tag{3.76}$$

3.5 Interpolation methods for electron and phonon distribution functions

To evaluate the statistics term $g^{+\,\eta}_{\beta\alpha,iu^i+x}$ we need to find f_{β,u^i+x} and $N^{\eta}_{v^i+x}$. A straight forward way of doing so is by linear interpolation. For the electron distribution function this reads

$$f_{\beta,u^i+x} = r_0^i f_{\beta,u^i} + r_1^i f_{\beta,u^i+1}, \tag{3.77}$$

by using again the set of linear weights (r_0^i, r_1^i). Furthermore, by taking (3.67) into account we obtain

$$\begin{aligned} f_{\beta,u^i+x} &= (1-x) f_{\beta,u^i} + x f_{\beta,u^i+1}, && (3.78)\\ &= f_{\beta,u^i} + x\left(f_{\beta,u^i+1} - f_{\beta,u^i}\right). && (3.79) \end{aligned}$$

Similar considerations lead us to

$$N^{\eta}_{v^i+x} = N^{\eta}_{v^i} + x\left(N^{\eta}_{v^i+1} - N^{\eta}_{v^i}\right). \tag{3.80}$$

3.5.1 Exponential interpolation of the electron distribution function:

We can exploit the knowledge of the distribution functions in thermal equilibrium to construct a better interpolation technique. For electron distribution functions it is based on the interpolation of the expression

$$\log\frac{f_{\beta,u^i+x}}{1-f_{\beta,u^i+x}} = r_0^i \log\frac{f_{\beta,u^i}}{1-f_{\beta,u^i}} + r_1^i \log\frac{f_{\beta,u^i+1}}{1-f_{\beta,u^i+1}}. \tag{3.81}$$

By using the symbol

$$\hat{f} = \frac{f_{\beta,u^i+x}}{1-f_{\beta,u^i+x}}, \tag{3.82}$$

we can transform (3.81) into

$$\hat{f} = \frac{(f_{\beta,u^i})^{r_0^i}(f_{\beta,u^i+1})^{r_1^i}}{(1-f_{\beta,u^i})^{r_0^i}(1-f_{\beta,u^i+1})^{r_1^i}}. \tag{3.83}$$

Again, using (3.67) yields:

$$\hat{f} = \frac{(f_{\beta,u^i})^{(1-x)}(f_{\beta,u^i+1})^x}{(1-f_{\beta,u^i})^{(1-x)}(1-f_{\beta,u^i+1})^x}. \tag{3.84}$$

$$\tag{3.85}$$

By inserting it back into (3.82) we get the final result:

$$f_{\beta,u^i+x} = \frac{\hat{f}}{1+\hat{f}}, \tag{3.86}$$

$$= \frac{\frac{(f_{\beta,u^i})^{(1-x)}(f_{\beta,u^i+1})^x}{(1-f_{\beta,u^i})^{(1-x)}(1-f_{\beta,u^i+1})^x}}{1+\frac{(f_{\beta,u^i})^{(1-x)}(f_{\beta,u^i+1})^x}{(1-f_{\beta,u^i})^{(1-x)}(1-f_{\beta,u^i+1})^x}}. \tag{3.87}$$

If we inspect (3.87), we see that its calculation involves a large amount of computation effort since it is based heavily on exponentiation. The solution f_{β,u^i+x} of this interpolation technique, however, represents a linear interpolation in energy space for Fermi-Dirac distribution functions. If the dispersion relation is linear the result coincides with the exact solution $f_\beta(k_{u^i+1})$. To proof this we will start with (3.83):

$$\hat{f} = \left(\frac{f_{\beta,u^i}}{1-f_{\beta,u^i}}\right)^{r_0^i}\left(\frac{f_{\beta,u^i+1}}{(1-f_{\beta,u^i i+1})}\right)^{r_1^i}. \tag{3.88}$$

Using the Fermi-Dirac distribution function (2.85) and (2.92) we subsequently get:

$$\tilde{f} = \frac{1}{\exp\left(\frac{r_0^i\left(E_\beta\left(k_{u^i}\right)-\mu\right)}{k_BT}\right)\exp\left(\frac{r_1^i\left(E_\beta\left(k_{u^i+1}\right)-\mu\right)}{k_BT}\right)}, \tag{3.89}$$

$$= \exp\left(-\frac{r_0^i E_{\beta,u^i} + r_1^i E_{\beta,u^i+1} - \mu}{k_BT}\right). \tag{3.90}$$

Inserting it back into (3.82) finally yields:

$$f_{\beta\, u^i+x} = \frac{\exp\left(-\frac{r_0^i E_{\beta,u^i}+r_1^i E_{\beta,u^i+1}-\mu}{k_B T}\right)}{1+\exp\left(-\frac{r_0^i E_{\beta,u^i}+r_1^i E_{\beta,u^i+1}-\mu}{k_B T}\right)}, \tag{3.91}$$

$$= \frac{1}{\exp\left(\frac{r_0^i E_{\beta,u^i}+r_1^i E_{\beta,u^i+1}-\mu}{k_B T}\right)+1}, \tag{3.92}$$

$$= \frac{1}{\exp\left(\frac{E_{\beta,u^i+x}-\mu}{k_B T}\right)+1}. \tag{3.93}$$

The final result shows that we have indeed accomplished a linear interpolation in energy space.

3.5.2 Exponential interpolation of phonon distribution function:

The starting point for the exponential interpolation of the phonon distribution function reads:

$$\log\frac{N^\eta_{v^i+x}+1}{N^\eta_{v^i+x}} = r_0^i \log\frac{N^\eta_{v^i}+1}{N^\eta_{v^i}} + r_1^i \log\frac{N^\eta_{v^i+1}+1}{N^\eta_{v^i+1}} \tag{3.94}$$

Similar to (3.82) we can define:

$$\hat{N} = \frac{N^\eta_{v^i+x}+1}{N^\eta_{v^i+x}} \tag{3.95}$$

Inserting it into (3.94) and transforming yields:

$$\hat{N} = \frac{(N^\eta_{v^i}+1)^{r_0^i}(N^\eta_{v^i+1}+1)^{r_1^i}}{(N^\eta_{v^i})^{r_0^i}(N^\eta_{v^i+1})^{r_1^i}} \tag{3.96}$$

$$= \frac{(N^\eta_{v^i}+1)^{(1-x)}(N^\eta_{v^i+1}+1)^{x}}{(N^\eta_{v^i})^{(1-x)}(N^\eta_{v^i+1})^{x}} \tag{3.97}$$

Subsequently we can plug our result back into (3.95) to get the final result:

$$N^\eta_{v^i+x} = \frac{1}{\frac{(N^\eta_{v^i}+1)^{(1-x)}(N^\eta_{v^i+1}+1)^{x}}{(N^\eta_{v^i})^{(1-x)}(N^\eta_{v^i+1})^{x}}-1} \tag{3.98}$$

Again we see that this interpolation method demands a lot of computational effort. The result again represents a linear interpolation in energy space as can be easily shown.

3.6 Discrete conservation laws

3.6.1 Conservation of the electron number

In the previous section we have discussed the numerical approximation of $C^{+\,\eta\,p}_{\alpha\beta,i}$. This section deals with the problem of calculating the corresponding collision term $C^{-\,\eta\,p}_{\beta\alpha,l}$ and how to ensure electron conservation numerically. We will construct $C^{-\,\eta\,p}_{\beta\alpha,l}$ at each grid point via the weighted sum over appropriate $C^{+\,\eta\,p}_{\alpha\beta,i}$. To proof that this is possible, we start with the expression

$$\int \Psi_\beta(k') C^{-\,\eta\,p}_{\beta\alpha}(k')dk' = -\int \Psi_\beta(\mathfrak{f}^{+\,\eta}_{\beta\alpha\,p}(k)) C^{+\,\eta}_{\alpha\beta}(k)dk, \tag{3.99}$$

which can be derived similarly to the transformation (2.128) by including an arbitrary function Ψ: We then approximate both integrals by using the midpoint rule:

$$\int \Psi_\beta(k') C^{-\,\eta\,p}_{\beta\alpha}(k')dk' \approx \Delta k \sum_l \Psi_{\beta,l} C^{-\,\eta\,p}_{\beta\alpha,l} \tag{3.100}$$

$$\int \Psi_\beta(\mathfrak{f}^{+\,\eta}_{\beta\alpha\,p}(k)) C^{+\,\eta\,p}_{\alpha\beta}(k)dk \approx \Delta k \sum_i \Psi_\beta(\mathfrak{f}^{+\,\eta}_{\beta\alpha\,p}(k_i)) C^{+\,\eta\,p}_{\alpha\beta,i} \tag{3.101}$$

As we know that $k' = \mathfrak{f}^{+\,\eta}_{\beta\alpha\,p}(k_i)$ does not necessarily coincide with a grid point, we, therefore, approximate $\Psi_\beta(f^{+\,\eta}_{\beta\alpha\,p}(k_i))$ by using the linear weights r^i_n:

$$\Psi_\beta(\mathfrak{f}^{+\,\eta}_{\beta\alpha\,p}(k_i)) \approx \sum_n r^i_n \Psi_{\beta,u^i_n} \tag{3.102}$$

Plugging this back into (3.101) yields:

$$\int \Psi_\beta(\mathfrak{f}^{+\,\eta}_{\beta\alpha\,p}(k)) C^{+\,\eta\,p}_{\alpha\beta}(k)dk \approx \Delta k \sum_i \sum_n r^i_n \Psi_{\beta,u^i_n} C^{+\,\eta\,p}_{\alpha\beta,i} \tag{3.103}$$

This can be expressed as a sum over all $\Psi_{\beta,l}$ by introducing δ_{l,u^i_n}

$$\int \Psi_\beta(\mathfrak{f}^{+\,\eta}_{\beta\alpha\,p}(k)) C^{+\,\eta\,p}_{\alpha\beta}(k)dk \approx \Delta k \sum_l \sum_i \sum_n r^i_n \Psi_{\beta,l} C^{+\,\eta\,p}_{\alpha\beta,i} \delta_{l,u^i_n} \tag{3.104}$$

and rearanging yields

$$\int \Psi_\beta(\mathfrak{f}^{+\,\eta}_{\beta\alpha\,p}(k_))C^{+\,\eta\,p}_{\alpha\beta}(k)dk \approx \Delta k \sum_l \Psi_{\beta,l} \sum_i \sum_n r^i_n C^{+\,\eta\,p}_{\alpha\beta,i}\delta_{l,u^i_n} \tag{3.105}$$

Finally, by comparing this result to (3.99) and (3.100) we conclude that

$$C^{-\,\eta\,p}_{\beta\alpha,l} = -\sum_i \sum_n r^i_n C^{+\,\eta\,p}_{\alpha\beta,i}\delta_{l,u^i_n} \tag{3.106}$$

This is the desired result. We can construct $C^{-\,\eta\,p}_{\beta\alpha,l}$ via corresponding $C^{+\,\eta\,p}_{\alpha\beta,i}$.

Consequently, we can ensure conservation of electron number numerically by imposing appropriate linear weights. To this end, we start again with (2.128) including two test function so that the expression

$$\int \Psi_\alpha(k)C^{+\,\eta\,p}_{\alpha\beta}(k)dk + \int \Psi_\beta(k')C^{-\,\eta\,p}_{\beta\alpha}(k')dk' \stackrel{!}{=} 0. \tag{3.107}$$

vanishes, similar to (2.136). Approximating both integrals as done before leads to:

$$\Delta k \sum_i \Psi_{\alpha,i}C^{+\,\eta\,p}_{\alpha\beta,i} + \Delta k \sum_l \Psi_{\beta,l}C^{-\,\eta\,p}_{\beta\alpha,l} = 0 \tag{3.108}$$

By inserting (3.106) we subsequently get

$$\sum_i \Psi_{\alpha,i}C^{+\,\eta\,p}_{\alpha\beta,i} - \sum_l \Psi_{\beta,l} \sum_i \sum_n r^i_n C^{+\,\eta\,p}_{\alpha\beta,i}\delta_{l,u^i_n} = 0. \tag{3.109}$$

By rearranging it we obtain

$$\sum_i C^{+\,\eta\,p}_{\alpha\beta,i}\Psi_{\alpha,i} - \sum_i C^{+\,\eta\,p}_{\alpha\beta,i} \sum_l \sum_n r^i_n \Psi_{\beta,l}\delta_{l,u^i_n} = 0. \tag{3.110}$$

Consequently, we can equate the coefficients

$$\Psi_{\alpha,i} - \sum_l \sum_n r^i_n \Psi_{\beta,l}\delta_{l,u^i_n} = 0 \tag{3.111}$$

and eliminating the Kronecker delta results in

$$\Psi_{\alpha,i} - \sum_n r^i_n \Psi_{\beta,u^i_n} = 0. \tag{3.112}$$

For the last step, we need to choose our test function. Equation (3.99) represents con-

servation of electron number, if we choose $\Psi_\alpha = \Psi_\beta = const.$ Pluging this back into (3.112) leads to

$$1 - \sum_n r_n^i 1 = 0 \tag{3.113}$$

and

$$\sum_n r_n^i = 1. \tag{3.114}$$

Consequently, we conclude that the linear weights r_n^i need to form a convex sum in order to ensure electron conservation.

3.6.2 Conservation of energy and momentum:

We have seen that the linear weights r_n^i needed to construct $C^{-\,\eta\,p}_{\beta\alpha,l}$ must form a convex sum in order to ensure the conservation of the number of electrons. We will now derive further restrictions for these weights based on the conservation of energy and momentum. The starting point is the relation (2.132) as condition for the conservation of the generalized moment $\mathcal{M}$ of the electrons and phonons. As we have seen, (2.136) holds for all partitions p. Consequently, we demand

$$\int \Psi_\alpha(k) C^{+\,\eta\,p}_{\alpha\beta}(k)dk + \int \Psi_\beta(k') C^{-\,\eta\,p}_{\beta\alpha}(k')dk' + \int \Psi^\eta(q) C^{\beta\alpha\,p}_{\eta}(q)dq \overset{!}{=} 0. \tag{3.115}$$

We can approximate the third integral by

$$\int \Psi^\eta(q) C^{\beta\alpha\,p}_{\eta}(q)dq \approx \Delta_k \sum_t \Psi^\eta_t C^{\beta\alpha\,p}_{\eta,t}. \tag{3.116}$$

Performing the same analysis as in Section 3.6.1 and using (2.145) leads to

$$C^{\beta\alpha\,p}_{\eta,t} = \sum_i \sum_m s^i_m C^{+\,\eta\,p}_{\alpha\beta,i} \delta_{t,v^i_m}. \tag{3.117}$$

Consequently, the integrals in (3.115) are approximated by using (3.100), (3.106), (3.116) and (3.117):

$$\sum_i C^{+\,\eta\,p}_{\alpha\beta,i} \Psi_{\alpha,i} - \sum_i C^{+\,\eta\,p}_{\alpha\beta,i} \sum_l \sum_n r^i_n \Psi_{\beta,l} \delta_{l,u^i_n} + \sum_i C^{+\,\eta\,p}_{\alpha\beta,i} \sum_t \sum_m s^i_m \Psi^\eta_t \delta_{t,v^i_m} = 0. \tag{3.118}$$

Finally, equating the coefficients leads to

$$\Psi_{\alpha,i} - \sum_l \sum_n r_n^i \Psi_{\beta,l} \delta_{l,u_n^i} + \sum_t \sum_m s_m^i \Psi_t^\eta \delta_{t,v_m^i} = 0 \tag{3.119}$$

and, therefore

$$\Psi_{\alpha,i} - \sum_n r_n^i \Psi_{\beta,u_n^i} + \sum_m s_m^i \Psi_{v_m^i}^\eta = 0. \tag{3.120}$$

Conservation of the total momentum is given by setting

$$\Psi_{\alpha,i} = k_i \qquad \Psi_{\beta,u_n^i} = k'_{u_n^i} \qquad \Psi_{v_m^i}^\eta = q_{v_m^i} \tag{3.121}$$

in (3.120). We further know (see (3.60)) that u_n^i can be decomposed into a starting index u^i plus an incremental index n. The same applies to v_i and m and we, therefore set

$$u_n^i = u^i + n \rightarrow k'_{u_n^i} = k'_{u^i+n}, \tag{3.122}$$

$$v_m^i = v^i + m \rightarrow q_{v_m^i} = q_{v^i+m}. \tag{3.123}$$

Inserting (3.121), (3.122) and (3.123) into (3.120) leads to

$$k_i - \sum_n r_n^i k'_{u^i+n} + \sum_m s_m^i q_{v^i+m} = 0. \tag{3.124}$$

For the discrete conservation of momentum to hold, we need to impose $r_n = s_n$ upon the linear weights. We will proof this by inserting this condition into (3.124):

$$k_i + \sum_n r_n^i (q_{v^i+n} - k'_{u^i+n}) = 0 \tag{3.125}$$

Remembering that $q_{v^i+n} = q_{v^i} + \Delta k\ n$ and $k'_{u^i+n} = k'_{u^i} + \Delta k\ n$ leads to

$$k_i + \sum_n r_n^i (q_{v^i} + \Delta k\ n - k'_{u^i} - \Delta k\ n) = 0, \tag{3.126}$$

$$k_i + \sum_n r_n^i (q_{v^i} - k'_{u^i}) = 0. \tag{3.127}$$

Finally, we know that the linear weights need to satisfy $\sum_n r_n^i = 1$:

$$k_i + (q_{v^i} - k'_{u^i}) \sum_n r_n^i = 0, \tag{3.128}$$

$$k_i + q_{v^i} - k'_{u^i} = 0. \tag{3.129}$$

Rearranging reveals that the discretized momenta are indeed conserved

$$q_{v^i} = k'_{u^i} - k_i, \tag{3.130}$$

by demanding

$$r_n = s_n. \tag{3.131}$$

We will now perform the same analysis by inserting the discrete energies

$$\Psi_{\alpha,i} = E_{\alpha,i} \qquad \Psi_{\beta,u_n^i} = E_{\beta,u_n^i} \qquad \Psi^\eta_{v_m^i} = W^\eta_{v_m^i}. \tag{3.132}$$

Further, we restrict ourselves to $n = 0, 1$. Consequently, (3.120) reads by using (3.131)

$$E_{\alpha,i} - r_0^i E_{\beta,u_0^i} - r_1^i E_{\beta,u_1^i} + r_0^i W^\eta_{v_0^i} + r_1^i W^\eta_{v_1^i} = 0. \tag{3.133}$$

For only two indices n, $\sum_n r_n^i = 1$ can simply be written as $r_1^i = 1 - r_0^i$ and we get

$$E_{\alpha,i} - r_0^i E_{\beta,u^i} - (1 - r_0^i) E_{\beta,u^i+1} + r_0^i W^\eta_{v^i} + (1 - r_0^i) W^\eta_{v^i+1} = 0, \tag{3.134}$$

$$E_{\alpha,i} - E_{\beta,u^i+1} + W^\eta_{v^i+1} + r_0^i (E_{\beta,u^i+1} - E_{\beta,u^i} + W^\eta_{v^i} - W^\eta_{v^i+1}) = 0. \tag{3.135}$$

Rearranging leads to

$$r_0^i = \frac{E_{\beta,u^i+1} - E_{\alpha,i} - W^\eta_{v^i+1}}{E_{\beta,u^i+1} - E_{\beta,u^i} + W^\eta_{v^i} - W^\eta_{v^i+1}}. \tag{3.136}$$

We can transform this expression using

$$H^{+\,\eta}_{\beta\alpha,iu^i+1} = E_{\beta,u^i+1} - E_{\alpha,i} - W^\eta_{v^i+1}, \tag{3.137}$$

$$H^{+\,\eta}_{\beta\alpha,iu^i} = E_{\beta,u^i} - E_{\alpha,i} - W^\eta_{v^i}, \tag{3.138}$$

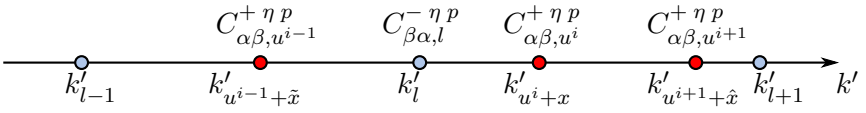

Figure 3.5: Illustration of the approximation process to calulate $C^{-\,\eta\,p}_{\beta\alpha,l}$. Possible values $k' = \mathfrak{f}^{+\,\eta}_{\beta\alpha\,p}(k_i)$ for k_{i-1}, k_i and k_{i+1} are shown along with corresponding collision operators $C^{+\,\eta\,p}_{\alpha\beta}$. Since the k' fall into an interval adjacent to k_l, all three collsion operators contribute to the value $C^{-\,\eta\,p}_{\beta\alpha,l} = r_1^{i-1} C^{+\,\eta\,p}_{\alpha\beta,u^{i-1}} + r_0^{i} C^{+\,\eta\,p}_{\alpha\beta,u^{i}} + r_0^{i+1} C^{+\,\eta\,p}_{\alpha\beta,u^{i+1}}$.

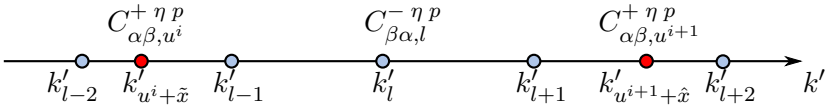

Figure 3.6: Again the approximation of $C^{-\,\eta\,p}_{\beta\alpha,l}$ is illustrated. In this case the values of $k' = \mathfrak{f}^{+\,\eta}_{\beta\alpha\,p}(k_i)$ are widespread and since $k'_{u^{i}+\tilde{x}}$ and $k'_{u^{i+1}+\hat{x}} \notin (k_{l-1}, k_{l+1})$, the collision operator at k'_l reads $C^{-\,\eta\,p}_{\beta\alpha,l} = 0$ This is a sampling problem since we need to have at least one data point for each interval (k'_l, k'_{l+1}) in order to approximate $C^{-\,\eta\,p}_{\beta\alpha,l}$ correctly.

according to (3.59). Subsequently the final result reads

$$r_0^i = \frac{H^{+\,\eta}_{\beta\alpha,iu^i+1}}{H^{+\,\eta}_{\beta\alpha,iu^i+1} - H^{+\,\eta}_{\beta\alpha,iu^i}}. \tag{3.139}$$

This exactly the same relation as (3.68). We, therefore, conclude that the restrictions derived in this section represent the linear interpolation used to find $\mathfrak{f}^{+\,\eta}_{\beta\alpha\,p}(k_i)$ in Section 3.4. Consequently, we can now interpret the construction of $C^{-\,\eta\,p}_{\beta\alpha,l}$ via the corresponding terms $C^{+\,\eta\,p}_{\alpha\beta,i}$. Figure 3.5 illustrates this process. All $C^{+\,\eta\,p}_{\alpha\beta,i}$ with $k'_{u^i+x} \in (k'_{l-1}, k'_{l+1})$ contribute to $C^{-\,\eta\,p}_{\beta\alpha,l}$. If $k'_{l-1} < k'_{u^i+x} < k'_l$ we need to use the linear weight r_1^i if on the other hand $k'_l \leqq k'_{u^i+x} < k'_{l+1}$ the weight r_0^i is used to calculate the contribution.

3.7 Supersampling

In the previous section we demonstared the construction of $C^{-\,\eta\,p}_{\beta\alpha,l}$ using linear weights and corresponding terms $C^{+\,\eta\,p}_{\alpha\beta,i}$. This method might lead to sapling probems as illustrated in Figure 3.6. Therefore, an oversampling or supersampling method is introduced

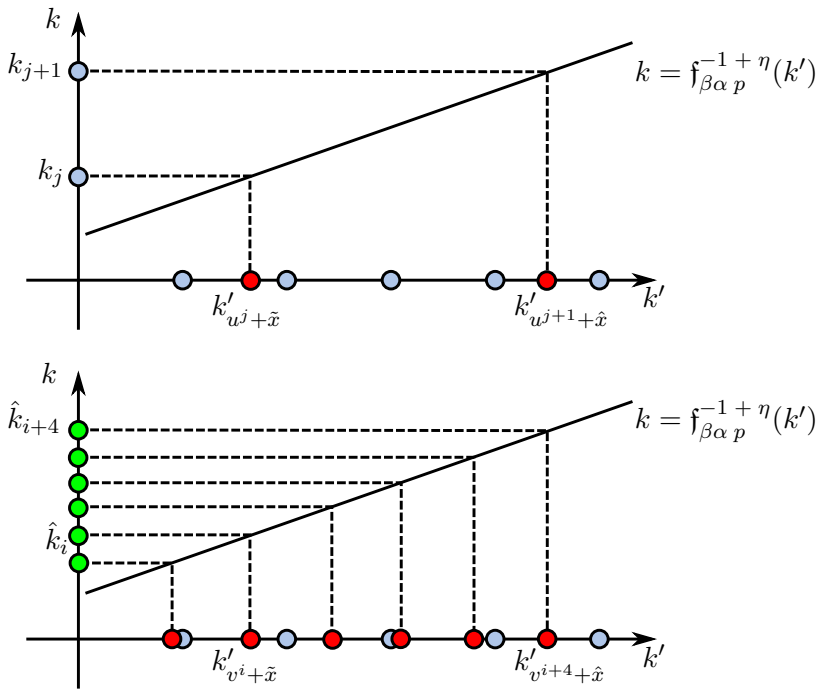

Figure 3.7: Illustration of the supersampling method. In the upper figure the problem of the previously introduced sampling method is highlited. Depending on the function $k' = \mathfrak{f}^{+\,\eta}_{\beta\alpha\,p}(k_j)$ the positions of corresponding k' values are either dense or sparse, since we only sample at the k_j gridpoints. We therefore introduce an additial set of grid points $\hat{k}_i$ that is more dense and allows us to sample $k' = \mathfrak{f}^{+\,\eta}_{\beta\alpha\,p}(k)$ in a way, so that for every interval (k'_l, k'_{l+1}) exists at least one $k'_{v^i+x} = \mathfrak{f}^{+\,\eta}_{\beta\alpha\,p}(\hat{k}_i)$. It should be noted that none of the supersampling gridpoints needs to coincide with the normal gridpoints.

(see Figure 3.7). The idea is to oversample $C^{+\,\eta}_{\alpha\beta,i}$ by introducing a finer supersampling grid in order to ensure that a $C^{-\,\eta}_{\beta\alpha,l}$ can be calculated correctly for every grid point. Since all functions are only defined at the normal grid points, we need to be able to calculate $\hat{C}^{+\,\eta}_{\alpha\beta,i}$ at the supersampling grid points $\hat{k}_i$. Furthermore, we need to reconstruct $C^{+\,\eta}_{\alpha\beta,j}$ as well as $C^{-\,\eta}_{\beta\alpha,l}$ at the normal grid points. To this end, we need to derive new constraints for the linear weights from the discrete conservation laws as before.

We start by introducing an additial finer grid to the initial grid (see Section (3.2)) by defining the set $\hat{\mathcal{I}}_k = \left\{\hat{k}_n | n = 0, \ldots, 2\hat{N}_k - 1\right\}$

$$\hat{k}_n = (n - \hat{N}_k)\Delta_{\hat{k}} \qquad \text{for} \quad n \in \hat{I}_k = \left\{0, \ldots, 2\hat{N}_k - 1\right\}, \tag{3.140}$$

covering the Brillouin zone uniformly, where $\Delta_{\hat{k}}$ denotes the supersampling discretization width and $\hat{N}_k = .\left\lfloor \frac{\pi}{a}\frac{1}{\Delta_{\hat{k}}} \right\rfloor$ For every electron band α and interval $\hat{\mathbb{I}}^{\alpha}_k = [k^{\alpha}_{\min}, k^{\alpha}_{\max}]$ we introduce the corresponding subsets $\hat{\mathcal{I}}^{\alpha}_k = \left\{\hat{k}_n | \hat{k}_n \in \hat{\mathbb{I}}^{\alpha}_k \wedge n \in \hat{I}_k\right\}$ and $\hat{I}^{\alpha}_k = \left\{n | n \in \hat{I}_k \wedge \hat{k}_n \in \hat{\mathbb{I}}^{\alpha}_k\right\}$. Subsequently, we can approximate the integral over the collision operator by

$$\int \Psi_{\alpha}(k) C^{+\,\eta\,p}_{\alpha\beta}(k) dk \approx \Delta_k \sum_j \Psi_{\alpha,j} C^{+\,\eta\,p}_{\alpha\beta,j}, \tag{3.141}$$

$$\int \Psi_{\alpha}(k) C^{+\,\eta\,p}_{\alpha\beta}(k) dk \approx \Delta_{\hat{k}} \sum_i \Psi_{\alpha}(\hat{k}_i) \hat{C}^{+\,\eta\,p}_{\alpha\beta,i}, \tag{3.142}$$

where

$$\hat{C}^{+\,\eta\,p}_{\alpha\beta,i} = C^{+\,\eta\,p}_{\alpha\beta}(\hat{k}_i), \quad \text{with} \quad i \in \hat{I}^{\alpha}_k \tag{3.143}$$

denotes the collision operator evaluated at the supersampling grid points. Since all moments of the distribution functions are defined at the original grid points, we need to approximate $\Psi_{\alpha}(\hat{k}_i)$ at the supersampling grid points by

$$\Psi_{\alpha}(\hat{k}_i) = \sum_n r^i_n \Psi_{\alpha\, u^i_n} \tag{3.144}$$

Inserting this back into (3.142) yields

$$\Delta_{\hat{k}} \sum_i \Psi_{\alpha}(\hat{k}_i) \hat{C}^{+\,\eta\,p}_{\alpha\beta,i} = \Delta_{\hat{k}} \sum_j \Psi_{\alpha,j} \sum_i \sum_n r^i_n \hat{C}^{+\,\eta\,p}_{\alpha\beta,i} \delta_{j,u^i_n}. \tag{3.145}$$

Finally, we can use the the equality of (3.141) and (3.142), leading to

$$\Delta_k \sum_j \Psi_{\alpha,j} C^{+\,\eta\,p}_{\alpha\beta,j} = \Delta_{\hat{k}} \sum_j \Psi_{\alpha,j} \sum_i \sum_n r^i_n \hat{C}^{+\,\eta\,p}_{\alpha\beta,i} \delta_{j,u^i_n}. \tag{3.146}$$

Equating coefficients and subsequent rearranging yields the final result

$$C^{+\,\eta\,p}_{\alpha\beta,j} = \frac{\Delta_{\hat{k}}}{\Delta_k} \sum_i \sum_n r^i_n \hat{C}^{+\,\eta\,p}_{\alpha\beta,i} \delta_{j,u^i_n}. \tag{3.147}$$

We will no perform the same analysis for $C^{-\,\eta\,p}_{\beta\alpha,l}$ starting with the approximation of the integrals

$$\int \Psi_\beta(k') C^{-\,\eta\,p}_{\beta\alpha}(k') dk' \approx \Delta_{k'} \sum_l \Psi_{\beta,l} C^{-\,\eta\,p}_{\beta\alpha,l} \tag{3.148}$$

$$\int \Psi_\beta(f^{+\,\eta}_{\beta\alpha\,p}(k))) C^{+\,\eta\,p}_{\alpha\beta}(k) dk \approx \Delta_{\hat{k}} \sum_i \Psi_\beta(f^{+\,\eta}_{\beta\alpha\,p}(\hat{k}_i)) \hat{C}^{+\,\eta\,p}_{\alpha\beta,i} \tag{3.149}$$

Please note that this time we did not restrict the k' discretization width of band β ($\Delta_{k'}$) to be equal to Δ_k. Repeating all steps as before leads to:

$$C^{-\,\eta\,p}_{\beta\alpha,l} = -\frac{\Delta_{\hat{k}}}{\Delta_{k'}} \sum_i \sum_m s^i_m \hat{C}^{+\,\eta\,p}_{\alpha\beta,i} \delta_{l,v^i_m} \tag{3.150}$$

with a new set of linear weights s^i_m. Finally, we can peform the same analysis for the phonon collision operator leading to

$$C^{\alpha\beta\,p}_{\eta,o} = -\frac{\Delta_{\hat{k}}}{\Delta_q} \sum_i \sum_l t^i_l \hat{C}^{+\,\eta\,p}_{\alpha\beta,i} \delta_{o,w^i_l} \tag{3.151}$$

where we again used a different discretization width Δ_q for the phonon branch η and introduced the linear weights t^i_l.

3.7.1 Conservation laws

As before, restrictions for the linear weights arise from discrete conservation laws, and we start our analysis, as done before, with the conservation of the electron number. Consequently, we use (3.107) and approximating the integrals by applying the midpoint

rule, like in (3.108), yields

$$\Delta_k \sum_j \Psi_{\alpha,j} C^{+\,\eta\,p}_{\alpha\beta\,j} + \Delta_{k'} \sum_l \Psi_{\beta,l} C^{-\,\eta\,p}_{\beta\alpha,l} = 0. \tag{3.152}$$

Subsequently, we can use (3.147) and (3.150), leading to

$$\Delta_k \sum_j \Psi_{\alpha,j} \frac{\Delta_{\hat{k}}}{\Delta_k} \sum_i \sum_n r^i_n \hat{C}^{+\,\eta\,p}_{\alpha\beta,i} \delta_{j,u^i_n} - \Delta_{k'} \sum_l \Psi_{\beta,l} \frac{\Delta_{\hat{k}}}{\Delta_{k'}} \sum_i \sum_m s^i_m \hat{C}^{+\,\eta}_{\alpha\beta,i} \delta_{l,v^i_m} = 0 \tag{3.153}$$

and by further rearrangement we get

$$\Delta_{\hat{k}} \sum_i \hat{C}^{+\,\eta\,p}_{\alpha\beta,i} \sum_j \sum_n r^i_n \Psi_{\alpha,j} \delta_{j,u^i_n} - \Delta_{\hat{k}} \sum_i \hat{C}^{+\,\eta}_{\alpha\beta,i} \sum_l \sum_m s^i_m \Psi_{\beta,l} \delta_{l,v^i_m} = 0. \tag{3.154}$$

Please note that the different discretization widths Δ_k and Δ'_k have dropped out. Consequently, by equating the coefficients, we get

$$\sum_j \sum_n r^i_n \Psi_{\alpha,j} \delta_{l,u^i_n} - \sum_l \sum_m s^i_m \Psi_{\beta,l} \delta_{l,v^i_m} = 0. \tag{3.155}$$

Further simplification finally leads to

$$\sum_n r^i_n \Psi_{\alpha,u^i_n} - \sum_m s^i_m \Psi_{\beta,v^i_m} = 0. \tag{3.156}$$

We again choose Ψ to be constant thus representing electron number, and get

$$\sum_n r^i_n - \sum_m s^i_m = 0. \tag{3.157}$$

We have chosen the linear weights r^i_n to satisfy $\sum_n r^i_n = 1$, which leads to

$$1 - \sum_m s^i_m = 0. \tag{3.158}$$

Finally, we see that in order for the electron number to be conserved, the weights s^i_m need to form a convex sum as well $\sum_m s^i_m = 1$.

Now, we turn to the conservation of energy and momentum. We start with (3.115) and approximate the integrals by using (3.147), (3.150) and (3.151), equating the coefficients

and finally eliminating the Kronecker delta we get

$$\sum_n r_n^i \Psi_{\alpha,u_n^i} - \sum_m s_m^i \Psi_{\beta,v_m^i} + \sum_l t_l^i \Psi_{w_l^i}^{\eta} = 0. \tag{3.159}$$

We will first investigate the conservation of momentum leading to:

$$\sum_n r_n^i k_{u_n^i} - \sum_m s_m^i k'_{v_m^i} + \sum_l t_l^i q_{w_l^i} = 0. \tag{3.160}$$

As before, we will use only two linear weights and assume that t_l^i also forms a convex sum leading to

$$r_1^i = 1 - r_0^i, \qquad s_1^i = 1 - s_0^i, \qquad t_1^i = 1 - t_0^i. \tag{3.161}$$

By plugging this into (3.160), and using

$$u_n^i = u^i + n, \qquad v_m^i = v^i + m, \qquad w_l^i = w^i + l \tag{3.162}$$

according to (3.60) and

$$k_{u_n^i} = \Delta_k u_n^i, \qquad k'_{v_m^i} = \Delta_{k'} v_m^i, \qquad q_{w_l^i} = \Delta_q w_l^i, \tag{3.163}$$

we consequently get by imposing $\Delta_k = \Delta_{k'} = \Delta_q$

$$\begin{aligned} &r_0^i \Delta_k u^i + (1 - r_0^i)\Delta_k (u^i + 1) - (s_0^i \Delta_k v^i + (1 - s_0^i)\Delta_k (v^i + 1)) \\ &\quad + t_0^i \Delta_k w^i + (1 - t_0^i)\Delta_k (w^i + 1) = 0. \end{aligned} \tag{3.164}$$

We can then simplify this to

$$r_0^i u^i + (1 - r_0^i)(u^i + 1) - (s_0^i v^i + (1 - s_0^i)(v^i + 1)) + t_0^i w^i + (1 - t_0^i)(w^i + 1) = 0, \tag{3.165}$$

which results in

$$u^i + 1 - r_0^i - (v^i + 1 - s_0^i) + w^i + 1 - t_0^i = 0. \tag{3.166}$$

By demanding

$$r_1^i - s_1^i + t_1^i = 0 \tag{3.167}$$

we retain the conservation of momentum, since by multiplying $u^i - v^i + w^i = 0$ with Δ_k we get $k_{u^i} - k'_{v^i} + q_{w^i} = 0$. Therefore, we see that we need to impose

$$t_1^i = r_0^i - s_0^i \tag{3.168}$$

on the linear weights. We can check this result by setting r_0 to one which means that the supersampling grid point coincides which the grid point k_i:

$$t_1^i = 1 - s_0^i \tag{3.169}$$

$$t_1^i = s_1^i \tag{3.170}$$

We see that this indeed transforms (3.168) back into (3.131).

In the last step, we will consider the conservation of energy by using (3.159) and (3.161) leading to

$$r_0^i E_{\alpha,u^i} + (1 - r_0^i) E_{\alpha,u^i+1} - (s_0^i E_{\beta,v^i} + (1 - s_0^i) E_{\beta,v^i+1}) + (1 - t_1^i) W^\eta_{w^i} + t_1^i W^\eta_{w^i+1} = 0. \tag{3.171}$$

By rearranging

$$r_0^i (E_{\alpha,u^i} - E_{\alpha,u^i+1}) + E_{\alpha,u^i+1} - (s_0^i (E_{\beta,v^i} - E_{\beta,v^i+1}) + E_{\beta,v^i+1}) \tag{3.172}$$

$$+ t_1^i (W^\eta_{w^i+1} - W^\eta_{w^i}) + W^\eta_{w^i} = 0 \tag{3.173}$$

and defining the short notations

$$\Delta E_{\alpha,u^i} = E_{\alpha,u^i+1} - E_{\alpha,u^i}, \tag{3.174}$$

$$\Delta E_{\beta,v^i} = E_{\beta,v^i+1} - E_{\beta,v^i}, \tag{3.175}$$

$$\Delta W^\eta_{w^i} = W^\eta_{w^i+1} - W^\eta_{w^i} \tag{3.176}$$

we get

$$E_{\alpha,u^i+1} - E_{\beta,v^i+1} + W^\eta_{w^i} - r_0^i \Delta E_{\alpha,u^i} + s_0^i \Delta E_{\beta,v^i} + t_1^i \Delta W^\eta_{w^i} = 0. \tag{3.177}$$

Subsequently using (3.168) yields

$$E_{\alpha,u^i+1} - E_{\beta,v^i+1} + W^\eta_{w^i} - r_0^i \Delta E_{\alpha,u^i} + s_0^i \Delta E_{\beta,v^i} + (r_0^i - s_0^i) \Delta W^\eta_{w^i} = 0, \tag{3.178}$$

and further

$$E_{\alpha,u^i+1} - E_{\beta,v^i+1} + W^{\eta}_{w^i} - r_0^i(\Delta E_{\alpha,u^i} - \Delta W^{\eta}_{w^i}) + s_0^i(\Delta E_{\beta,v^i} - \Delta W^{\eta}_{w^i}) = 0. \tag{3.179}$$

Therefore, we get the final result:

$$s_0^i = -\frac{E_{\alpha,u^i+1} - E_{\beta,v^i+1} + W^{\eta}_{w^i} - r_0^i(\Delta E_{\alpha,u^i} - \Delta W^{\eta}_{w^i})}{\Delta E_{\beta,v^i} - \Delta W^{\eta}_{w^i}}. \tag{3.180}$$

We can again check this by setting $r_0 = 1$, which means that

$$s_0^i = -\frac{E_{\alpha,u^i+1} - E_{\beta,v^i+1} + W^{\eta}_{w^i} - (E_{\alpha,u^i+1} - E_{\alpha,u^i} - W^{\eta}_{w^i+1} + W^{\eta}_{w^i})}{E_{\beta,v^i+1} - E_{\beta,v^i} - (W^{\eta}_{w^i+1} - W^{\eta}_{w^i})}. \tag{3.181}$$

Consequently, canceling yields

$$s_0^i = -\frac{E_{\alpha,u^i} - E_{\beta,v^i+1} + W^{\eta}_{w^i+1}}{E_{\beta,v^i+1} - E_{\beta,v^i} - W^{\eta}_{w^i+1} + W^{\eta}_{w^i}} \tag{3.182}$$

and by using (3.137) and (3.138) we get

$$s_0^i = \frac{H^{+\,\eta}_{\beta\alpha\; iu^i+1}}{H^{+\,\eta}_{\beta\alpha\; iu^i+1} - H^{+\,\eta}_{\beta\alpha\; iu^i}} \tag{3.183}$$

where we remeber that $u^i = i$ since $r_0 = 1$ and rename $v^i \to u^i$, $w^i \to v^i$. This result is equal to (3.139) which shows that we retain the original conditions for the linear weight if a supersampling grid point coincides with an original grid point.

4 Single walled carbon nanotubes

In the previous chapters we have developed the transport model for one-dimensional systems and its discretized version. We test it by applying it to an actual physical problem. Carbon nanotubes (CNT) are a very well understood system from its morphology and, therefore, are very well suited for that purpose. They comprise a hollow cylinder formed by carbon atoms with a diameter in the order of nanometer and a length ranging up to several hundred micrometers. CNTs can therefore be looked at as essentially one-dimension systems with translational periodicity along its tube axis.

4.1 Structure and electron band structure

This chapter is mainly based on the book of S. Reich et al.[5] and review atricle of M.S. Dresselhaus et al. [2]. For additional summarization of carbon nanotube properties please refer to the following review papers [3] and [4].

Single walled carbon nanotubes can be thought of as a single sheet of graphite, which is commonly referred to as graphene, rolled up into a tube.

Graphene has a two-dimensional hexagonal, also called honeycomb, lattice structure. The primitive cell is spanned by the two vectors $\mathbf{a}_1$ and $\mathbf{a}_2$ forming an angle of 60°, both having the length $a_0 = \sqrt{3}a_C = 2.461\,\text{Å}$ where $a_C = 1.42\,\text{Å}$ denotes the carbon-carbon bond length.

The vector around the circumference of the nanotube $\mathbf{C} = n_1\mathbf{a}_1 + n_2\mathbf{a}_2$, called chiral vector, is given by the set of integers n_1, n_2, called chiral indices, and defines the nanotube uniquely. Nanotubes with chiral indices of the form $(n, 0)$ are called zig-zag, whereas the ones with (n, n) are called armchair tubes. The diameter d_t of a tube is given by

$$d_t = \frac{|\mathbf{C}|}{\pi} = \frac{a_0}{\pi}\sqrt{n_1^2 + n_1 n_2 + n_2^2}. \tag{4.1}$$

The translational vector $\mathbf{T}$ is the shortest lattice vector perpendicular to the chiral vector

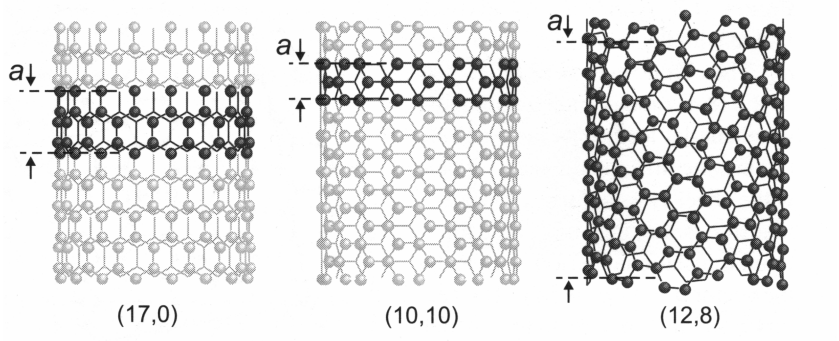

Figure 4.1: Illustration of the structure of a $(17, 0)$ zig-zag, $(10, 10)$ armchair and $(12, 8)$ chiral tube taken from the book of S. Reich et al. [5]. It should be noted that in this figure a denotes the length of the translational vector.

and given by

$$\mathbf{T} = -\frac{2n_2 + n_1}{n\mathcal{R}}\mathbf{a}_1 + \frac{2n_1 + n_2}{n\mathcal{R}}\mathbf{a}_2, \tag{4.2}$$

with n the greatest common divisor of (n_1, n_2) and

$$\mathcal{R} = \begin{cases} 3 & \text{if} \quad (n_1 - n_2)/3n \in \mathbb{N} \\ 1 & \text{otherwise} \end{cases} . \tag{4.3}$$

The translational period T is then given by

$$T = |\mathbf{T}| = \frac{\sqrt{3(n_1^2 + n_1 n_2 + n_2^2)}}{n\mathcal{R}} a_0. \tag{4.4}$$

Zig-zag and armchair tubes are achiral and for both (4.1) and (4.4) can be simplified to

$$T_{\mathcal{Z}} = \sqrt{3}a_0, \qquad |\mathbf{C}_{\mathcal{Z}}| = na_0 \qquad \text{(zig-zag)}, \tag{4.5}$$

$$T_{\mathcal{A}} = a_0, \qquad |\mathbf{C}_{\mathcal{A}}| = \sqrt{3}na_0 \qquad \text{(armchair)}, \tag{4.6}$$

following [5]. We see that achiral tubes have a very high translational periodicity, whereas for chiral tubes the unit cell can be very long depending on the chiral indices.

Subsequently, we can now construct the Brillouin zone for the nanotube. Graphene and nanotubes are closely related. Figure 4.2 shows the Brillouin zone of graphene. For nanotubes we define the z-axis to be along the tube axis and, consequently, the

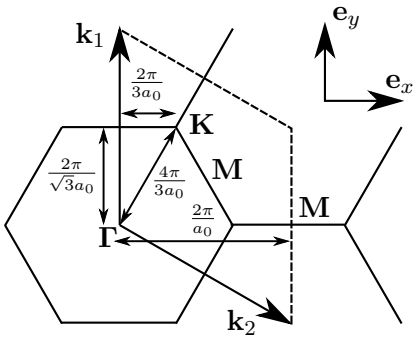

Figure 4.2: Illustration of the Brillouin zone of graphene with the high symmetry points $\mathbf{\Gamma}$, $\mathbf{K}$ and $\mathbf{M}$ as well as the important dimensions following [5].

reciprocal lattice vector reads

$$k_z = \frac{2\pi}{T}. \tag{4.7}$$

The nanotube is assumed to have a macroscopic length and, therefore, k_z can be assumed to be continuous. Consequently, the first Brillouin zone in z-direction spans the interval $(-\frac{\pi}{T}, \frac{\pi}{T}]$. The wave vector $k_\perp$ along the circumference is quantized according to

$$k_{\perp,m} = \frac{2}{d_t} m, \tag{4.8}$$

with the integer $m \in [-n, n]$ for achiral tubes. Consequently, we see that the first Brillouin zone consists of $2n$ equally spaced lines parallel to k_z. Figures 4.3a and 4.3b illustrate the construction of the Brillouin zone for a zig-zag and armchair nanotube, respectively. It should be noted that the position of the line $m = 0$, crossing the $\mathbf{\Gamma}$ point, and $m = n$ is the same for all zig-zag and all armchair tubes, respectively, independet of the diameter. The spacing between all other lines decreases with increasing radius.

We are now able to derive the electronic band structure of nanotubes from graphene using the so called zone-folding approximation. The basic idea is that the band structure is given by the graphene band structure along the allowed k lines. This is a very good approximation for nanotubes with sufficiently large diameters, since in this case confinement effects can be neglected.

A nanotube is metallic if an allowed k line crosses the $\mathbf{K}$ point. This is obviously true for all armchair tubes since the position of the n-th line is independent of n and crosses

both the **K** and **K′** point. Furthermore, one can derive the relation

$$3m = n_1 - n_2, \tag{4.9}$$

stating $n_1 - n_2$ needs to be a multiple of three in order for a nanotube to be metallic. This is obviously true for all armchair and for 1/3 of all zig-zag tubes. Nanotubes not fulfilling this relation are semiconducting with a varying band gap depending on the chiral indices. The band structure of a $(4, 0)$ and a $(4, 4)$ tube is illustrated in the subplots 4.3(c) and 4.3(d).

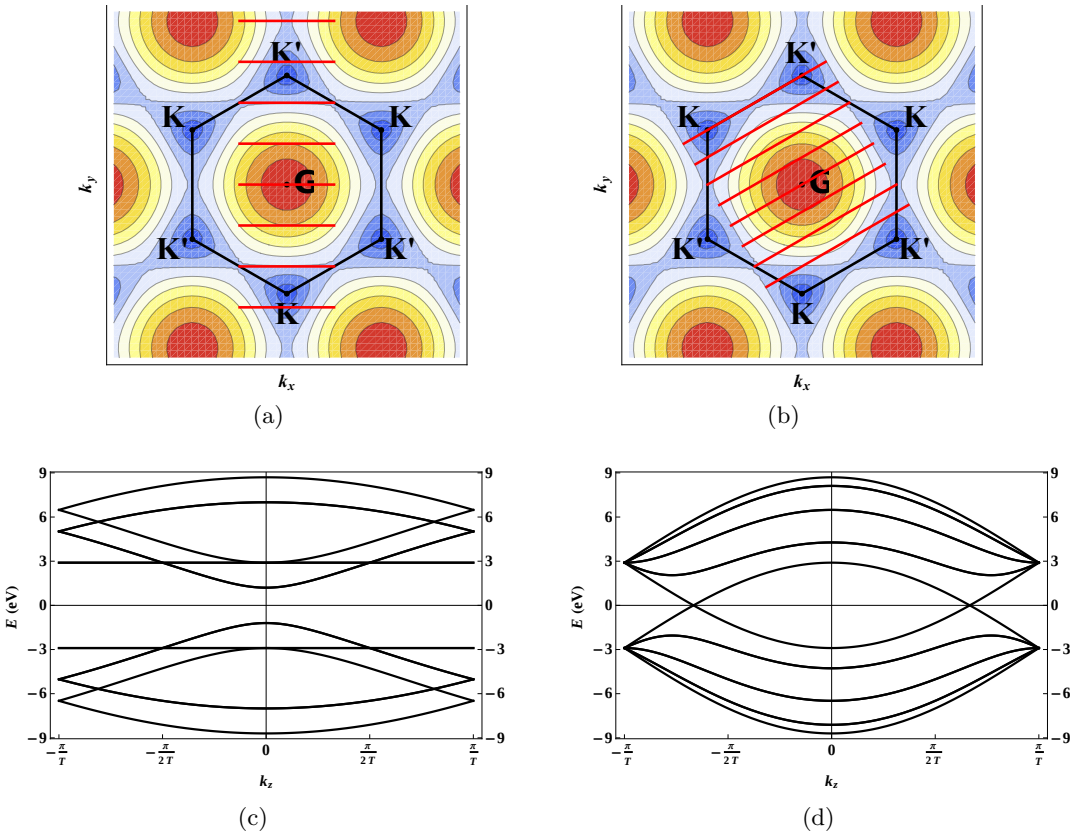

Figure 4.3: Brillouin zone of a $(4, 0)$ zig-zag nanotube (a) and a $(4, 4)$ armchair tube (b). The backgound is a contour plot of the graphene conduction band calculated with a first neighbour thight-binding approximation (TB). The subplots (c) and (d) show the corresponding band structure of the $(4, 0)$ and $(4, 4)$, respectively, using the zone folding approximation. The graphene conduction and valence band again were calculated using first neighbour TB. These plots were created using Mathematica and [28].

For our further investigations we will only consider metallic armchair tubes. In sub-

plot 4.3(d) we see that in a small region around the K and K', where the conduction and valence band touch, the dispersion relation is to a good approximation linear. The group velocity can be approximated by v_F. Furthermore, we see that for sufficiently small energies, we can neglect all other bands and concentrate on a small region around the K K' points. It is convenient to use continuous bands of left and right moving electrons crossing each other instead of conduction and valence bands. The corresponding dispersion relations read

$$E_{R_1/L_1}(K + k) = E_{R_2/L_2}(K' + k) = \pm\hbar v_F k, \tag{4.10}$$

where v_F denotes the Fermi velocity. The reduced electron band structure used for the transport calculation is illustrated in Figure 4.4.

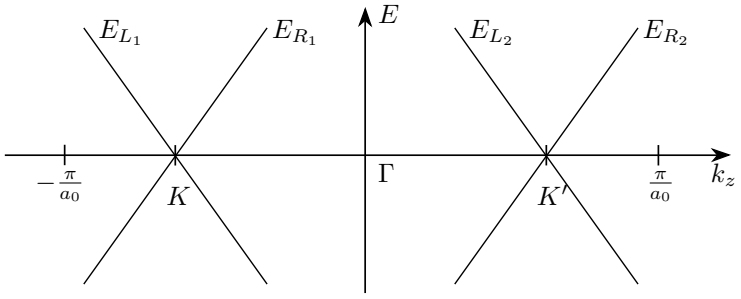

Figure 4.4: Illustration of the reduced band structure with two continuous dispersion relations for left and right moving electrons, respectively.

We will see later on that the electron distributions for left and right moving electrons within each valleys evolves identically. It is, therefore, sufficient to consider just a single region around the K point for the transport calculations.

4.2 Phonon band structure and electron phonon coupling

Similar to the electron band structure, the band structure for the phonon system can be calculated using zone folding, which gives rise to a multitude of phonon branches. Fortunately, only a few phonon branches exhibit a sufficiently large electron phonon coupling (EPC) for certain wave vectors leading to electron scattering. There are only three optical phonon types of interest for the transport model: **K**-phonons and $\mathbf{\Gamma}_{\mathrm{LO/TO}}$-phonons [9, 11, 29]. The most important branch causing back-scattering is the A_1 branch for $q \approx \pm K$, therefore, commonly referred to as **K** or zone boundary phonons, with an

energy of $W_K = 161\,\text{meV}$. Because of the large wave vector involved, this phonon branch causes only intravalley scattering. Transversal optical (TO) and longitudinal optical (LO) phonons with small quasi momentum, thus called $\mathbf{\Gamma}$ phonons, and an energy of $W_{TO} = W_{LO} = 196\,\text{meV}$ cause intervalley forward- and back-scattering. A process is called forward scattering if the electron retains its direction of motion after the scattering event, otherwise it is called back-scattering.

The matrix element for the scattering of elecrons with optical phonons in nanotubes has the same form as in graphen and reads following [19]

$$s^{\eta}_{\alpha\beta}(k_1, k_2) = \frac{2\pi}{\hbar} \frac{\hbar \left| D^{\eta}_{\alpha\beta}(k_1, k_2) \right|^2}{2N m_C \omega_{\eta}(k_1, k_2)}, \tag{4.11}$$

where N denotes the number of unit cells along the device, m_C the mass of a carbon atom and ω_η the phonon vibration frequency. The quasi momenta k_1 and k_2 in this case are measured from the corresponding $\mathbf{K}$-points. The vector notation for the wave vectors k_1 and k_2 can be dropped for nanotubes since they are one-dimensional quantities. The electron phonon coupling (EPC) $\left|D^{\eta}_{\alpha\beta}\right|^2$ in nanotubes can be derived from the graphene EPC $\left|\tilde{D}^{\eta}_{\alpha\beta}\right|^2$. For optical phonons we can use the Einstein approximation

$$W^{\eta}(q) = W^{\eta} = const. \tag{4.12}$$

and therefore

$$\omega_{\eta}(k_1, k_2) = \omega_{\eta} = \frac{W^{\eta}}{\hbar}. \tag{4.13}$$

In graphene the electron phonon coupling is symmetric with respect to $\mathbf{k_1}$ and $\mathbf{k_2}$ and depends on the angle spanned by the two vectors. It should be noted that for graphene we need to used the vector notation for the quasi momenta and both are measured from the corresponding $\mathbf{K}$ point. For the $\mathbf{\Gamma}$ phonons the EPC (see [19, 11]) reads

$$\left|\tilde{D}^{\mathrm{LO/TO}}_{\alpha\neq\beta}(\mathbf{k_1}, \mathbf{k_2})\right|^2 = D^2_{\Gamma}\left[1 \pm \cos(\theta + \theta')\right], \tag{4.14}$$

$$\left|\tilde{D}^{\mathrm{LO/TO}}_{\alpha=\beta}(\mathbf{k_1}, \mathbf{k_2})\right|^2 = D^2_{\Gamma}\left[1 \mp \cos(\theta + \theta')\right], \tag{4.15}$$

where $\theta \measuredangle (\mathbf{k_1}, \mathbf{k_2} - \mathbf{k_1})$ and $\theta' \measuredangle (\mathbf{k_2}, \mathbf{k_2} - \mathbf{k_1})$. Here α and β denote the graphene con-

duction and valence band π^* and π. For **K** phonons the relation is given by

$$\left|\tilde{D}^K_{\alpha\neq\beta}(\mathbf{k_1},\mathbf{k_2})\right|^2 = D_K^2\left[1+\cos(\theta'')\right], \tag{4.16}$$

$$\left|\tilde{D}^K_{\alpha=\beta}(\mathbf{k_1},\mathbf{k_2})\right|^2 = D_K^2\left[1-\cos(\theta'')\right], \tag{4.17}$$

where $\theta'' \measuredangle(\mathbf{k_2},\mathbf{k_1})$.

Considering nanotubes, being one-dimensional systems, this angles can only take the values π or 0 [11]. As a result back-scattering is only possible for **Γ**-LO and **K** phonons and the EPC reads

$$\left|\tilde{D}^{\mathrm{LO}}_{\mathrm{bs}}(k_1,k_2)\right|^2 = 2D_\Gamma^2, \tag{4.18}$$

$$\left|\tilde{D}^{\mathrm{K}}_{\mathrm{bs}}(k_1,k_2)\right|^2 = 2D_K^2. \tag{4.19}$$

Forward scattering on the other hand is only possible for **Γ**-TO phonons with an EPC of

$$\left|\tilde{D}^{\mathrm{TO}}_{\mathrm{fs}}(k_1,k_2)\right|^2 = 2D_\Gamma^2. \tag{4.20}$$

Finally, the EPC derived from graphene needs to be scaled (see [11]) according to

$$S|D^\eta_{\alpha\beta}|^2 = \tilde{S}|\tilde{D}^\eta_{\alpha\beta}|^2, \tag{4.21}$$

where $S = |\mathbf{C}_\mathcal{A}\times\mathbf{T}|$ denotes the surface of the nanotube unit-cell and $\tilde{S} = a_0^2\sqrt{3}/2$ the one of the graphene unit-cell. With $S = \pi d_t T$ we see that

$$|D^\eta_{\alpha\beta}|^2 = \frac{\sqrt{3}a_0^2}{2}\frac{1}{\pi d_t T}|\tilde{D}^\eta_{\alpha\beta}|^2. \tag{4.22}$$

By considering (4.18), (4.19), (4.20) and using (4.13) and (4.22), expression (4.11) consequently reads

$$s^\eta_{\alpha\beta} = \frac{2\pi}{\hbar}\frac{\hbar}{2Nm_C\omega_\eta}\frac{\sqrt{3}a_0^2}{2}\frac{1}{\pi d_t T}|\tilde{D}^\eta_{\alpha\beta}|^2, \tag{4.23}$$

where we can drop the k_1 and k_2 dependence. We see that the scattering matrix element is a constant and only depends on the electron bands α, β and the phonon branch η involved.

4.3 Scaling law and electron/phonon collision operator

We can now derive an expression for the scattering length of optical phonons, which is proportional to the nanotube diameter by collecting all prefactors. We start with the known relations (2.64), (2.65)

$$C_{\alpha\beta}^{\pm\,\eta}(k) = \frac{L}{2\pi} s_{\alpha\beta}^{\eta} \left(\left| \frac{\partial H_{\beta\alpha}^{\pm\,\eta}(k',k)}{\partial k'} \right|^{-1} \chi_{\beta\alpha\,p}^{\pm\,\eta}(k) g_{\beta\alpha}^{\pm\,\eta}(k',k) \right)_{k'=\mathfrak{f}_{\beta\alpha\,p}^{\pm\,\eta}(k),\, k=k} \tag{4.24}$$

for the electron collision operator where we used that $s_{\alpha\beta}^{\eta}$ is a constant. We dropped the index p since $H_{\beta\alpha}^{\pm\,\eta}(\mathfrak{f}_{\beta\alpha\,p}^{\pm\,\eta}(k),k) = 0$ is an amplicit definition for just one bijective function $\mathfrak{f}_{\beta\alpha\,p}^{\pm\,\eta}(k)$ if we use the approximations (4.10) and (4.12). This can also be expressed as

$$C_{\alpha\beta}^{\pm\,\eta}(k) = \frac{1}{\tau_\eta} g_{\beta\alpha}^{\pm\,\eta}(\mathfrak{f}_{\beta\alpha}^{\pm\,\eta}(k),k), \tag{4.25}$$

where τ_η denotes the mean scattering time and we dropped $\chi_{\beta\alpha}^{\pm\,\eta}(k)$ for simplicity. Consequently, we see that

$$\frac{1}{\tau_\eta} = \frac{L}{2\pi} s_{\alpha\beta}^{\eta} \left| \frac{\partial H_{\beta\alpha}^{\pm\,\eta}(k',k)}{\partial k'} \right|_{k'=\mathfrak{f}_{\beta\alpha}^{\pm\,\eta}(k)}^{-1}. \tag{4.26}$$

We first evaluate the partial derivative using (2.34), (2.35), the linear approximation of the electron bands (4.10) and the Einstein approximation (4.12) for phonons:

$$\left| \frac{\partial H_{\beta\alpha}^{\pm\,\eta}(k',k)}{\partial k'} \right|^{-1} = \left| \pm\partial_{k'} E_\beta(k') \mp \partial_{k'} E_\alpha(k) - \partial_{k'} W^\eta(\pm(k'-k)) \right|^{-1}, \tag{4.27}$$

$$= \frac{1}{|\partial_{k'} E_\beta(k')|} = \frac{1}{\hbar v_F}. \tag{4.28}$$

Inserting this back into (4.26) yields

$$\frac{1}{\tau_\eta} = \frac{L}{2\pi} \frac{1}{\hbar v_F} s_{\alpha\beta}^{\eta} \tag{4.29}$$

and by using (4.23), (4.29) consequently reads

$$\frac{1}{\tau_\eta} = \frac{L}{2\pi} \frac{1}{\hbar v_F} \frac{2\pi}{\hbar} \frac{\hbar}{2N m_C \omega_\eta} \frac{\sqrt{3} a_0^2}{2} \frac{1}{\pi d_t T} |\tilde{D}_{\alpha\beta}^{\eta}|^2 \tag{4.30}$$

By canceling and remembering that the length of the nanotube can be expressed as $L = NT$ (see Section 4.2) we get

$$\frac{1}{\tau_\eta} = \frac{\sqrt{3}a_0^2|\tilde{D}^\eta_{\alpha\beta}|^2}{4\pi\hbar v_F^2 m_C \omega_\eta}\frac{v_F}{d_t}. \tag{4.31}$$

Finally, we define the scattering frequency

$$\gamma_\eta = \frac{1}{\tau_\eta} = \frac{v_F}{l_\eta d_t} \tag{4.32}$$

as done in [9] where l_η is a scaling constant and $l_\eta d_t$ denotes the scattering length. An expression for the scaling constant can be found by comparing (4.32) to (4.31):

$$l_\eta = \frac{4\pi\hbar v_F^2 m_C \omega_\eta}{\sqrt{3}a_0^2|\tilde{D}^\eta_{\alpha\beta}|^2}. \tag{4.33}$$

To match the result of [11] we now introduce the symbol $\beta = \hbar v_F$ and rewrite (4.33) into

$$l_\eta = \frac{4\pi m_C \omega_\eta \beta^2}{\sqrt{3}\hbar a_0^2|\tilde{D}^\eta_{\alpha\beta}|^2} \tag{4.34}$$

It should be noted that in [11] $\omega_{K/\Gamma}$ is given in meV suggesting that the $\omega_{K/\Gamma}$ is an energy which might lead to confusion. It should of course read $\hbar\omega_\Gamma = 196\,\text{meV}$ and $\hbar\omega_K = 161.2\,\text{meV}$ instead. The values for electron phonon coupling following [11] is given by $\tilde{D}_\Gamma^2 = 45.60\,(\text{eV/Å})^2$ and $\tilde{D}_K^2 = 92.05\,(\text{eV/Å})^2$. If we further use $\beta = 5,52\,\text{ÅeV}$, $m_C = 12,0107\,\text{u} = 1.6605 \times 10^{-26}\,\text{kg}$, where $u = 1,66 \times 10^{-27}\,\text{kg}$ denotes the atomic mass unit and $a_0 = 2.461\,\text{Å}$ we get

$$l_K = 92.0, \qquad l_\Gamma = 225.6. \tag{4.35}$$

which matches the values chosen for the transport model in [9] and in this work. Using (4.32), the collision terms for the electron interaction with optical phonons finally reads

$$C^{\pm\,\eta}_{\alpha\beta}(k) = \gamma_\eta\, \chi^{\pm\,\eta}_{\beta\alpha}(k)\, g^{\pm\,\eta}_{\beta\alpha}(\mathfrak{f}^{\pm\,\eta}_{\beta\alpha}(k), k). \tag{4.36}$$

Subsequently, we now derive the collision operator of **K** and **Γ**-LO phonons starting

with (2.84)

$$C_{\eta}^{\alpha\beta\,p}(q) = \frac{L}{2\pi} s_{\alpha\beta}^{\eta} \left(\left| \frac{\partial H_{\beta\alpha}^{+\,\eta}(k', k'-q)}{\partial k'} \right|^{-1} \phi_{\beta\alpha\,p}^{+\,\eta}(q) g_{\beta\alpha}^{+\,\eta}\left(k', k\right) \right)_{k'=\mathfrak{h}_{\beta\alpha\,p}^{+\,\eta}(q),\, k=\mathfrak{g}_{\beta\alpha\,p}^{-1\,+\,\eta}(q)} . \tag{4.37}$$

where we again used that $s_{\alpha\beta}^{\eta} = const$ and dropped the index p. Evaluating the partial derivative yields

$$\left| \frac{\partial H_{\beta\alpha}^{+\,\eta}(k', k'-q)}{\partial k'} \right|^{-1} = \left| \partial_{k'} E_{\beta}(k') - \partial_{k'} E_{\alpha}(k'-q) - \partial_{k'} W^{\eta}(q) \right|^{-1} . \tag{4.38}$$

We can now use (4.10), (4.12) and by remembering that for back-scattering the dispersion relations E_{β} and E_{α} have always opposite slopes, we get

$$\left| \frac{\partial H_{\beta\alpha}^{+\,\eta}(k', k'-q)}{\partial k'} \right|^{-1} = \frac{1}{|\pm 2\hbar v_F|}. \tag{4.39}$$

Again we can combine all prefactors using (4.39) and by comparing this to (4.29) and (4.32) we see that

$$\frac{L}{2\pi} \frac{1}{2\hbar v_F} s_{\alpha\beta}^{\eta} = \frac{1}{2\tau_{\eta}} = \frac{\gamma_{\eta}}{2} \tag{4.40}$$

Therefore, the collision operator for **K** and **Γ**-LO phonons finally reads

$$C_{\eta}^{\alpha\beta}(q) = \frac{\gamma_{\eta}}{2} \left(\phi_{\beta\alpha}^{+\,\eta}(q) g_{\beta\alpha}^{+\,\eta}\left(k', k\right) \right)_{k'=\mathfrak{h}_{\beta\alpha}^{+\,\eta}(q),\, k=\mathfrak{g}_{\beta\alpha}^{-1\,+\,\eta}(q)} . \tag{4.41}$$

We can not derive the same expression for forward-scattering **Γ**-LO phonons due to the approximations we chose for the electron and phonon band structure. If we consider (2.34)

$$H_{\beta\alpha}^{+\,\eta}(k', k'-q) = E_{\beta}(k') - E_{\alpha}(k'-q) - W^{\eta}(q) \tag{4.42}$$

we see that by using (4.10), (4.12) and remebering that for forward scattering of **Γ**-LO

phonons $\alpha = \beta$, (2.34) reads

$$H^{+\,\eta}_{\alpha\alpha}(k', k'-q) = \pm\hbar v_F k' \mp \hbar v_F (k'-q) - W^\eta, \tag{4.43}$$

$$= \pm\hbar v_F q - W^\eta. \tag{4.44}$$

This expression is independent of k'.

Therefore, we can not use (2.84) because the term $\left|\partial_{k'} H^{+\,\eta}_{\beta\alpha}(k', k'-q)\right|^{-1}$ diverges and we need to start at the integral form (2.82) where we again use the partition into bijective subintervals introduced in (2.51) (2.52) (2.55). For $q_\eta \in (q^{+\,\eta}_{\beta\alpha\,p\,L}, q^{+\,\eta}_{\beta\alpha\,p\,U})$, (2.82) for the p-th interval reads

$$C^{\alpha\alpha\,p}_\eta(q) = \frac{L}{2\pi} \int_{k'^{+\,\eta}_{\alpha\alpha\,p\,L}}^{k'^{+\,\eta}_{\alpha\alpha\,p\,U}} \delta(H^{+\,\eta}_{\alpha\alpha}(k', k'-q)) s^\eta_{\alpha\alpha} g^{+\,\eta}_{\alpha\alpha}(k', k'-q) dk', \tag{4.45}$$

where we remebered that $s^\eta_{\alpha\alpha} = const.$ Using the approximations (4.10), (4.12) there is only one interval and we again drop the index p. Since the delta distribution is independent of k' we can write

$$C^{\alpha\alpha}_\eta(q) = \frac{L}{2\pi} s^\eta_{\alpha\alpha} \delta(\pm\hbar v_F (q - q_\eta)) \int_{k'^{+\,\eta}_{\alpha\alpha\,L}}^{k'^{+\,\eta}_{\alpha\alpha\,U}} s^\eta_{\alpha\alpha} g^{+\,\eta}_{\alpha\alpha}(k', k'-q) dk', \tag{4.46}$$

by defining

$$q_\eta = \pm \frac{W^\eta}{\hbar v_F}. \tag{4.47}$$

Using $\delta(ax) = 1/|a|\delta(x)$ yields

$$C^{\alpha\alpha}_\eta(q) = \frac{L}{2\pi} \frac{1}{\hbar v_F} s^\eta_{\alpha\alpha} \delta(q - q_\eta) \int_{k'^{+\,\eta}_{\alpha\alpha\,L}}^{k'^{+\,\eta}_{\alpha\alpha\,U}} g^{+\,\eta}_{\alpha\alpha}(k', k'-q) dk'. \tag{4.48}$$

Subsequently we use (4.29) and (4.32) to get the final representation

$$C^{\alpha\alpha}_\eta(q) = \gamma_\eta \delta(q - q_\eta) \int_{k'^{+\,\eta}_{\alpha\alpha\,L}}^{k'^{+\,\eta}_{\alpha\alpha\,U}} g^{+\,\eta}_{\alpha\alpha}(k', k'-q) dk'. \tag{4.49}$$

Numerically the delta distribution does not cause any problems since the integral of the collision operator over the grid cell is used in solving the Boltzmann equation by means of the finite volume method.

4.4 Collision geometry and transport model

As we have seen in Section 4.1 the band structure necessary for the simulation of the electron transport in armchair nanotubes consists of two one-dimensional cones around the K and K' points. It suffices, however, to calculate the evolution of the distribution functions around just one cone by using a local coordinate system. Since for both cones the dispersion relation of the left and right moving bands are identical, one can define:

$$f_L(k,t) := f_{L_1}(K+k,t) = f_{L_2}(K'+k,t), \tag{4.50}$$

$$f_R(k,t) := f_{R_1}(K+k,t) = f_{R_2}(K'+k,t). \tag{4.51}$$

This is, however, only true if the phonon distribution evolves in an equally symmetric way. We assume

$$\bar{N}^K(q,t) := N^K(K+q,t) = N^K(K'+q,t), \tag{4.52}$$

where $N^K(K+q)$ and $N^K(K'+q)$ denotes the phonon distribution function of branch **K** around the K and K' point and $N^K(q)$ the phonon distribution function in the reduced coordinate system. We will now show that the time evolution of the phonon distribution function satisfies

$$\frac{\partial \bar{N}^K(q,t)}{\partial t} := \frac{\partial N^K(\hat{q},t)}{\partial t} = \frac{\partial N^K(\tilde{q},t)}{\partial t}, \tag{4.53}$$

with $\hat{q} = K+q$ and $\tilde{q} = K'+q$, then, (4.52) holds for all times. The starting point to do so is the collision operator derived for back-scattering (4.41)

$$C_\eta^{\alpha\beta}(q) = \frac{\gamma_\eta}{2}\phi^{+\,\eta}_{\beta\alpha\,p}(q)\left\{\left[N^\eta(q)+1\right]f_\beta(k_2)\left[1-f_\alpha(k_1)\right] - N^\eta(q)f_\alpha(k_1)\left[1-f_\beta(k_2)\right]\right\}, \tag{4.54}$$

where we used (2.32) and dropped the time dependence t for simplicity. We also introduced the short notation $k_2 = \mathfrak{h}^{+\,\eta}_{\beta\alpha\,p}(q)$ and $k_1 = \mathfrak{g}^{-1\,+\,\eta}_{\beta\alpha\,p}(q)$ to emphasis that these two functions represent electron quasi momenta. The collision operator for **K** phonons following (2.73) reads

$$C_K = \sum_\alpha \sum_\beta C_K^{\alpha\beta}, \tag{4.55}$$

$$= C_K^{L_1R_2} + C_K^{R_2L_1} + C_K^{L_2R_1} + C_K^{R_1L_2}. \tag{4.56}$$

where we dropped all terms where $s^{\eta}_{\alpha\beta} = 0$ like $C_K^{L_1R_1}$. We will now consider the two quasi momenta $\hat{q}$ and $\tilde{q}$ around the K and K' point, respectively, for (4.56) If we look at Figure 4.5 we see that only a process $C_K^{L_1R_2}$ can affect phonons with quasi momenta around K. Similarly only $C_K^{L_2R_1}$ affects phonons around K'. The analysis perfomed in Figure 4.5 can be repeated for $C_K^{R_1L_2}$ and $C_K^{R_2L_1}$ and we similarly find that process $C_K^{R_1L_2}$ only affect phonons with quasi momenta around K and $C_K^{R_2L_1}$ those around K'. Therefore, we conclude that

$$C_K(\hat{q}) = C_K^{L_1R_2}(\hat{q}) + C_K^{R_1L_2}(\hat{q}), \tag{4.57}$$

$$C_K(\tilde{q}) = C_K^{L_2R_1}(\tilde{q}) + C_K^{R_2L_1}(\tilde{q}). \tag{4.58}$$

By inserting (4.41) and subsequently (4.54) into $C_K^{L_1R_2}(\hat{q})$ we get

$$C_K^{L_1R_2}(\hat{q}) = \frac{\gamma_K}{2} g^{+\,K}_{R_2L_1}(K' + k_2, K + k_1), \tag{4.59}$$

$$= \frac{\gamma_K}{2} \left\{ \left[N^K(K+q) + 1 \right] f_{R_2}(K' + k_2) \left[1 - f_{L_1}(K + k_1) \right] \right. \tag{4.60}$$

$$\left. - N^K(K+q) f_{L_1}(K + k_1) \left[1 - f_{R_2}(K' + k_2) \right] \right\}, \tag{4.61}$$

where we used Figure 4.5 to construct the corresponding electron quasi momenta. Consequently, we us (4.50), (4.51), (4.52)

$$C_K^{L_1R_2}(\hat{q}) = \frac{\gamma_K}{2} \left\{ \left[\bar{N}^K(q) + 1 \right] f_R(k_2) \left[1 - f_L(k_1) \right] - \bar{N}^K(q) f_L(k_1) \left[1 - f_R(k_2) \right] \right\} \tag{4.62}$$

and define

$$C_K^{LR}(q) := \frac{\gamma_K}{2} \left\{ \left[\bar{N}^K(q) + 1 \right] f_R(k_2) \left[1 - f_L(k_1) \right] - \bar{N}^K(q) f_L(k_1) \left[1 - f_R(k_2) \right] \right\}, \tag{4.63}$$

$$= C_K^{L_1R_2}(\hat{q}). \tag{4.64}$$

Now, we turn to expression $C_K^{L_2R_1}(\tilde{q})$ and us again (4.41), (4.54) and Figure 4.5:

$$C_K^{L_2R_1}(\tilde{q}) = \frac{\gamma_K}{2} g^{+\,K}_{R_1L_2}(K + k_2, K' + k_1), \tag{4.65}$$

$$= \frac{\gamma_K}{2} \left\{ \left[N^K(K'+q) + 1 \right] f_{R_1}(K + k_2) \left[1 - f_{L_2}(K' + k_1) \right] \right. \tag{4.66}$$

$$\left. - N^K(K'+q) f_{L_2}(K' + k_1) \left[1 - f_{R_1}(K + k_2) \right] \right\}. \tag{4.67}$$

Finally inserting (4.50), (4.51), (4.52) yields

$$C_K^{L_2R_1}(\tilde{q}) = \frac{\gamma_K}{2}\left\{\left[\bar{N}^K(q)+1\right] f_R(k_2)\left[1-f_L(k_1)\right] - \bar{N}^K(q) f_L(k_1)\left[1-f_R(k_2)\right]\right\} \quad (4.68)$$

and we see that

$$C_K^{LR}(q) := C_K^{L_1R_2}(\hat{q}) = C_K^{L_2R_1}(\tilde{q}). \quad (4.69)$$

Using the same analysis we can show that

$$C_K^{RL}(q) := C_K^{R_1L_2}(\hat{q}) = C_K^{R_2L_1}(\tilde{q}). \quad (4.70)$$

Using (4.57), (4.58), (4.69) and (4.70) we conclude that

$$C_K(q) := C_K(\hat{q}) = C_K(\tilde{q}) = C_K^{LR}(q) + C_K^{RL}(q). \quad (4.71)$$

Therefore, we get the desired result

$$\frac{\partial N^K(q)}{\partial t} := \frac{\partial N^K(\hat{q})}{\partial t} = \frac{\partial N^K(\tilde{q})}{\partial t} = 2C_K(q), \quad (4.72)$$

by using (2.71) where we included a factor two to account for the spin degeneracy of the electron system.

Consequently, we need to derive a similar relation for **Γ**-LO phonons. Since they cause intravalley scattering we do not need to use a local coordinate system. The collision operator for **Γ**-LO phonons following (2.73) reads:

$$C_\Gamma(q) = \sum_\alpha \sum_\beta C_\Gamma^{\alpha\beta}(q), \quad (4.73)$$

$$= C_\Gamma^{L_1R_1}(q) + C_\Gamma^{R_1L_1}(q) + C_\Gamma^{L_2R_2}(q) + C_\Gamma^{R_2L_2}(q). \quad (4.74)$$

For a small quasi momentum q the intravalley scattering operator for left to right moving electron band around the K point reads (see 4.54))

$$C_\Gamma^{L_1R_1}(q) = \frac{\gamma_\Gamma}{2}\left\{\left[N^\Gamma(q)+1\right] f_{R_1}(K+k_2)\left[1-f_{L_1}(K+k_1)\right]\right.$$
$$\left. -N^\Gamma(q) f_{L_1}(K+k_1)\left[1-f_{R_1}(K+k_2)\right]\right\}, \quad (4.75)$$

$$= \frac{\gamma_\Gamma}{2}\left\{\left[N^\Gamma(q)+1\right] f_R(k_2)\left[1-f_L(k_1)\right] - N^\Gamma(q) f_L(k_1)\left[1-f_R(k_2)\right]\right\}, \quad (4.76)$$

$$=: C_\Gamma^{LR}(q). \quad (4.77)$$

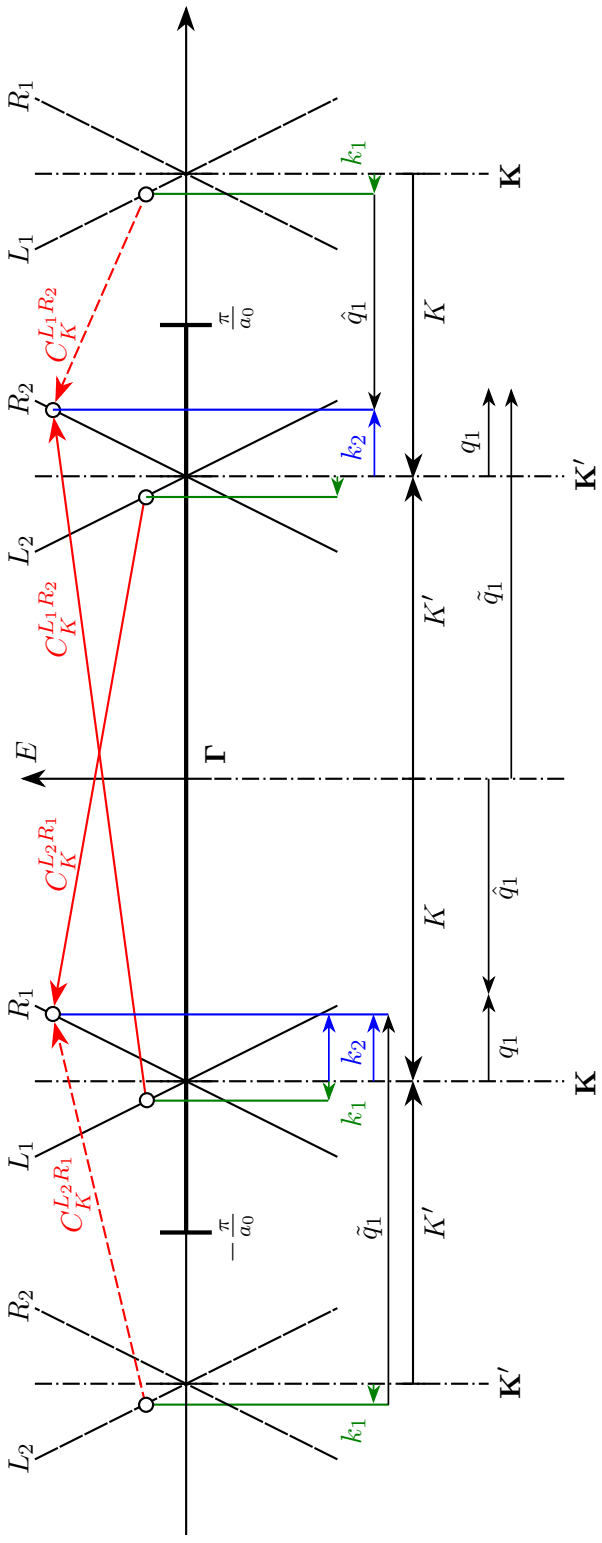

Figure 4.5: Illustration of the construction of the local coordinate system for **K**-phonons. If we look at scattering processes $C_K^{L_1R_2}$ and $C_K^{L_2R_1}$, we see that the phonon wave vector involved is larger than $\frac{\pi}{a_0}$ and we are, therefore, dealing with an Umklapp process. To construct the resulting phonon quasi momentum, we need to consider the corresponding cone in the adjacent Brillouin zone. This process is illustrated for $C_K^{L_1R_2}$ and $\tilde{q}_1$ as well as $C_K^{L_2R_1}$ and $\hat{q}_1$. We consequently see that the process $C_K^{L_1R_2}$ can only affect phonons around the **K** point, whereas only the process $C_K^{L_2R_1}$ can affect phonons around the **K**′ point. Furthermore, we conclude that the local phonon wave vector q_1 around **K** and **K**′ can be constructed by using only the local electron vectors k_1 and k_2 and is the same for both processes.

A similar expression can be derived for $C_\Gamma^{L_2R_2}(q)$:

$$\begin{aligned} C_\Gamma^{L_2R_2}(q) = \frac{\gamma_\Gamma}{2} \Big\{ &\left[N^\Gamma(q)+1\right] f_{R_2}(K'+k_2)\left[1-f_{L_2}(K'+k_1)\right] \\ &-N^\Gamma(q) f_{L_2}(K'+k_1)\left[1-f_{R_2}(K'+k_2)\right] \Big\}, \qquad (4.78) \\ = \frac{\gamma_\Gamma}{2} \Big\{ &\left[N^\Gamma(q)+1\right] f_R(k_2)\left[1-f_L(k_1)\right] - N^\Gamma(q) f_L(k_1)\left[1-f_R(k_2)\right] \Big\}, \qquad (4.79) \\ = C_\Gamma^{LR}(q). \qquad & (4.80) \end{aligned}$$

Using (4.77) and (4.80) we conclude that

$$C_\Gamma^{LR}(q) = C_\Gamma^{L_1R_1}(q) = C_\Gamma^{L_2R_2}(q), \qquad (4.81)$$

$$C_\Gamma^{RL}(q) = C_\Gamma^{R_1L_1}(q) = C_\Gamma^{R_2L_2}(q), \qquad (4.82)$$

where (4.82) can be derived similar to (4.81). Consequently, inserting (4.82) and (4.81) into (4.74) yields

$$C_\Gamma(q) = 2C_\Gamma^{LR}(q) + 2C_\Gamma^{RL}(q). \qquad (4.83)$$

We see that an additional factor two appears if we use the reduced coordinate system. This accounts for the fact that each scattering event happens in both cones simultaneously. The rate of change caused by collisions due to (2.71), therefore, reads

$$\frac{\partial N^\Gamma(q)}{\partial t} = 2C_\Gamma(q) = 4C_\Gamma^{LR}(q) + 4C_\Gamma^{RL}(q), \qquad (4.84)$$

where we again need to included the factor two to account for the spin degeneracy of the electron system.

Finally, the interaction of electrons with acoustic phonons is modeled in agreement to [9] as

$$C_{\alpha,\beta}^{ac}(k) = \frac{v_F}{l_{ac}} \left(f_\beta(-k) - f_\alpha(k)\right). \qquad (4.85)$$

5 Tests, results and conclusion

We will now discuss several tests and results for the numerical model based on the physical system outlined in Chapter 4. For the numerical simulations we use the following parameters if not stated otherwise, which are in agreement with [9]: The discretization width in x-direction is $\Delta_x = L/25$, where L denotes tube length. We use a k-space discretization width of $\Delta_k = \Delta_E/\hbar v_F$ with $\Delta_E = 40\,\text{meV}$ and the Fermi velocity $v_F = 8.4 \times 10^5\,\text{m/s}$. Since $\Delta_k \propto \Delta_E$ it suffices to specify either the k-space or energy discretization width. The transmission constant for ohmic contacts is set to $t^2 = 0.95$. Regarding the phonon energies we use $W_K = 160\,\text{meV}$ and $W_{\Gamma\text{-LO/TO}} = 200\,\text{meV}$. The relaxation time for the decay of optical phonons is assumed to be $\tau_\eta = 3.5\ ps$ for all phonon branches. Although we use the Einstein approximation to calculate the collision integrals, we use a group velocity for backscattering phonons in the advection term and set $v_K = 5000\,\text{m/s}$, $v_{\Gamma\text{-LO}} = 2950\,\text{m/s}$ and $v_{\Gamma\text{-TO}} = 0\,\text{m/s}$. Acoustic phonons are assumed to be at room temperature $T_{ac} = 300\,\text{K}$ with an elastic mean free path for electrons of $l_{ac} = 700\,\text{nm}$. Finally, the nanotube diameter is used as a fitting parameter and we choose $l_K = 92.0$ and $l_{\Gamma\text{-LO/TO}} = 225.6$ for the coupling coefficient (4.32).

5.1 Ballistic transport

Transport without the influence of scattering processes is called ballistic transport. For metallic nanotubes a very simple formula (see [9]) can be derived describing the correlation of current density and applied electric field

$$j = \frac{4e_0^2 U}{2\pi\hbar}, \tag{5.1}$$

where e_0 denotes the elementary charge and U the applied voltage. This result can be easily derived by evaluating (2.4) for the reduced model derived in (4.10) at the right contact and zero temperature. The distribution function of the left moving electrons distribution function equals the equilibrium distribution function whereas for the right moving electrons the Fermi surface is shifted along the device due to the applied electric

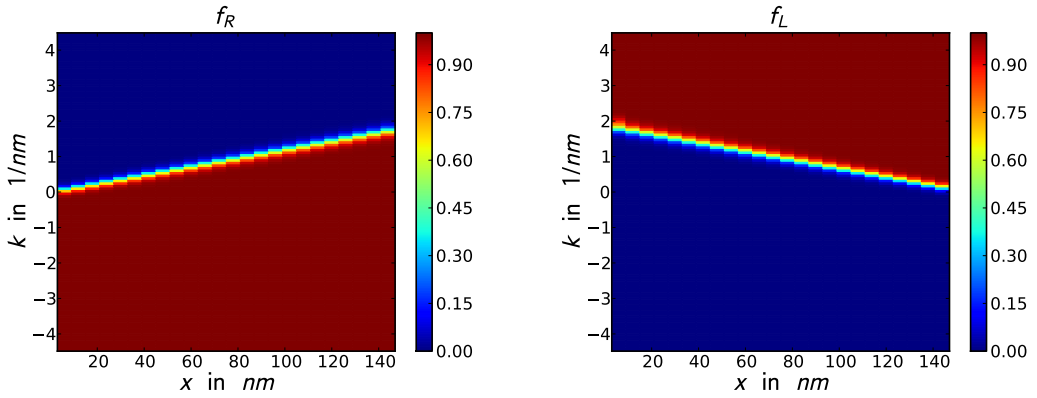

(a) (b)

Figure 5.1: Plot of the steady state distribution functions for right (a) and left propagating electrons (b) in the ballistic transport case.

field. Again the factor four needs to be included due to the spin degeneracy and the two equal cones. It should be noted that perfect contacts are assumed.

By excluding electron-phonon interaction entirely, the calculation of the numerical fluxes as well as the dimensional splitting method and the time integration scheme can be tested. We thus compare the numerical results to the expected physical behavior of the system. First of all, we consider the distribution functions of left and right moving electrons f_L and f_R. Figure 5.1 clearly shows the shift of the Fermi surface along the device, as expected. This is a good indicator that the right side of the Boltzmann equation is modeled correctly. Furthermore, we can compare the calculated electron current density to the theoretical predicted value (5.1). Figure 5.2 shows the result for various applied voltages. The simulation result matches the theoretical result remarkably well.

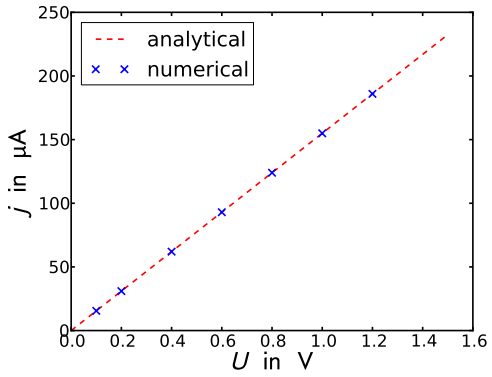

Figure 5.2: Electron current density versus applied voltage in the ballistic case. Comparison of analytical to numerical results.

5.2 Collision operator

In the next step we check the calculation of the collision operator. To this end, we will consider electron and phonon equilibrium distribution functions at different temperatures. This allows us to calculate the exact values for the collision operator and compare them to the numerical results. We assume the electron temperature to be $T_e = 300\,\mathrm{K}$ and $T_K = 1500\,\mathrm{K}$ for the **K**-phonon branch. To see the influence of discretization and supersampling we will vary the grid spacing.

Electron collision operator:

$\Delta_E = 20\,\mathrm{meV}$ - supersampling=off: Figure 5.3a

In this test case the phonon energy is a multiple of Δ_E. Consequently $k' = \mathfrak{f}_{LR}^{+\,K}(k_i)$ coincides with a grid point and, therefore, the collision operator (3.76) (N) must be exactly equal to the analytical expression (2.64) evaluated at grid points k_i (A). We can see that the error $= C_{RL}^{K\,\mathrm{N}} - C_{RL}^{K\,\mathrm{A}}$ is of the order of the numerical precision ($\max(C_{RL}^{K\,\mathrm{N}}) = 0.085\,{}^1/_{\mathrm{fs}}$, $\max(\mathrm{error}) = 2.7 \times 10^{-17}\,{}^1/_{\mathrm{fs}}$)

$\Delta_E \approx 16,58\,\mathrm{meV}$ - supersampling=off: Figure 5.3c

For arbitrary discretization widths the numerical and analytical solution still match. We, however, observe a numerical error caused by the construction of $C_{LR,i}^{-\,K}$ using linear weights outlined in Sections 3.6.1 and 3.6.2. It should be noted that $C_{LR,i}^{+\,K}$ is still equal to the analytical solution if the exponential interpolation method is used.

$\Delta_E \approx 16,58\,\text{meV}$ - supersampling=on ($N_{ss} = 2$): Figure 5.3e

Considering this test case, we can now conclude that supersampling indeed works and gives the correct result. The error is of the same order of magnitude as in 5.3c but slightly higher since both $C^{+\,K}_{RL,i}$ and $C^{-\,K}_{RL,i}$ need to be constructed.

Phonon collision operator:

$\Delta_E = 20\,\text{meV}$ - supersampling=off: Figure 5.3b

Choosing this discretization width $q^{+}_{v^i+x}$ as well as k'_{u^i+x} coincides with a grid point. We can, however, observe that the resulting phonon collision operator is not constructed correctly. The resulting values are twice as big as expected and every other collision operator vanishes. This is obviously a sampling problem similar to the one illustrated in Figure 3.6.

$\Delta_E \approx 16,58\,\text{meV}$ - supersampling=off: Figure 5.3d

We see that using an arbitrary discretization width yields the same problem.

$\Delta_E \approx 16,58\,\text{meV}$ - supersampling=on ($N_{ss} = 2$): Figure 5.3f

Finally using supersampling solves this problem and the **K**-phonon collision operator (4.41) is calculated correctly.

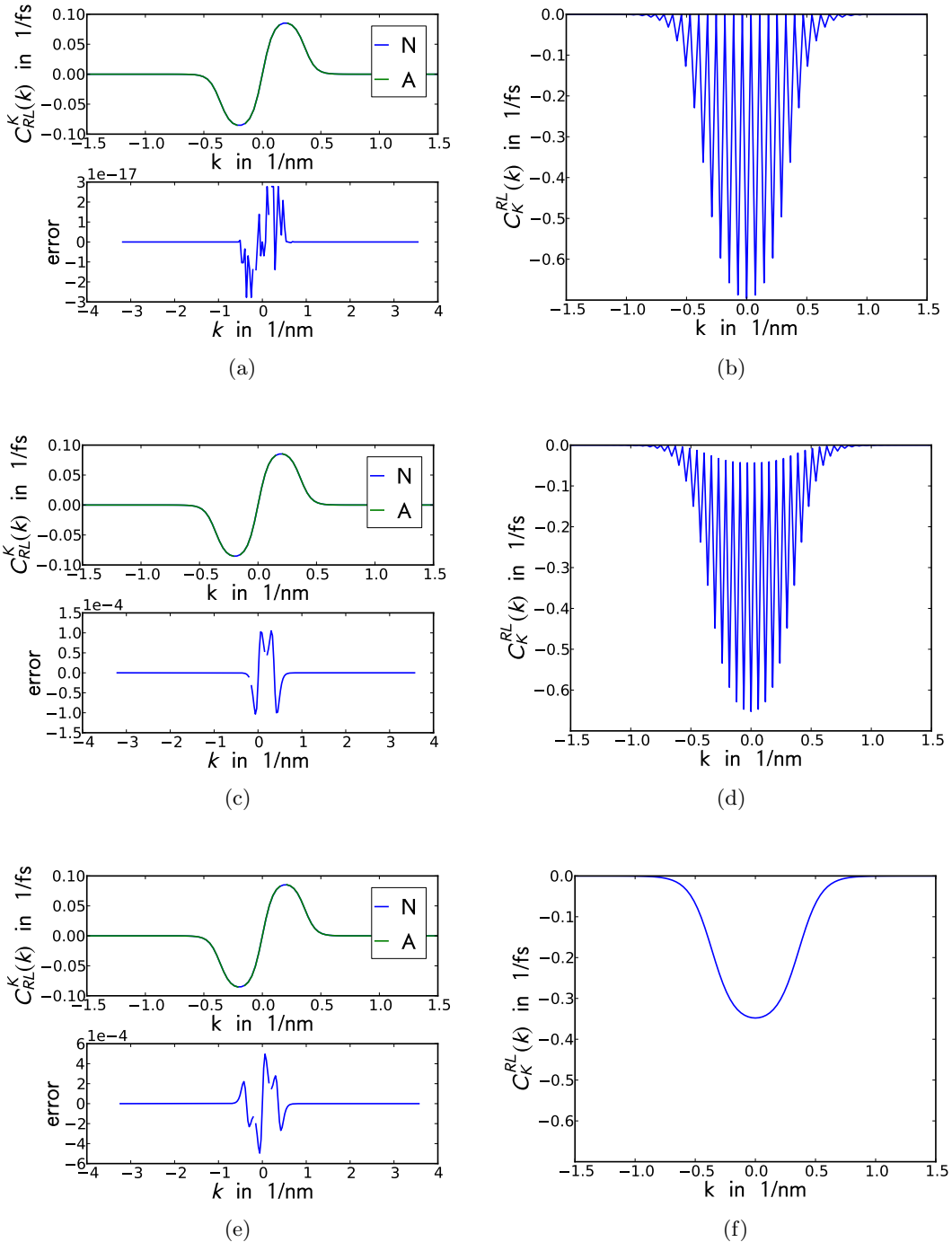

Figure 5.3: Illustration of the electron collision operator and its error $= C^{K\,\mathrm{N}}_{RL} - C^{K\,\mathrm{A}}_{RL}$ for different sampling widths and supersamping turned off and on. On the right hand side the corresponding values of the **K**-phonon collision operators are plotted.

5.3 Bulk simulations

Now, we consider bulk simulations for electrons (2.15) and **K**-phonons (2.70), respectively, by disregarding any x dependence without an electric field applied to check if the time evolution approaches the thermal equilibrium. Consequently, we fix either the electron distribution at $T_e = 300\,\mathrm{K}$ or **K**-phonon distribution $T_{ph} = 1500\,\mathrm{K}$ and calculate the time evolution of the other system. The simulation result for electrons is shown in Figure 5.4a. We can see that the electron system heats up to the phonon temperature. For comparison the corresponding Fermi-Dirac distribution functions at $T = 1500\,\mathrm{K}$ for left and right moving electron has been included. Similarly, we observe in Figure 5.4b that the phonon system cools down. Compared to electrons this process takes a very long time and only small wave vector are affected since for large wave vectors k the Fermi-Dirac functions for $T = 300\,\mathrm{K}$ and $T = 1500\,\mathrm{K}$ differ only slightly. It should also be noted that it is important to choose the time step very carefully in this test case since for to too large time steps the phonon distribution function can take on negative values.

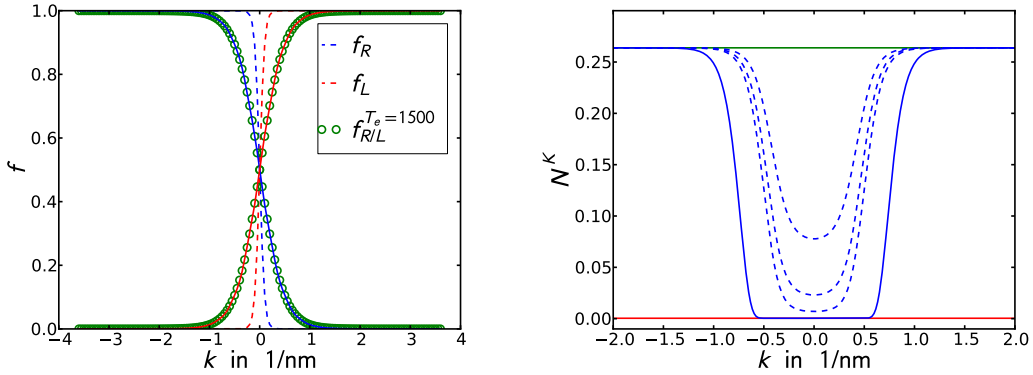

(a) (b)

Figure 5.4: Bulk simulations: Plot (a) illustrates the heating of electron system where the dashed line shows the initial and the solid line shows final distribution. Plot (b) illustrates the phonon distribution function N^K for various time steps while cooling to the electron temperature. The solid green line shows the initial, the blue line the final ($t_f = 3\,\mathrm{ps}$) and the red line the equilibrium distribution function. The dashed blue lines denote intermediate timesteps at $t_1 = 0.075\,\mathrm{ps}$, $t_2 = 0.15\,\mathrm{ps}$ and $t_3 = 0.225\,\mathrm{ps}$. As we can see the calculated phonon distribution function approaches slowly the thermal equilibrium.

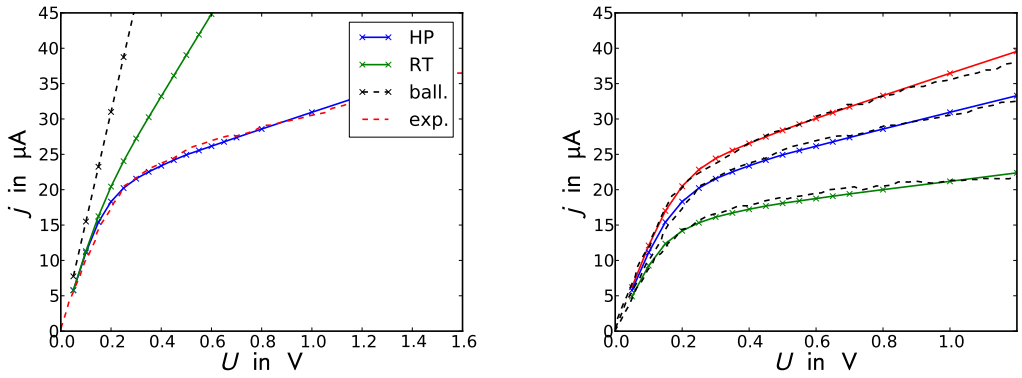

(a) (b)

Figure 5.5: Device simulations, steady state current density versus applied voltage. Plot (a) compares simulations including dynamic phonons out of equilibrium also called hot-phonons (HP) to experimental data (exp.) as well as to current densities calculated using phonons at room temperature (RT) and the ballistic limit (ball.) for a 150 nm nanotube with $d_t = 1.75$ nm diameter. Plot (b) compares the results (solid lines) for different carbon nanotube lengths using the tube diameter as a fitting parameter to the corresponding experimental data (dashed lines) taken from [7]: Red: 85 nm $d_t = 1.45$ nm, Blue: 150 nm $d_t = 1.75$ nm, Green: 300 nm $d_t = 1.6$ nm

5.4 Device simulations

Finally, we turn to device simulations for electrons (2.15) and **K**-phonons (2.70) including electron-phonon interaction by using static phonon distribution functions and dynamically calculated ones. As boundary conditions we use (3.52) and (3.53) for electrons and (3.55) and (3.56) for phonons, respectively.

Experimental data provided in [7] are compared to calculated current densities in Figure 5.5. The simulation results are in good agreement with measurements by including dynamically calculated phonons (hot-phonons) as predicted in [8]. Figure 5.5a shows that static phonon distributions at room temperature can not account for the severe drop of the conductance at about $0.2\,V$ in the the experimental data. This, however, can be correctly reproduced by including hot phonons. Furthermore, the decrease of the conductance for increasing nanotube lengths is modeled properly as seen Figure 5.5b.

The steady state distribution functions for electrons and phonons, respectively, are illustrated in Figure 5.6. If we consider the **K**-phonon distribution function in Figure 5.6f and compare it to the findings in [8], [9] and [10] we notice that the peaks in our calculations are significantly lower. Since for **K**-phonons the rate of change caused by

collisions differs by a factor of two (see (4.72) compared to above mentioned works, this was expected. As a consequence, we see that the $N^{\Gamma-LO}$ peaks are slightly higher than in the works of Auer et. al. see Figure 5.6c. Consequently, if the same scaling constants are used as in [9] the nanotube diameter used as a fitting parameter needs to be lower compared to [9] to match the experimental data as shown in Figure 5.5. This accounts for the smaller out of equilibrium **K**-phonon distribution function. One could also conclude that the electron phonon coupling implicitly assumed in [9] via the scaling constant is underestimated.

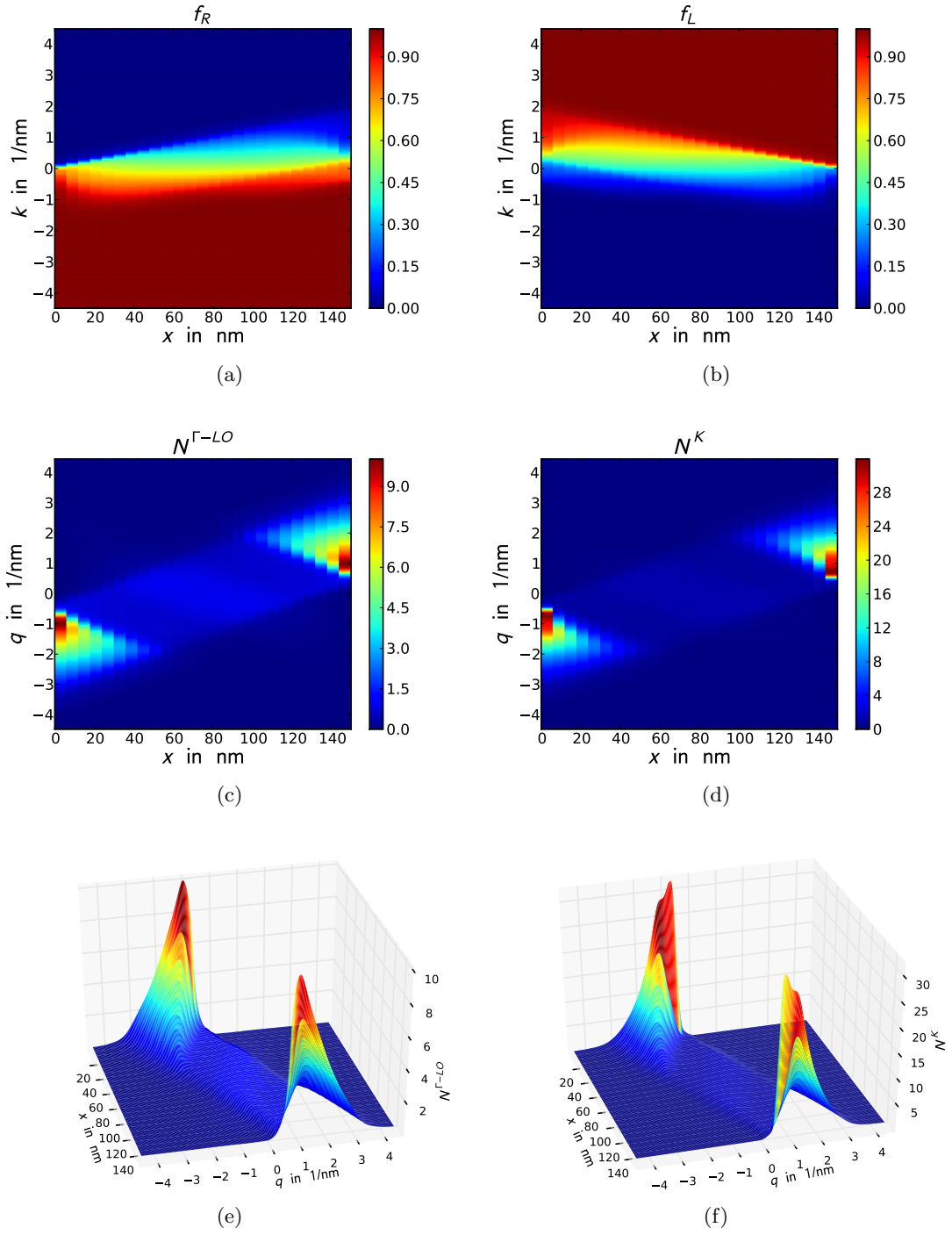

Figure 5.6: Device simulation using dynamic phonons for a nanotube of length $L = 150\,\text{nm}$ with an applied voltage of $U = 1\,\text{V}$ and $d_t = 1.75\,\text{nm}$. Plot (a) and (b) show the steady state distributions for right and left propagating electrons whereas in (c) - (f) phonon steady state distribution functions are depicted.

5.4.1 Comparison of the upwind to the WENO method

Finally, we compare the effect of using the upwind or WENO method to the device simulations.

We start by considering ballistic transport. Figure 5.7a shows the steady state distribution function of right moving electrons obtained by using the upwind method to calculate the numerical fluxes. If we compare this plot to Figure 5.1a, we notice strong numerical diffusion. Figure 5.7b compares the calculated distribution functions f_R at the right contact by using upwind and WENO schemes. Both distribution functions are shifted correctly but by using the upwind method the distribution appears to have a much higher temperature due to the spreading caused by numerical diffusion along the device. For comparison, a Fermi-Dirac distribution at the temperature of $T_e = 1900\,K$ has been included. It should be noted that in this setup the numerical diffusion has no impact on the calculated current density since the Fermi surface is shifted correctly.

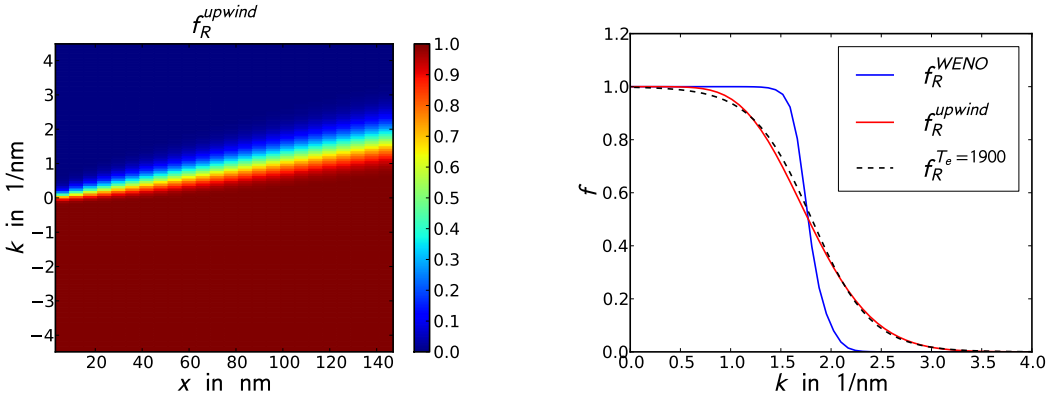

(a) (b)

Figure 5.7: Figure (a) shows the electron distribution function for right propagating electrons for ballistic transport calulated by using the upwind scheme. Figure (b) compares f_R at the right contact in the ballistic transport case. The blue line was calculated by using the WENO scheme and the red line by using the upwind scheme. The dashed line shows a shifted Fermi-Dirac distribution function at $T_e = 1500\,\mathrm{K}$.

This is however not the case for device simulations, see Figure 5.8. The resulting conductance is lower if an upwind scheme is used. The emission of phonons along the device starts earlier due to the apparent higher temperature. This might be a good explanation for this phenomenon. The resulting steady state distribution functions are compared in Figure 5.9.

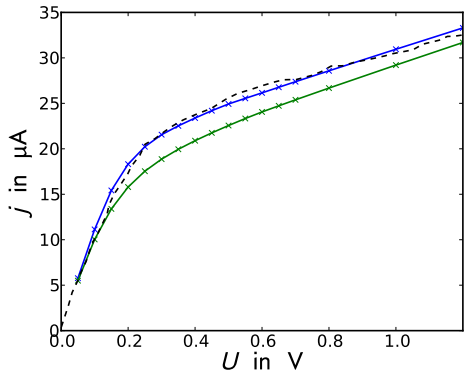

Figure 5.8: Illustration of the electron current density versus the applied voltage calculated by using the WENO (blue) or upwind scheme (green) for the simulation parameters: $L = 150\,\mathrm{nm}$, $U = 1\,\mathrm{V}$ and $d_t = 1.75\,\mathrm{nm}$. The dashed lines represents the corresponding experimental data.

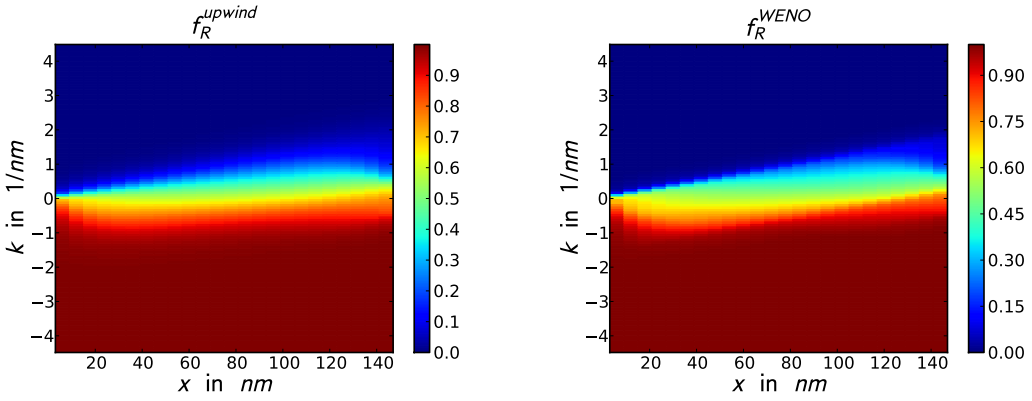

(a) (b)

Figure 5.9: Comparison of the steady state distribution functions including dynamically calculated phonons using the upwind (a) or WENO (b) scheme. Simulation parameters: $L = 150\,\mathrm{nm}$, $U = 1\,\mathrm{V}$ and $d_t = 1.75\,\mathrm{nm}$.

5.4.2 Conclusion

In this thesis a kinetic transport model for the coupled dynamics of electrons and phonons in one-dimensional systems has been developed without using prior information on the band structure of the electron and phonon system. Subsequently, a numerical model has been presented to solve the transport equations for which the conservation of electron number, energy and moment was proved. To overcome numerical sampling problems, a supersampling algorithm was proposed. Furthermore, as opposed to the common energy discretization of the electron bands, a k-space discetization was used in order to be able to work with very flat bands. Based on the model the algorithm was implemented and successfully tested on metallic carbon nanotubes. The results are in accordance to the findings of Auer et al. [9, 10] and the measurements presented in [7]

6 Acknowledgement

First of all I want to express my gratitude to my advisors Ao. Univ.-Prof. Dr. Ferdinand Schürrer and Dipl.-Ing. Dr.techn. Peter Lichtenberger. Without their their support and supervision as well as extensive experience and knowledge this thesis would not have been possible. Moreover, I want to thank all members of the research group, especially Manfred Gruber and Benjamin Stickler for all the fruitful discussions and the good time during my work on this thesis.

I also want to express my deepest thanks to my family for all their support and help. Furthermore, I want to thank all my friends and study colleagues for making my whole studies an unforgettable time. Finally, I want to thank my girlfriend Claudia for always supporting me and enduring my increasing level of lunacy during the final stages for my work.

Bibliography

[1] M. Monthioux and V. L. Kuznetsov. Who should be given the credit for the discovery of carbon nanotubes? *Carbon*, 44(9):1621–1623, 2006.

[2] M.S. Dresselhaus, G. Dresselhaus, and A. Jorio. Unusual properties and structure of carbon nanotubes. *Annual Review of Materials Research*, 34(1):247–278, 2004.

[3] E. Thune and C. Strunk. Quantum transport in carbon nanotubes.

[4] J.-C. Charlier, X. Blase, and S. Roche. Electronic and transport properties of nanotubes. *Rev. Mod. Phys.*, 79(2):677–732, May 2007.

[5] S. Reich, C. Thomsen, and J. Maultzsch. *Carbon Nanotubes*. WILEY-VCH, Weinheim, 2004.

[6] Z. Yao, C. Kane, and C. Dekker. High-field electrical transport in single-wall carbon nanotubes. *Phys. Rev. Lett.*, 84(13):2941–2944, Mar 2000.

[7] A. Javey, J. Guo, M. Paulsson, Q. Wang, D. Mann, M. Lundstrom, and H. Dai. High-field quasiballistic transport in short carbon nanotubes. *Phys. Rev. Lett.*, 92(10):106804, Mar 2004.

[8] C. Auer. *Efficient Numerical Methods for Semiclassical Kinetic Equations for Electrons and Phonons in Semiconductors*. PhD thesis, Graz University of Technology, 2005.

[9] C. Auer and F. Schürrer. Hot phonon effects on the high-field transport in metallic carbon nanotubes. *Phys. Rev. B*, 74, 2006.

[10] C. Auer and F. Schürrer. Influence of hot phonons on the transport properties of single-wall carbon nanotubes. *J. Comput. Electron.*, 6:325–328, 2007.

[11] M. Lazzeri, S. Piscanec, F. Mauri, A. C. Ferrari, and J. Robertson. Electron transport and hot phonons in carbon nanotubes. *Phys. Rev. Lett.*, 95:236802, 2005.

[12] M. Lazzeri and F. Mauri. Coupled dynamics of electrons and phonons in metallic nanotubes: Current saturation from hot-phonon generation. *Phys. Rev. B*, 73(16):165419, Apr 2006.

[13] A. Javey, J. Guo, Q. Wang, M. Lundstrom, and H. Dai. Ballistic carbon nanotube field-effect transistors. *Nature*, 424:654–657, Jun 2003.

[14] S. Hasan, M. A. Alam, and M. S. Lundstrom. Simulation of carbon nanotube fets including hot-phonon and self-heating effects. *IEEE Trans. El. Dev.*, 54(9):2352 – 2361, Sep 2007.

[15] H.-M. So, B.-K. Kim, D.-W. Park, B. S. Kim, J.-J. Kim, K.-j. Kong, H. Chang, and J.-O Lee. Selective suppression of conductance in metallic carbon nanotubes. *JACS*, Mar 2007.

[16] H.-M. So, K. Won, Y. H. Kim, B.-K. Kim, B. H. Ryu, P. S. Na, H. Kim, and J.-O Lee. Single-walled carbon nanotube biosensors using aptamers as molecular recognition elements. *JACS*, Aug 2005.

[17] J. Lu, S. Nagase, X. Zhang, D. Wang, M. Ni, Y. Maeda, T. Wakahara, T. Nakahodo, T. Tsuchiya, T. Akasaka, Z. Gao, D. Yu, H. Ye, W. N. Mei, and Y. Zhou. Selective interaction of large or charge-transfer aromatic molecules with metallic single-wall carbon nanotubes: Critical role of the molecular size and orientation. *JACS*, 126:5114–5118, Mar 2006.

[18] M. Lundstrom. *Fundamentals of carrier transport.* Cambridge University Press, Camebridge, 2000.

[19] P. Lichtenberger. *Kinetic Modeling of the Nonlinear Dynamics of Particles in Low-Dimensional and Non-Equilibrium Systems.* PhD thesis, Graz University of Technology, 2009.

[20] P. A. Markowich, C. A. Ringhofer, and C. Schmeiser. *Semiconductor Equations.* Springer, Wien, 1990.

[21] E. F. Toro. *Riemann solvers and numerical methods for fluid dynamics.* Springer, Berlin / Heidelberg, 1997.

[22] X.-D. Liu, S. Osher, and T. Chan. Weighted essentially nonoscillatory schemes. *J. Comput. Phys.*, 115:200–212, 1994.

[23] A. Harten, B. Engquist, S. Osher, and S. Chakravarthy. Uniformly high order accurate essentially non-oscillatory schemes, iii. *J. Comput. Phys.*, 71:231–303, 1987.

[24] C.-W. Shu and S. Osher. Efficient implementation of essentially nonoscillatory shock-capturing schemes. *J. Comput. Phys.*, 77:439, 1988.

[25] G. Jiang and C.-W. Shu. Efficient implementation of weighted ENO schemes. *J. Comput. Phys.*, 126:202–228, 1996.

[26] C.-W. Shu. High order weighted essentially nonoscillatory schemes for convection dominated problems. *SIAM Review*, 51:82–126, 2009.

[27] R. J. LeVeque. *Finite Volume Methods for Hyperbolic Problems.* Cambridge University Press, Camebridge, 2004.

[28] J. Alfonsi. Electronic band structure of a single-walled carbon nanotube by the zone-folding method. The Wolfram Demonstrations Project, 07 2010. `http://demonstrations.wolfram.com/ElectronicBandStructureOfASingleWalledCarbonNanotubeByTheZon/`.

[29] S. Piscanec, M. Lazzeri, F. Mauri, A. C. Ferrari, and J. Robertson. Kohn anomalies and electron-phonon interactions in graphite. *Phys. Rev. Lett.*, 93(18):185503, Oct 2004.

[30] D.K. Ferry. *Semiconductor Transport.* Taylor & Francis, London, 2000.

[31] N. W. Ashcroft and N. D. Mermin. *Solid State Physics.* Thomson Learning, Cornell University, 1976.

[32] S. Gottlieb and C.-W. Shu. Total variation diminishing Runge-Kutta schemes. *Math. Comp.*, 67:73–85, 1998.

[33] H. W. Kroto, J. R. Heath, S. C. O'Brien, R.F. Curl, and R. E. Smalley. C60: Buckminsterfullerene. *Nature*, 318, 1985.

[34] S. Iijima. Helical microtubules of graphite carbon. *Nature*, 354:56–58, 1991.

[35] S. Iijima and T. Ichihashi. Single-shell carbon nanotubes of 1-nm diameter. *Nature*, 363:603–605, 1993.

[42] D. Adams. *The Hitchhiker's Guide to the Galaxy.* Ballantine Books, New York, 2002